THEORETICAL STUDY OF NONLINEAR AND NON-HERMITIAN ELECTRODYNAMICS IN CHAINS OF PLASMONIC NANOPARTICLES

MOK TSZ CHUNG

M.Phil

The Hong Kong Polytechnic University

2017

The Hong Kong Polytechnic University

Department of Applied Physics

Theoretical Study of Nonlinear and Non-Hermitian Electrodynamics in Chains of Plasmonic Nanoparticles

Mok Tsz Chung

A thesis submitted in partial fulfillment of the requirements for the degree of Master of Philosophy

January 2016

CERTIFICATE OF ORIGINALITY

I hereby declare that this thesis is my own work and that, to the best of my knowledge and belief, it reproduces no material previously published or written, nor material that has been accepted for the award of any other degree or diploma, except where due acknowledgement has been made in the text.

_____ (Signed)

Mok Tsz Chung Ivan (Name of student)

Abstract

In view of the recent advancement in the development of techniques for fabrication of metal nanoparticles, plasmonic chains of nanoparticle, has been widely studied theoretically and experimentally in recent years. In this thesis, we focus on the nonlinear and non-Hermitian electrodynamics in chains of plasmonic nanoparticles. Two special configurations, namely, the plasmonic resonator and the diatomic plasmonic chain were studied and presented. The ideology of a plasmonic resonator, which presumes metal nanoparticles in a one-dimensional array as mechanical resonators, can greatly simplify the mathematics behind. A proper design of the one-dimensional plasmonic chain was outlined, in which the respective linear and nonlinear behaviour were studied by the method of linearization, eigenvalue problem and Runge-Kutta iterations. With the data sets obtained by the Runge-Kutta method, Fourier analysis and mode energy analysis could be exploited which led to various phenomena in the classical FPU model, such as the equipartition and the spatial energy localization. In the meanwhile, the diatomic plasmonic chain also performs various astonishing features due to its distinctive spatial configuration to open up band gap in the dispersion relation. A finite one-dimensional diatomic chain having coated metal nanoparticles with alternatively changing separations was investigated. The coupled dipole equation together with quasistatic polarizability having radiation corrections suggested the existence of edge state localized at the two edges of the finite chain, which was then further verified by setting up a compatible simulation in Lumerical FDTD. Upon

implementing balanced gain/loss into the system, the diatomic plasmonic chain could be PT-symmetric by nature, which would eventually induce the disappearance of the extinction of the edge state supported by the chain. The aforesaid effect was examined through a precise formulation of the coupled dipole equation, and by simulations conducted in FDTD together with an analytic calculation using the multiple scattering theory (MST). Both results suggested that the zero extinction property was given by the perfect cancelation of the scattering and absorbing behaviour within the diatomic chain at the edge state frequency.

Acknowledgements

I would like to acknowledge the support of the Department of Applied Physics, The Hong Kong Polytechnic University, and in particular my supervisors Dr. K. H. Fung and Dr. C. H. Lam for their advices and supports in my study period.

Also I would like to give thanks to my colleagues, research-group members, especially Ling Chi Wai and Raymond Wu Pak Hong, who gives me a lot of ideas on my research work.

Table of contents

List of figures

2.3 (a) The displacement graph, with y-axis being the longitudinal displacement of the center of mass in terms of m and x-axis being the site number representing 10 discrete electron clouds along the one-dimensional plasmonic chain. (b) The velocity graph, with y-axis being the longitudinal velocity of the center of mass in terms of $\mathrm{m/s}$ and x-axis being the site number. The above figure is capped when time $= 3000/\omega_0$, i.e. 3×10^7 RK iterations.

2.4 (Color online) Time-domain simulation of the net dipole moment, with x-axis being the site number representing 10 discrete electron clouds, y-axis being the time in terms of s and z-axis being the dipole moment normalized by electron charge $e = 1.602 \times 10^{-19}\mathrm{C}$. This graph is in the early cutoff of the RK iterations. The small black dots indicate the corresponding dipole strength at each iteration. The colored surface formed by dots is for the purpose of a more distinguishable results along different sites in the chain. The most vigorous oscillation stays in site 1, 4, 7, and 10.

2.5 (Color online) The net dipole moment-time graph of the 9^{th} electron cloud along the plasmonic chain, i.e. site number = 9, with y-axis being the dipole moment normalized by $e = 1.602 \times 10^{-19}\mathrm{C}$ and x-axis being the time in terms of s. The program executed at around $5.5 \times 10^{-13}\mathrm{s}$ results in an execution of the dipole moment.

2.6 (Color online) (a) The net dipole moment-time graph of the 9^{th} electron cloud along the plasmonic chain, with $B = 1.25 \times 10^{-8}\mathrm{m}$. Note that the deep blue and light blue color in the graph is meaningless because it is related to a compression of large quantities of data points. (b) Time-domain simulation of the net dipole moment with respect to 10 electron clouds. Through the two figures, a quasi-linear behavior is observed.

2.7 (Color online) (a) The net dipole moment-time graph of the 9^{th} electron cloud along the plasmonic chain, with $B = 1.5 \times 10^{-8}$m. (b) Time-domain simulation of the net dipole moment with respect to 10 electron clouds. A nonlinear oscillation is observed after time $t = 1 \times 10^{-13}$s.

2.8 The total energy-time graph of the system using initial multiplying parameter $B = 0.5 \times 10^{-8}$m, having 10 sites along the one-dimensional array, using the 4^{th} eigenmode as initial configuration. The program executes at 3×10^{7} RK iterations, i.e. $t = 5.5 \times 10^{-13}$s.

2.9 Fourier transform of the dipole moment-time data of the 9^{th} electron cloud in the one-dimensional plasmonic chain using initial configuration of eigenvector corresponds to 4^{th} eigenfrequency and an initial multiplying parameter $B = 0.5 \times 10^{-8}$m. At spiky peak at 8.35×10^{14}Hz is observed.

2.10 Fourier transform of the dipole moment-time data of the 9^{th} electron cloud in the one-dimensional plasmonic chain using initial configuration of eigenvector corresponds to the 4^{th} eigenfrequency and an initial multiplying parameter $B = 1.0 \times 10^{-8}$m. A spiky peak at 8.33×10^{14}Hz is observed with the existence of small peaks from other frequencies.

2.11 (a) The pick off normalized displacement vector, with x-axis being the site number representing 512 discrete electron clouds along the one-dimensional plasmonic chain and y-axis being the normalized longitudinal displacement vector of the center of mass. Here the pick off displacement vector is of the 1^{st} eigenfrequency (fundamental mode). (b) The dispersion band of the 512 discrete eigenfrequencies, with x-axis being the mode number k, and y-axis being the eigenfrequency in terms of rad s^{-1}.

2.12 (Color online) (a) The net dipole profile right before program execute, with y-axis being the dipole moment normalized by $e = 1.602 \times 10^{-19}\mathrm{C}$ and x-axis being the site number representing 512 discrete electron clouds; Time-domain simulation of the net dipole moments on individual particle sites in a chain of $N = 512$ particles (b) and in a chain of $N = 10$ particles (c). Both cases are initially excited with the fundamental eigenmode, i.e., all dipole moments are almost in phase; nanoparticle radius $R = 5\mathrm{nm}$; lattice constant $a = 15\mathrm{nm}$; time step for RK-4 $dt = 10^{-4}/\omega_0$ while the displaying time step for the graph $dt' = 0.1/\omega_0$, and the resonance frequency $\omega_0 = 5.420 \times 10^{15}\mathrm{rad\ s^{-1}}$ (Au). For (c), the black dots indicate the corresponding dipole strength at each iteration. The colored surface formed by dots is for the purpose of a more distinguishable results along different sites in the chain. The data shown here is in an early cut off. While for (b), the dots are omitted and only the surface is displayed. The simulation stops at $t = 1.2307 \times 10^{-12}\mathrm{s}$.

2.13 (Color online) Energy indicating-time graph of the data set obtained in Fig. 2.12(b). An 'equipartition' is likely to be acquired as energy distributes along modes by symmetry. The energy here is with arbitrary unit as it is a comparative value for modes. Modes 2, 4, 6...etc. cannot be found in the graph as they have a comparatively zero energy with respect to the excited eigenmode.

3.1 Schematic figure of a one-dimensional coated diatomic plasmonic chain for which the above setup is assumed to be duplicated till infinite. There are two spherical dispersive metal nanoparticles with dielectric function ϵ_1 coated with non-dispersive dielectric of different permittivity ϵ_2 and ϵ_3 in one single unit cell having two sites, namely A and B. All coated nanoparticles are of the same size with outer radius b, inner radius a. The length of the unit cells and the separation between site A and site B are denoted as d and t respectively. There is also a dashed-line rectangle showing the unit cell of the one-dimensional diatomic chain. The chain is assumed to be embedded in a medium with relative permittivity $\epsilon_{\mathrm{m}} = 1$.

3.2 Schematic figure of a 'two-nanoparticles system' picking from the unit cell of the diatomic plasmonic chain. The distance between site A and B is denoted as r, site A and site B's nanoparticle is having dipole moment $\mathbf{p}_1$ and $\mathbf{p}_2$ respectively.

3.3 Band dispersion of a 1-D diatomic plasmonic chain using identical coated metal nanoparticles for both site A and site B, with x-axis being the wave vector $kd/2$ covering both the 1^{st} and 2^{nd} Brillouin zone, y-axis being the normalized plasma frequency ω/ω_p. It shows the longitudinal dispersion relation of the diatomic chain with $d = 57.1\mathrm{nm}$, $t = 34.3\mathrm{nm}$. Since there are two coated metal nanoparticles in one unit cell, two non-degenerated longitudinal bands are observed. A band gap ranging from $0.515\omega_p$ to $0.542\omega_p$ is observed as $t \neq d/2$ for a diatomic chain.

3.4 Plotting of $1/\min|\lambda|$ against normalized plasma frequency ω/ω_p for a one-dimensional diatomic plasmonic chain using identical coated metal nanoparticles for both site A and site B, with chain length $N = 32$. Results are obtained using quasistatic approximation and nearest neighbor approximation on Green's function, a quasistatic polarizability with core of coated nanoparticle described by lossless-Drude model. It shows the coupled longitudinal modes supported in the diatomic chain whenever a large quantity of $1/\min|\lambda|$ appears. The diatomic chain is with $d = 57.1\text{nm}$, $t = 34.3\text{nm}$. A band gap is observed in between $0.515\omega_p$ and $0.542\omega_p$, also a supported longitudinal mode is found in between the band gap at about $0.529\omega_p$, which should be the topological edge state as expected.

3.5 (Color online) Plotting of magnitude of the dipole moment p_n along the finite one-dimensional diatomic chain at three eigenstates suggested in Fig. 3.4. (a) Eigenstate below the band gap for $\omega = 0.515\omega_p$; (b) Eigenstate in between the band gap for $\omega = 0.529\omega_p$; (c) Eigenstate above the band gap for $\omega = 0.545\omega_p$; The blue line represents real part of the magnitude of the dipole moment, the orange line represents complex part. Fig. 3.5(b) verifies the supported mode found in between the band gap in Fig. 3.4 is an edge state having fields localized in two edges of the diatomic chain.

3.6 Plotting of $1/\min|\lambda|$ against normalized plasma frequency ω/ω_p for a one-dimensional diatomic plasmonic chain using identical coated metal nanoparticles for both site A and site B, with chain length $N = 32$. Results are obtained without using quasistatic approximation and nearest neighbor approximation on Green's function, a quasistatic polarizability with core of coated nanoparticle described by Drude model having loss $= 0.0001 \times \omega_p$. It shows the coupled longitudinal modes supported in the diatomic chain whenever a large quantity of $1/\min|\lambda|$ appears. The diatomic chain is with $d = 57.1\text{nm}$, $t = 34.3\text{nm}$. A band gap is observed in between $0.515\omega_p$ and $0.542\omega_p$, also a supported longitudinal mode is found in between the band gap at about $0.529\omega_p$, which should be the topological edge state as expected.

3.7 (Color online) Plotting of magnitude of the dipole moment p_n along the finite one-dimensional diatomic chain at three eigenstates suggested in Fig. 3.6. (a) Eigenstate below the band gap for $\omega = 0.515\omega_p$; (b) Eigenstate in between the band gap for $\omega = 0.529\omega_p$; (c) Eigenstate above the band gap for $\omega = 0.545\omega_p$; The blue line represents real part of the magnitude of the dipole moment, the orange line represents complex part. Fig. 3.7(b) verifies the supported mode found in between the band gap in Fig. 3.6 is an edge state having fields localized in two edges of the diatomic chain.

3.8 Illustration of the setup in FDTD simulation. We can see the diatomic chain is with configuration mentioned in Fig. 3.1. The two short dotted lines in the edge of the chain simply means you can pad the chain with more unit cells. The box with grey-colored dash-line denotes the TFSF source and must cover the entire chain. Inside the box it calculates the total field, while only scattered field will be calculated outside the box. The red arrow denotes the polarization direction (i.e. electric field oscillating along) and the blue arrow denotes the propagating direction.

3.9 Illustration of a general setup in calculating the extinction cross section of a cluster of scatters. The incident electric field is polarized along the chain axis, and propagates in the $\mathbf{k}_0$ direction. There will be excited dipole moment $\mathbf{p}_j$ on the j^{th} nanoparticles which having distance $\mathbf{r}_j$ from origin. The observing point has displacement $\mathbf{R}$ from origin and experiences the dipole electric field $\mathbf{E}_j$ generated by $\mathbf{p}_j$. From the figure, we know $\mathbf{n}_0 \cdot \mathbf{p}_j = 0$, $\mathbf{n}_0 \cdot \mathbf{r}_j =$ constant, $\mathbf{E}_0^* \cdot \mathbf{p}_j = E_0 p_j$.

3.10 Plotting of $1/\min|\lambda|$ against normalized plasma frequency ω/ω_p for a one-dimensional diatomic plasmonic chain using identical coated metal nanoparticles for both site A and site B, with chain length $N = 8$. Results are obtained using dynamic Green's function without nearest neighbor approximation, a quasistatic polarizability with core of coated nanoparticle described by Drude model having loss $= 0.0001 \times \omega_p$. It shows the coupled longitudinal modes supported in the diatomic chain whenever a large quantity of $1/\min|\lambda|$ appears. The diatomic chain is with $d = 57.1\text{nm}$, $t = 34.3\text{nm}$. The supported mode in the middle is at about $0.530\omega_p$, which is in between two other supported mode at about $0.515\omega_p$ and $0.546\omega_p$, are presumed to be the edge state and the range of band gap, respectively.

3.11 Analytic extinction cross section (in unit of $\lambda_p/8\pi^2 d^3$) of the one-dimensional diatomic plasmonic chain using identical coated metal nanoparticles for both site A and site B mentioned in Fig. 3.1, with chain length $N = 8$, against normalized plasma frequency ω/ω_p. The three peaks are at around $0.499\omega_p$, $0.515\omega_p$ and $0.530\omega_p$ such that they are all supported mode shown in Fig. 3.10 and are presumed to be coming from the lower band for the $0.499\omega_p$ and the $0.515\omega_p$ one, and an edge state for the $0.530\omega_p$ one. This figure tells the actual response of the diatomic chain among various frequencies.

3.12 (Color online) Cross sections (in unit of m^2) of the one-dimensional diatomic plasmonic chain using identical coated metal nanoparticles for both site A and site B mentioned in Fig. 3.1 using setup explained in Fig. 3.8, with chain length $N = 8$, against normalized plasma frequency ω/ω_p. The mesh in use is $1.5\mathrm{nm}$ within the TFSF source and the simulation time is long enough for a relevant Fourier-transform to take place. Extinction, absorption and scattering cross sections are plotted in different color. The three peaks are at around $0.476\omega_p$, $0.483\omega_p$ and $0.499\omega_p$ such that they are presumed to be the three excited mode shown in Fig 3.11 with slightly shifted frequencies coming from the lower band and the edge state.

3.13 (Color online) (a) The spatial magnitude profile of the dipole moments calculated analytically in the one-dimensional diatomic plasmonic chain with identical coated metal nanoparticles being the individuals, having chain length $N = 8$, at three different picked off frequencies described in Fig. 3.11, (i) $\omega = 0.499\omega_p$, (ii) $\omega = 0.515\omega_p$, (iii) $\omega = 0.530\omega_p$ such that it corresponds to the edge state. (b) The electric field profile obtained by setting the similar setup in FDTD using 2D field monitor to record the magnitude of E_x throughout the entire spatial distribution of the setup at three different picked off frequencies described in Fig. 3.12, (i) $\omega = 0.476\omega_p$, (ii) $\omega = 0.483\omega_p$, (iii) $\omega = 0.499\omega_p$. The mesh in use is $1.5\mathrm{nm}$. By comparing the magnitude of the dipole moments in (a) with the electric field profile in (b), one can justify the three peaks mentioned in Fig. 3.11 match those mentioned in Fig. 3.12 with Fig. 3.13(a.iii) and Fig. 3.13(b.iii) being the edge state.

3.14 Schematic figure of a PT-symmetric one-dimensional coated diatomic plasmonic chain. There are two spherical dispersive metal nanoparticles with dielectric function ϵ_1 coated with non-dispersive dielectrics of different permittivity ϵ_2 and $\epsilon_3 = \epsilon_2^*$ in one single unit cell having two sites, namely A and B. All coated nanoparticles are of the same size with outer radius b, inner radius a. The length of the unit cells and the separation between site A and site B are denoted as d and t respectively. The chain is assumed to be embedded in a medium with relative permittivity ϵ_m = 1. Also an illustration of defining origin in the diatomic chain having number of unit cells an odd number is shown.

3.15 Analytic extinction cross section (in unit of $\lambda_p/8\pi^2 d^3$) of the diatomic plasmonic chain using (a) identical coated metal nanoparticles and (b) coated nanoparticles with gain/loss dielectric shells alternatively, PT-symmetric; against normalized plasma frequency ω/ω_p are plotted for comparison. The two diatomic chains have chain length $N = 8$, with $d = 57.1\text{nm}$, $t = 34.3\text{nm}$, $b = 10\text{nm}$, $a = 7.14\text{nm}$, plasma collision frequencies for the cores are set to be $v_c = 0.0001\omega_p$. By comparing Fig. 3.15(a) and (b), we can see that at the edge state frequency $\omega = 0.530\omega_p$, the extinction cross section C_{ext} is significantly reduced and almost vanished when the system switches from a non-PT-symmetric one to a PT-symmetric one.

3.16 (Color online) The spatial magnitude profile of the excited dipole moments calculated analytically in the PT-symmetric diatomic plasmonic chain having chain length $N = 8$, at the edge state frequency $\omega = 0.530\omega_p$ found in non-PT-symmetric diatomic chain, see Fig. 3.11. The blue and orange line represent real and imaginary part of the excited dipole moments, respectively. The real part of the magnitude forms an even function of x while the imaginary part forms an odd function of x, most likely.

3.17 (Color online) Cross sections (in unit of m^2) of the PT-symmetric diatomic plasmonic chain using coated metal nanoparticles with setup mentioned in Fig. 3.14, with chain length $N = 8$, against normalized plasma frequency ω/ω_p. The mesh in use is 1.5nm within the TFSF source and the simulation time is short due to the divergence of electric field. Extinction, absorption and scattering cross sections are plotted in red, blue and green color respectively. The three peaks are at around $0.476\omega_p$, $0.483\omega_p$ and $0.499\omega_p$ such that they are presumed to be the three excited mode mentioned in Fig 3.15(b) with slightly shifted frequencies. The most right-hand side peak corresponds to the edge state and is of great fluctuation. The fluctuation mainly comes from the Fourier-transform as the simulation time is not long enough.

3.18 (Color online) (a) The spatial magnitude profile of the dipole moments calculated analytically in the PT-symmetric diatomic plasmonic chain with coated metal nanoparticles having setup mentioned in Fig. 3.14, adopting chain length $N = 8$, at three different picked off frequencies described in Fig. 3.15(b), (i) $\omega = 0.499\omega_p$, (ii) $\omega = 0.515\omega_p$, (iii) $\omega = 0.530\omega_p$ such that it corresponds to the edge state. (b) The electric field profile obtained by setting the similar setup in FDTD using 2D field monitor to record the magnitude of E_x throughout the entire spatial distribution of the setup at three different picked off frequencies described in Fig. 3.17, (i) $\omega = 0.476\omega_p$, (ii) $\omega = 0.483\omega_p$, (iii) $\omega = 0.499\omega_p$. The mesh in use is 1.5nm. By comparing the magnitude of the dipole moments in (a) with the electric field profile in (b), one can justify the three peaks mentioned in Fig. 3.15(b) match those mentioned in Fig. 3.17 with Fig. 3.18 (a.iii) and (b.iii) being the edge state with vanished extinction.

3.19 (Color online) (a) Cross sections (in unit of m^2) of the PT-symmetric diatomic plasmonic chain using coated metal nanoparticles with setup mentioned in Fig. 3.14, with chain length $N = 8$, against normalized plasma frequency ω/ω_p. The mesh in use is $1.5\mathrm{nm}$ within the TFSF source. The simulation time is doubled compare to the results obtained in Fig. 3.17. The field diverges as the peak at the resonant frequency of the edge state is having magnitude over 100times bigger than that in Fig. 3.17. The absorption cross section and scattering cross section seems like about to cancel each other to obtain a zero extinction cross section. (b) Plotting of the cross sections with the absorption cross section having a flipped sign, i.e. $-C_{\mathrm{abs}}$, it shows that the negative absorption cross section is almost the same as the scattering cross section, i.e. $-C_{\mathrm{abs}} = C_{\mathrm{sca}}$, and supposes to give a zero extinction at the edge state frequency $\omega = 0.499\omega_p$.

3.20 (Color online) Normalized cross sections of the diatomic plasmonic chain using (a) identical coated nanoparticles with no gain/loss in its dielectric shell, (b) coated nanoparticles with gain/loss dielectric shells alternatively, therefore PT-symmetric, against normalized plasma frequency ω/ω_p. The diatomic chain has chain length $N = 8$, with $d = 57.1\mathrm{nm}$, $t = 34.3\mathrm{nm}$, $b = 10\mathrm{nm}$, $a = 7.14\mathrm{nm}$, plasma collision frequencies for the cores are set to be $v_c = 0.0001\omega_p$. Absorption, scattering and extinction cross sections are plotted using red-dashed line, blue-dashed line and dark line respectively. The three peaks (include the 'vanished peak') is at around $0.493\omega_p$, $0.508\omega_p$ and $0.525\omega_p$. The non-PT-symmetric chain shares same resonant frequencies with the PT-symmetric one, which is of expected. Looking into the 'vanished extinction' of resonant state at the edge state frequency, it shows the cancelation effect of the absorption and scattering cross sections.

A.1 (Color online) Energy indicator-time graph of several modes, with y-axis being the energy-level indicator and the x-axis being the time. The plot stops at 6238 oscillations. Note that there does not have the plot of modes 1, 2, 4, 5, 6…etc. because those modes have comparatively zero energy with respect to the excited one. Also other than modes $3, 9, 15$, others are plotted with doted lines as they are not of interests. The denoted red spots pointed by yellow doted arrows are points picked, such that at those particular time, a specified mode is somewhat dominated. From left to right, we denotes the marked point as point $1, 2, 3 \ldots 7$ as it will be useful later.

A.2 The initial configuration of the normalized displacement vector corresponding to the 3^{rd} eigenmode, with x-axis being the site number representing 512 discrete electron clouds, y-axis being the normalized u. The 3 red arrows point at the 3 picked particular sites, which is the 128^{th}, 170^{th} and the 256^{th} one.

A.3 (Color online) (a) Using the 128^{th} eigenmode as the initial configuration, the energy indicator-time graph of several modes, with y-axis being the energy-level indicator and x-axis being the time, this system does not have the overlapping of electron cloud within the simulation time. (b) Using the 384^{th} eigenmode as the initial configuration, the energy indicator-time graph of several modes, with y-axis being the energy-level indicator and the x-axis being the time, the plot stops at 2487 oscillations as overlapping happens.

A.4 (Color online) Energy indicator-time graph of several modes using the 256^{th} eigenmode as the initial configuration, with y-axis being the energy-level indicator and the x-axis being the time, the plot stops at 594 oscillations.

A.5 Energy indicator-time graph of several modes using the 512^{th} eigenmode as the initial configuration, with y-axis being the energy-level indicator and the x-axis being the time, the plot stops at 547 oscillations.

List of tables

Chapter 1 Introduction

1.1 Electrodynamics in arrays of plasmonic nanoparticles

The immense flow of research in plasma started in 1879 after it was recognized as one of the four fundamental states of matter (others are solid, liquid and gas) by Sir William Crookes [1]. Plasma is generally described as a neutral medium consisting of unbound positive and negative particles, interacting each other through electromagnetic fields [2, 3]. Similar to the relationship between photons and electromagnetic vibrations, plasmon comes from the quantization of plasma oscillations, which is a collective oscillation of the free electron gas density with respect to its positive ion. Collective excitation of these plasma-like charge carries can exist in metal nanoparticles, especially at their surfaces. A chain of plasmonic nanoparticles with tunable setting can be considered as a kind of electromagnetic metamaterial which consists of meta-atoms. The meta-atoms here form an exacting structures with repeating patterns which poses desirable properties, such kind of artificial engineered material are called Metamaterial [4-6]. One-dimensional chain of plasmonic metal nanoparticles has been investigated intensively as it had been considered to be an extremely good intermediary for light confinement and wave guiding [7, 8]. Such an aggregation of the nanoparticles could allow some specified modes to propagate by the coupling between the localized plasmon among them, and is of great interest to study.

While we are studying the one-dimensional plasmonic chain and electromagnetic metamaterials, not only do we want to investigate the respective linear aspect as it has been studied in a number of publications [9-11], but also to perform the analysis in a nonlinear approach because of the needs of a desired nonlinear response, such that it could be found in the electromagnetic metamaterials compared to the conventional nonlinearity in natural materials recently [12]. Unlike the traditional researching approach, the rapid development in metamaterials has significantly enhanced the control of lights, which in turn has also reinforced the development of plasmonic devices in both linear and nonlinear regimes.

1.2 Overview on nonlinear metamaterials

The concept of nonlinear metamaterials was first introduced by three groups independently [13-15], and the publications on such topic have started growing since 2005. With the present of nonlinearity in the metamaterials, Shadrivov [20] suggested that it might lead to the creation of new families of waves known as solitons. Such solitons can be further classified into spatial solitons and temporal solitons [21]. Under the intense discussions, a wide range of nonlinear phenomena was discovered, yet the discussion on nonlinear plasmonics has just begun.

To get familiar with the nonlinear plasmonics, we have to first look into the nonlinear metamaterials. In the numerical perspective of the nonlinear metamaterials, Zeng et al. [16] suggested an alternative approach by analyzing the eigenmodes of the substrates, which appeared to be useful

in describing the resulting phenomena linearly. Furthermore, second harmonic generation (SHG) depends strongly on shape and symmetry of particles and their couplings. While the impact on the SHG by particle shape have been generally discussed in a few publications [17-19], the effect of their couplings is not well-understood. Since the nonlinear aspects of the one-dimensional plasmonic chain and the nonlinear coupling among plasmonic particles are of great interest to look at, we would provide a number of ways to analyze the one-dimensional nonlinear plasmonic chain by covering the theoretical aspects of the design and results in Chapter 2, and explaining various nonlinear phenomena in the field of nonlinear metamaterials.

1.3 FPU-model

Although the plasmonic chain is a kind of electromagnetic metamaterials, FPU model perhaps is the one that shares the largest similarity with the plasmonic chain if we treat the chain as a system of coupled resonators. Here the term 'resonator' simply represents the one as described in classical mechanics. As we are considering a one-dimensional nonlinear plasmonic chain with evenly separated plasmonic metal nanoparticles in Chapter 2, the interactions between the respective on-site electron cloud will result in an oscillating behavior like resonators. Although the mathematical equations are different, we will consider a situation where the nonlinear plasmonic would behave like an FPU model. In the following paragraphs, we will introduce the FPU model.

The FPU paradox, named after three scientists Fermi, Pasta and Ulam, consists of a chain of masses connected by springs with nonlinear components in the relation between deformation and restoring force. Fig. 1.1 shows a schematic picture of the nonlinear mass-spring system investigated by Fermi et al. If u_n denotes the displacement of the n^{th} mass from its original position in the longitudinal direction, and α denotes the nonlinear coefficient of the quadratic terms in the force between the neighboring sites and β denotes the nonlinear cubic term, a general FPU model were governed by the following equations:

$$\ddot{u_n} = (u_{n+1} + u_{n-1} - 2u_n) + \alpha[(u_{n+1} - u_n)^2 - (u_n - u_{n-1})^2], \quad (1.1)$$

$$\ddot{u_n} = (u_{n+1} + u_{n-1} - 2u_n) + \beta[(u_{n+1} - u_n)^3 - (u_n - u_{n-1})^3]. \quad (1.2)$$

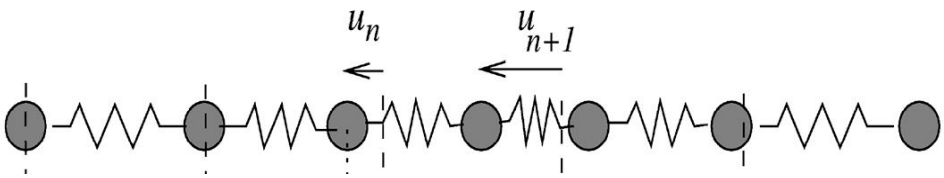

Figure 1.1: Schematic picture of the FPU model: masses that can move only in one dimension are coupled by nonlinear spring, u_n is the relative displacement with respect to the equilibrium position of the n^{th} mass in longitudinal direction.

The evenly separated one-dimensional nonlinear plasmonic chain in Chapter 2 can thus transform into a FPU model once the electron clouds and the electrostatic force between them are regarded as masses and nonlinear coupling springs respectively, where the masses in the FPU case are also resonators. Upon considering the classical FPU model, Fermi [22] expected that setting the system into motion in a way that all of the energy was initially in one of the normal mode of the linear system would lead to a state called equipartition, which energy was shared equally among all normal

modes. To the great surprise of Fermi, the equipartition did not take place, the energy was instead shared among few modes and then returned to the starting mode, known as the 'super-recurrence relation' [23]. In order to explain the 'FPU phenomenon', Zabusky and Kruskal [24] suggested the numerical integration of the Korteweg-de-Vries equation led to a generation of solitons emerged from the generic initial conditions and travelled through the media in 1965. In order to achieve the equipartition, Zabusky and Deem [25] were the first to consider putting energy into a high frequency mode. The numerical calculations later found that such a condition with large amplitude oscillation could lead to equipartition. Systematic studies summarized by Lichtenberg et al. [26] showed the existence of two thresholds; a transition from regular motion to weakly chaotic state with the dominance of regular motion within the first threshold, and a quick equipartition led by strong chaos in the second threshold. Besides the aforementioned, there are a lot of topics to be discussed in the area of FPU paradox: Metastability and the blow-up conditions [27, 28], questions on the dimension dependent, 'breathers and travelling breathers' [29], applicability of KAM theory [30], etc. Note that all these analyses were done by using the classical FPU model only, it is a worthy topic to study when such a system is being applied to the field of nonlinear plasmonic chain and perform the 'numerical experiments' to see how it will differ from the classical FPU model, which would be discussed in chapter 2.

1.4 Non-Hermitian one-dimensional diatomic plasmonic chain

In chapter 3, we switch our focus from the evenly separated

one-dimensional nonlinear plasmonic chain to a non-Hermitian diatomic plasmonic chain.

From the previous sections, we know the one-dimensional plasmonic chain had been put under extensive investigations and most of them were regarded as 'monatomic' chains, including the setup we mentioned in Chapter 2. The term 'monatomic' here implies the plasmonic chain is formed by uniformly spaced identical plasmonic nanoparticles, for which they are having one single plasmonic nanoparticle to be the unit cell. Now, we consider a dimer consisting of two plasmonic nanoparticles A and B (they might not be necessarily identical), and the dimer eventually linked together to form a one-dimensional chain. With this spatial configuration, the chain is known as a 'diatomic' chain as it has a dimer (2 nanoparticles, A and B) in its unit cell. This kind of configuration had an increasing significance recently owing to their possibility to have topological edge states, nonreciprocal bands and unidirectional wave propagations [44, 45]. In Chapter 3, we would like to consider a one-dimensional diatomic plasmonic chain with a unit cell dimer consisting of coated metal nanoparticles. Nanoparticles with coated layers could support astonishing phenomena such as parity-time (PT) symmetry phase transition and the gain or loss could be easily implemented into the system to consider the non-Hermitian aspects.

1.5 Overview on PT-symmetric system

In the late Chapter 3, efforts would be spent on a recent material

advancement which challenged the traditional conception of light-matter interaction, known as the parity-time (PT) symmetric media, using the configuration of one-dimensional coated diatomic plasmonic chain.

Over the years, intensive investigations on the Hermitian Hamiltonian systems are of great success because of the calculation on the allowed bands and forbidden gaps [31]. It was widely accepted in quantum mechanics that the physical observables are associated with the eigenvalues of Hermitian operators, which are real quantities in reality. For example, a Hamiltonian operator, $\widehat{H}$, has only real eigenvalues would result in a real energy spectrum. This feature is implied by that the Hamiltonian is Hermitian (self adjoint), i.e. $H^{+} = H$ [32]. In contrast, the so-called non-Hermitian system had far less attention until the late 1900's. When considering a non-Hermitian system, a ubiquitous configuration is adopting gain and loss and hence posing a non-Hermitian Hamiltonian. Bender and Boettcher were known as the first to introduce the idea of parity-time symmetry to study this kind of system in the approach of quantum field theory [33]. In this work they found that a broad family of non-Hermitian Hamiltonian could exhibit the entire real spectra and so as the real eigenvalues in the presence of PT (parity-time) symmetry. Indeed, the eigenvalues are purely real only below a certain critical threshold of those non-Hermiticity parameter [34], above which the eigenvalues will enter the complex plane such that the system undergoes a spontaneous PT-symmetry-breaking, materials will exhibit an increased gain and loss, results in entering a broken PT symmetry regime [33 ,35]. The point for which the eigenvalues transit from real to complex plane is known as the

'exceptional point' nowadays [36]. Such kind of phase transition is of great interest as it was unexpected to have same features with Hermitian systems under some circumstances.

Recently, PT-symmetry in optics has an area of intense study [38-43]. These include the band merging effects in PT-symmetric lattices [39], double refraction, power oscillation associated with dynamic beam evolution and unidirectional invisibility [40-42]. Also, optical solitons are being excited in the numerical calculation using nonlinear material having PT-systems [38], nonreciprocal wave propagation in combing PT-symmetry and nonlinearity [43].

1.5.1 *PT*-Symmetry

In the field of conventional quantum mechanics, a PT-symmetric system simply means that a non-Hermitian Hamiltonian theory having PT-symmetric condition imposed on the Hermitian Hamiltonian, that is, a PT-symmetric Hamiltonian should share the same eigenfunctions with the $\hat{P}\hat{T}$ operator, also:

$$\hat{P}\hat{T}\ \ \hat{H} = \hat{H}\ \ \hat{P}\hat{T}. \tag{1.3}$$

Here, the Hamiltonian $\hat{H}$ can be written as

$$\hat{H} = \hat{p}^2/m\ \ +\ \ V(\hat{x}), \tag{1.4}$$

$\hat{p}$ and $\hat{x}$ are the momentum operator and position operator respectively. The parity operator $\hat{P}$, whose effect is to make spatial inversion, and the time operator $\hat{T}$, which is a time reversal operator, i.e.

$$\hat{P}: \quad \hat{p} \to -\hat{p}, \quad \hat{x} \to -\hat{x}, \tag{1.5.1}$$

$$\hat{T}: \quad \hat{p} \to -\hat{p}, \quad \hat{x} \to -\hat{x}, \quad t \to -t. \tag{1.5.2}$$

To conclude, Bender and Boettcher demonstrated that a real spectra could be obtained if the Hamiltonian was PT-symmetric even it was non-Hermitian by itself, while entering a broken PT-phase (complex eigenspectrum) if it did not share the same eigenfunctions with the $\hat{P}\hat{T}$ operator. However, the PT-symmetry in optics was not witnessed until 2007. Recently, D. N. Christodoulides et al. suggested the possibility to observe the complex PT-symmetric effect within an optical framework [37-39]. A PT-symmetric system will guarantee Eq. (1.3) to be true and impose the Hamiltonian to commute with the $\hat{P}\hat{T}$ operator such that:

$$\hat{P}\hat{T} \;\; \hat{H} = \hat{p}^2/m + V^*(-\hat{x}), \tag{1.6}$$

$$\hat{H} \;\; \hat{P}\hat{T} = \hat{p}^2/m + V(\hat{x}). \tag{1.7}$$

Thus, Eq. (1.3) implies that:

$$V^*(-\hat{x}) = V(\hat{x}), \tag{1.8}$$

Eq. (1.8) basically gives constraint to the potential by stating that the real part of the potential must be an even function and the imaginary part must be an odd function, in terms of position x. Such a condition was then modified by D. N. Christodoulides et al. who postulated to include a symmetric index guiding and an anti-symmetric gain/loss profile in order to realize the PT-symmetric effect in optics [37]. Notice that such kind of gain profile cannot be obtained naturally in reality, but can be achieved by various way, such as two-wave mixing, etc. In general, by substituting wave propagation direction $\hat{z}$ to the time evolution term when dealing with the paraxial wave equation and Schrodinger equation, the refractive index plays

the role of potential in optics, rewrite Eq. (1.8), we have:

$$n^*(-\hat{x}) = n(\hat{x}), \tag{1.9}$$

$$\varepsilon^*(-\hat{x}) = \varepsilon(\hat{x}). \tag{1.10}$$

That is, if the real part of the refractive index profile is an even function of position x while the imaginary part is an odd function, light will propagate as if it undergoes a PT-symmetric potential, for which Eq. (1.9) and (1.10) are equivalent.

1.6 Objective

Owing to the extensive development in linear and nonlinear metamaterials which use plasmonic material as the 'building blocks', it is definitely a good starting point to give a closer look into the one-dimensional plasmonic chain first. In Chapter 2, we would like to first build up a model of a one-dimensional nonlinear plasmonic chain for which its nonlinearity comes from the Coulomb interaction of charges using Nearest Neighbour Approximation (NNA), then we would perform the linear analysis through linearization and solving eigenvalue-problem, and obtain the time-domain behaviour through the Runge-Kutta Method. Next, we would provide evaluation on Hamiltonian and the Fourier analysis to explain the nonlinear results. Finally, in the last part of Chapter 2, we would end up with the FPU approach on analysing the energy-indicator diagram and discussing the nonlinear localization and frequency conversion found in long finite chain system.

In Chapter 3, as aforementioned, we switched our focus to the

non-Hermitian PT-symmetric diatomic chain. Efforts would be spent on the verification of edge state in a one-dimensional coated diatomic plasmonic chain through coupled dipole equation and dynamic Green's function in the analytic approach, and also the realization on simulations of Finite-difference time-domain (FDTD) in the numerical approach, as FDTD is a powerful Maxwell solver in calculating the EM-waves. An interesting scattering phenomena [46] in the system would also be discussed, which was described as the zero extinction cross section of edge state in PT-symmetric coated diatomic plasmonic chain.

In the last chapter, an overall summary on the topic would be given.

Chapter 2 One-dimensional nonlinear plasmonic chain

2.1 Modelling

In order to investigate the plasmonic oscillation, we always consider a collective oscillation of the free electron gas density with respect to the positive ion. And inside the model world, we want to leave out as much of the complexity as we can. Therefore, we only consider a one-dimensional nonlinear plasmonic nanoparticle chain with equally-spaced nanoparticles of identical sizes. Through external electric field excitation, charges within nanoparticles oscillate, thus each of the nanoparticle can be characterized by a movable negatively charged electron cloud $(-q)$ and a fixed positive volume charge $(+q)$. To start with, we assume the positive volume charge having center of mass always fixed at the entries along the one-dimensional chain, while the negatively charged electron cloud are given a slightly push in direction parallel to the chain axis so as to undertake a back and forth oscillation (longitudinal motion) with respect to the overlapped positive volume charge and its movement is being affected by the neighbouring charges, see Fig. 2.1.

Here the displacing electron clouds form plasmonic oscillation, which gives energy to the system so that the electron cloud can gain a degree of freedom with respect to the positive ion.

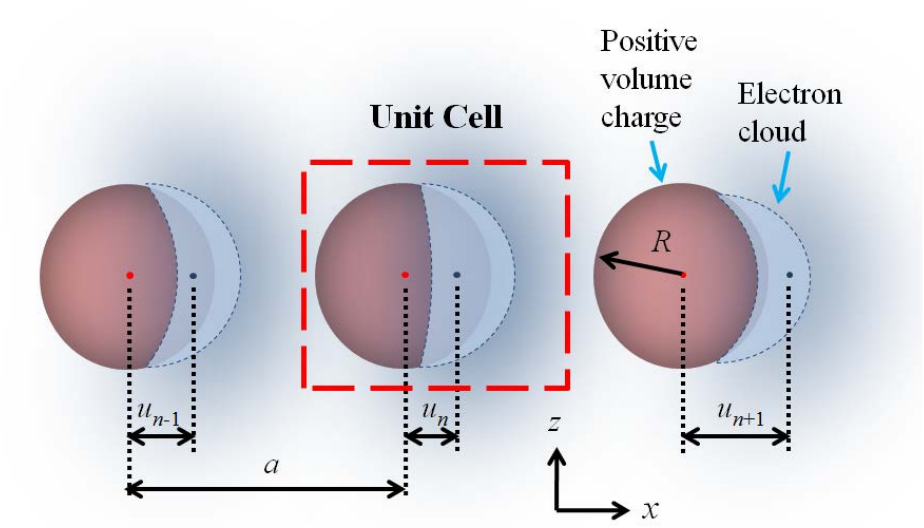

Figure 2.1: (Color online) Schematic of a nonlinear plasmonic nanoparticle chain with oscillating electron clouds. The chain contains fixed positive volume charge and movable negatively charged electron cloud in a unit cell, denoted by red solid spheres and blue semi-transparent clouds with dashed boundaries, respectively. All nanoparticles are of the same size with radius R, and the charges have centers of mass represented by the red/blue spots. The nanoparticles are separated by a fixed distance a. The electron cloud are assumed to be undertaken a longitudinal motion such that that the nth one has its center of mass displaced by u_n with respect to the center of mass of the nth positive volume charge along the chain axis x.

We assume the longitudinal motion of the n^{th} negatively charged electron cloud can be denoted by u_n, the displacement of center of mass with respect to the n^{th} positive volume charge (the displacement here does not state the particle oscillates, but describing an electron oscillation); the corresponding velocity and acceleration are defined as follow:

$$v_n = \frac{d}{dt}(u_n), \tag{2.1}$$

$$a_n = \frac{d}{dt}(v_n) = \frac{d^2}{dt^2}(u_n). \tag{2.2}$$

In the model world, the motion or say the trajectory of the n^{th} electron cloud is affected by the n^{th} positive volume charge, the $(n-1)^{\text{th}}$ positive volume charge/electron cloud, the $(n+1)^{\text{th}}$ positive volume charge/electron cloud. If we use all other parameters denoted in the past (separation = a, radius of nanoparticle = R, total charge in the electron cloud = $-q$), one can easily write down the equation of motion by considering the force exerting on the n^{th} negatively charged electron cloud, that is:

$$\begin{aligned} F = m\ddot{u_n} = -m\omega_0^2 u_n + \frac{q^2}{4\pi\varepsilon_0}\frac{1}{(a-u_n)^2} \\ - \frac{q^2}{4\pi\varepsilon_0}\frac{1}{(a+u_{n+1}-u_n)^2} - \frac{q^2}{4\pi\varepsilon_0}\frac{1}{(a+u_n)^2} \\ + \frac{q^2}{4\pi\varepsilon_0}\frac{1}{(a+u_n-u_{n-1})^2}, \end{aligned} \tag{2.3}$$

where in the right-hand side, the first term is the influence of the n^{th} positive volume charge, ω_0 is a constant such that it is obtained from the plasma frequency of the respective material and is directly proportional to the charge density. The terms later on are describing the influences of the adjacent positive volume charge and negatively charged electron cloud. Notice that the nonlinearity inside our equation of motion basically comes from the Coulomb interaction, that is, to assume the charged medium being a point charge. Back to the equation, we then divide m on each side:

$$\begin{aligned} \ddot{u_n} = -\omega_0^2 u_n + \frac{q^2}{4\pi\varepsilon_0 m}\frac{1}{(a-u_n)^2} - \frac{q^2}{4\pi\varepsilon_0 m}\frac{1}{(a+u_{n+1}-u_n)^2} \\ - \frac{q^2}{4\pi\varepsilon_0 m}\frac{1}{(a+u_n)^2} + \frac{q^2}{4\pi\varepsilon_0 m}\frac{1}{(a+u_n-u_{n-1})^2}. \end{aligned} \tag{2.4}$$

Since the problem is a plasmonic oscillation, we can do the following replacement:

$$\omega_0^2 R^3 = \frac{q^2}{4\pi\varepsilon_0 m}\left(= \frac{\omega_p^2 R^3}{3}\right), \tag{2.5}$$

$$\therefore \ddot{u_n} = -\omega_0^2 u_n + \omega_0^2 R^3 \left[\frac{1}{(a-u_n)^2} - \frac{1}{(a+u_{n+1}-u_n)^2} - \frac{1}{(a+u_n)^2} + \frac{1}{(a+u_n-u_{n-1})^2}\right], \tag{2.6}$$

where ω_p is the material plasma frequency which can be found by a given plasmon energy in terms of eV, take Au as an example. Assume Au has a plasmon energy 6.18eV, therefore:

$$\omega_p = \frac{6.18 \times 1.602 \times 10^{-19} \times 2\pi}{6.626 \times 10^{-34}} = 9.388 \times 10^{15}\text{rad s}^{-1}, \tag{2.7}$$

$$\omega_0 = \frac{\omega_p}{\sqrt{3}} = 5.420 \times 10^{15}\text{rad s}^{-1}. \tag{2.8}$$

The above equations imply that there will be a specific ω_0 corresponds to a specific material. Also, Eq. (2.6) is a useful equation of motion in computing the acceleration mentioned in Chapter 2.3.

But for now, in Eq. (2.6), we can see the only not unified term is the acceleration on the left-hand side, by making the following change:

$$\ddot{u_n} = -\omega^2 u_n, \tag{2.9}$$

where ω is the oscillating frequency of the whole system we are interested in, Eq. (2.6) will eventually turn into:

$$-\omega^2 u_n = -\omega_0^2 u_n + \omega_0^2 R^3 \left[\frac{1}{(a-u_n)^2} - \frac{1}{(a+u_{n+1}-u_n)^2} - \frac{1}{(a+u_n)^2} + \frac{1}{(a+u_n-u_{n-1})^2}\right]. \tag{2.10}$$

2.2 Linear analysis (Linearization & Eigenvalue-problem)

We first linearize the model by considering that x is small enough,

$$(1+x)^p \approx 1 + px. \tag{2.11}$$

In this case, we have

$$\frac{1}{(a-x)^2} \approx \frac{1}{a^2}\left(1 + 2\frac{x}{a}\right), \tag{2.12}$$

and

$$\frac{1}{(a+x)^2} \approx \frac{1}{a^2}\left(1 - 2\frac{x}{a}\right). \tag{2.13}$$

The above relation will then transform the complex equation of motion into a simple and solvable eigenvalue-problem, i.e. Eq. (2.10) will transform to:

$$\begin{aligned} -\omega^2 u_n = &-\omega_0^2 u_n \\ &+ \omega_0^2 R^3 \left[4\frac{u_n}{a^3} - 2\frac{u_n}{a^3} + 2\frac{u_{n-1}}{a^3} + 2\frac{u_{n+1}}{a^3} - 2\frac{u_n}{a^3}\right] \\ &= -\omega_0^2 u_n + \frac{2\omega_0^2 R^3}{a^3} u_{n-1} + \frac{2\omega_0^2 R^3}{a^3} u_{n+1}, \end{aligned} \tag{2.14}$$

which implies that:

$$\omega^2 u_n = \omega_0^2 u_n - \frac{2\omega_0^2 R^3}{a^3} u_{n-1} - \frac{2\omega_0^2 R^3}{a^3} u_{n+1}. \tag{2.15}$$

Indeed, we can now see the equation of motion of the n^{th} negatively charged electron cloud has transformed into a recurrence equation such that the n^{th} term depends on its $(n-1)^{\text{th}}$, n^{th} and $(n+1)^{\text{th}}$ terms.

Recall the form of an eigenvalue-problem,

$$\mathbf{A}\mathbf{v} = \lambda\mathbf{v}, \tag{2.16}$$

we rewrite Eq. (2.15) using the format of Eq. (2.16) and eventually get:

$$\mathbf{A}\begin{bmatrix} u_1 \\ \vdots \\ u_n \\ \vdots \end{bmatrix} = \omega^2 \begin{bmatrix} u_1 \\ \vdots \\ u_n \\ \vdots \end{bmatrix}, \tag{2.17}$$

where $\mathbf{A}$ is an $n \times n$ matrix having dimension depends on the number of charged nanoparticles in the one-dimensional plasmonic chain, and is defined by:

$$\mathbf{A} = \begin{bmatrix} \omega_0^2 & -\frac{2\omega_0^2 R^3}{a^3} & 0 & 0 & \cdots & 0 \\ -\frac{2\omega_0^2 R^3}{a^3} & \omega_0^2 & -\frac{2\omega_0^2 R^3}{a^3} & 0 & \cdots & 0 \\ 0 & -\frac{2\omega_0^2 R^3}{a^3} & \omega_0^2 & -\frac{2\omega_0^2 R^3}{a^3} & \cdots & 0 \\ \vdots & \ddots & \ddots & \ddots & \ddots & \vdots \\ \vdots & \ddots & 0 & -\frac{2\omega_0^2 R^3}{a^3} & \omega_0^2 & -\frac{2\omega_0^2 R^3}{a^3} \\ 0 & \cdots & \cdots & 0 & -\frac{2\omega_0^2 R^3}{a^3} & \omega_0^2 \end{bmatrix} \tag{2.18}$$

Here zero boundary condition is adopted as shown in Eq. (2.18), i.e. there will not be extra nanoparticles beyond two ends of the chain. Eq. (2.17) has a similar form with the eigenvalue-problem, where the square-root of the eigenvalue of matrix $\mathbf{A}$ is the oscillating frequency ω of the system, and its corresponding eigenvector is the displacement vector of the center of mass of the negatively charged electron cloud in the entire chain.

The main concept of this method is that, once we know the form of $\mathbf{A}$, we can get n discrete eigenvalues (ω^2) and n corresponding eigenvectors (displacement of the center of mass of the negatively charged electron cloud throughout the whole chain).

Here we use MATLAB as the simulation tool as it works with essentially one kind of object, a rectangular numerical matrix with possibly complex entries. To proceed, we first consider 10 nanoparticles in the chain (i.e. $n = 10$) and use Au as the material having natural resonant frequency $\omega_0 = 5.420 \times 10^{15}\text{rad s}^{-1}$; the nanoparticles are having the same size such that its radius $R = 5\text{nm}$ and are evenly separated by $a = 15\text{nm}$ initially.

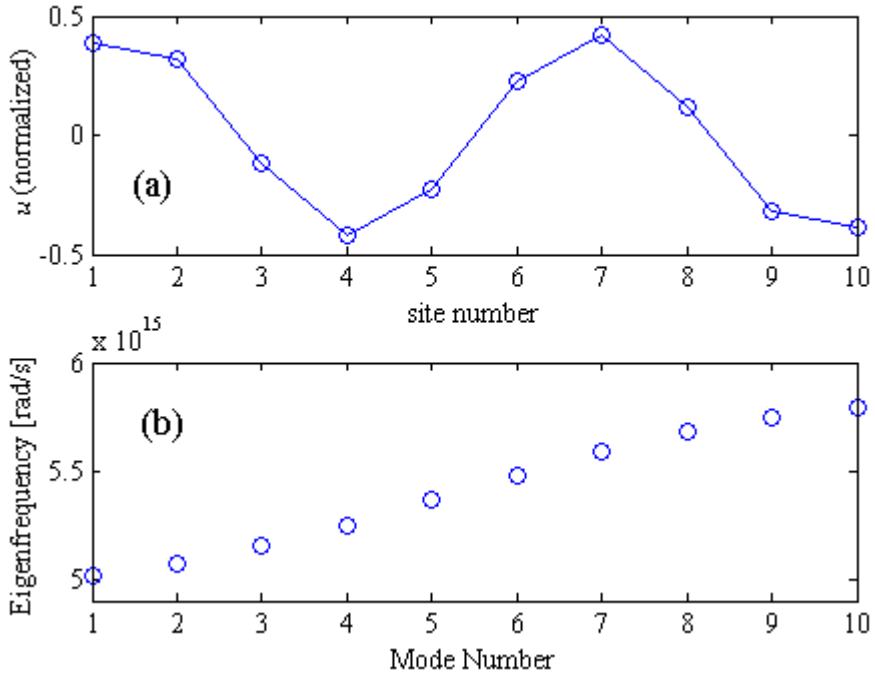

Figure 2.2: (a) The pick off normalized displacement vector, with x-axis being the site number representing 10 discrete electron clouds along the one-dimensional plasmonic chain, and y-axis being the normalized longitudinal displacement of the center of mass. Here the pick off eigenmode is at the 4^{th} eigenfrequency found in Fig. 2.2(b). (b) The dispersion band of the 10 discrete eigenfrequencies, with x-axis being the mode number k, and y-axis being the eigenfrequency in terms of rad s^{-1}.

The output is shown above, see Fig. 2.2. The graph is divided into 2

parts. Fig. 2.2(a) displays the eigenvector of the selected eigenfrequency, while Fig. 2.2(b) displays the dispersion band of the eigenfrequencies. This gives us a basic idea of how the system behave – if the oscillation is linear, there should exist 10 kinds of waveform correspond to those 10 eigenfrequencies, since $\mathbf{A}$ is a 10×10 matrix.

The outcome is of expectation since there are 10 discrete eigenfrequencies shown in Fig. 2.2(b), ranging from $5.0 \times 10^{15}\text{rad s}^{-1}$ to $5.8 \times 10^{15}\text{rad s}^{-1}$. It suggests that practically, the range of oscillating frequency when oscillating linearly should be about $0.9\omega_0$ to $1.1\omega_0$. Notice that the y-axis of Fig. 2.2(b) is in the unit of rad s^{-1} which shows the exact value of the eigenfrequencies. To obtain the ratio toward ω_0, one should over the value by the importing ω_0 initially, in this case it is 5.420×10^{15} rad s^{-1}. We can expect later on, when we consider about the time-domain simulations, the system will have its oscillation property depends on what initial condition of displacement vector is in used.

Trivially, if there are N sites in the chain, we will have N discrete normalized eigenvectors. Such a normalized eigenvector is useful for being an initial condition in next part by multiplying a factor B, which allows a considerable control on the inputting energy into the system, that is:

$$\mathbf{u}_0 = B \times \text{normalized mode} \begin{bmatrix} u_1 \\ \vdots \\ u_n \\ \vdots \end{bmatrix}, \tag{2.19}$$

for some value B, $\mathbf{u}_0$ is the collective displacement vector formed by u_i of the i^{th} negatively electron cloud describing initial condition.

2.3 Nonlinear analysis (Runge-Kutta Method)

From the previous section, what we get is 10 sets of eigenfrequencies with their corresponding initial displacement vectors (normalized eigenvector). In this part, we will try to examine its time domain behaviour by a method called Classical Runge-Kutta Method (RK-4).

The Classical Runge-Kutta Method, also known as 'RK4', is a useful mathematical tool in solving differential equations. The concept of RK4 is as follow:

We first have a differential equation of function y, with a known expression or value of the initial condition, that is:

$$\dot{y} = f(t, y), \qquad y(t_o) = y_o. \tag{2.20}$$

Instead of solving it analytically, we define a time step h, for each step size $h > 0$, RK4 states that:

$$\begin{cases} y_{n+1} = y_n + \frac{1}{6}h(k_1 + 2k_2 + 2k_3 + k_4) \\ t_{n+1} = t_n + h \\ k_1 = f(t_n, y_n) \\ k_2 = f\left(t_n + \frac{1}{2}h, y_n + \frac{h}{2}k_1\right) \\ k_3 = f\left(t_n + \frac{1}{2}h, y_n + \frac{h}{2}k_2\right) \\ k_4 = f(t_n + h, y_n + hk_3) \end{cases}, \tag{2.21}$$

for $n = 0, 1, 2, 3 \ldots\ldots$

When we considering the nonlinear oscillation of electron cloud with respect to a fixed positive volume charge, the relation between

displacement vector, velocity vector and acceleration vector is always a differential equation with EM components. Knowing that such differential equations are difficult to solve, RK4 gives an alternative way to obtain the answer y respect to time t without solving the differential equation but doing iteration against time t instead. By using this method, the time corresponding displacement vector, velocity vector and acceleration vector of plasmonic oscillation can be found easily.

In order to use RK4, there are three things to fulfil. First, we must have a known form of $\dot{y} = f(t, y)$. Second, a known initial condition for $y(t_o) = y_o$ is needed. Finally, we have to define a suitable time step h.

We first apply the RK4 on the displacement vector $\mathbf{u}$ and velocity vector $\mathbf{v}$ of the one-dimensional plasmonic chain simultaneously. Using the form of Eq. (2.20), we have:

$$\begin{cases} \dfrac{d\mathbf{u}}{dt} = \mathbf{v}, & \dot{\mathbf{u}} = \mathbf{v} = \mathbf{f}(t_n, \mathbf{u}_n), \\ \dfrac{d\mathbf{v}}{dt} = \mathbf{a}, & \dot{\mathbf{v}} = \mathbf{a} = \mathbf{f}(t_n, \mathbf{v}_n), \\ \text{define } h = \text{interval of one iteration} = dt, \end{cases} \tag{2.22}$$

to proceed, we then write down the iteration equations. Using the form of Eq. (2.21), iteration equations of displacement vector:

$$\begin{cases} \mathbf{u}_{n+1} = \mathbf{u}_n + \dfrac{1}{6}h(\mathbf{m}_1 + 2\mathbf{m}_2 + 2\mathbf{m}_3 + \mathbf{m}_4) \\ \mathbf{m}_1 = \mathbf{f}(t_n, \mathbf{u}_n) \\ \mathbf{m}_2 = \mathbf{f}\left(t_n + \dfrac{1}{2}h, \mathbf{u}_n + \dfrac{h}{2}\mathbf{m}_1\right) \\ \mathbf{m}_3 = \mathbf{f}\left(t_n + \dfrac{1}{2}h, \mathbf{u}_n + \dfrac{h}{2}\mathbf{m}_2\right) \\ \mathbf{m}_4 = \mathbf{f}(t_n + h, \mathbf{u}_n + h\mathbf{m}_3) \end{cases}, \tag{2.23}$$

for $n = 0, 1, 2, 3 \ldots\ldots$

Iteration equations of velocity vector:

$$\begin{cases} \mathbf{v}_{n+1} = \mathbf{v}_n + \frac{1}{6}h(\mathbf{k}_1 + 2\mathbf{k}_2 + 2\mathbf{k}_3 + \mathbf{k}_4) \\ \mathbf{k}_1 = \mathbf{f}(t_n, \mathbf{v}_n) \\ \mathbf{k}_2 = \mathbf{f}\left(t_n + \frac{1}{2}h, \mathbf{v}_n + \frac{h}{2}\mathbf{k}_1\right) \\ \mathbf{k}_3 = \mathbf{f}\left(t_n + \frac{1}{2}h, \mathbf{v}_n + \frac{h}{2}\mathbf{k}_2\right) \\ \mathbf{k}_4 = \mathbf{f}(t_n + h, \mathbf{v}_n + h\mathbf{k}_3) \end{cases}, \qquad (2.24)$$

for $n = 0, 1, 2, 3 \ldots\ldots$

Indeed, the concept of RK4 is to divide each time step h into 4 parts, $\mathbf{m}_1$, $\mathbf{k}_1$ represent the change of first small increment, $\mathbf{m}_2$, $\mathbf{k}_2$ represent the change of second small increment…etc. And each iteration equals to different proportion of those four increments. In the next part, I will evaluate the first iteration deeply.

Here, let us look at the table of $\mathbf{u}$, $\mathbf{v}$, $\mathbf{a}$ in first iteration:

Table 2.1: Illustration of displacement vector, velocity vector and acceleration vector in first time step of iterations of RK4.

Time: 0 → h	**u**	**v**	**a**
1st increment	$\mathbf{u}_0$	$\mathbf{v}_0$	$\mathbf{a}_0$
2nd increment	unknown	unknown	$\mathbf{a}_1$
3rd increment	unknown	unknown	$\mathbf{a}_2$
4th increment	unknown	unknown	$\mathbf{a}_3$

Note that we only have $\mathbf{u}_0$ from the previous part and assume $\mathbf{v}_0$ equals 0, also we assume we can compute the value of acceleration at any time by some sort of equations. Throughout the first iteration,

$$\begin{cases} \mathbf{u}_1 = \mathbf{u}_0 + \dfrac{1}{6}h(\mathbf{m}_1 + 2\mathbf{m}_2 + 2\mathbf{m}_3 + \mathbf{m}_4) \\ \mathbf{m}_1 = \mathbf{f}(t_0, \mathbf{u}_0) = \mathbf{v}_0 \\ \mathbf{m}_2 = \mathbf{f}\left(t_0 + \dfrac{\mathrm{d}t}{2}, \mathbf{u}_0 + \dfrac{\mathrm{d}t}{2}\mathbf{m}_1\right) = \mathbf{v} \text{ at } 2^{\text{nd}} \text{ increment} = \mathbf{v}_0 + 0.5 \times \mathrm{d}t \times \mathbf{a}_0. \\ \mathbf{m}_3 = \mathbf{f}\left(t_0 + \dfrac{\mathrm{d}t}{2}, \mathbf{u}_0 + \dfrac{\mathrm{d}t}{2}\mathbf{m}_2\right) = \mathbf{v} \text{ at } 3^{\text{rd}} \text{ increment} = \mathbf{v}_0 + 0.5 \times \mathrm{d}t \times \mathbf{a}_1 \\ \mathbf{m}_4 = \mathbf{f}(t_0 + \mathrm{d}t, \mathbf{u}_0 + \mathrm{d}t \times \mathbf{m}_3) = \mathbf{v} \text{ at } 4^{\text{th}} \text{ increment} = \mathbf{v}_0 + \mathrm{d}t \times \mathbf{a}_2 \end{cases} \tag{2.25}$$

Here we obtain the expressions of velocity at different increments in the set of iteration equations of velocity vector as shown below,

$$\begin{cases} \mathbf{v}_1 = \mathbf{v}_0 + \dfrac{1}{6}h(\mathbf{k}_1 + 2\mathbf{k}_2 + 2\mathbf{k}_3 + \mathbf{k}_4) \\ \mathbf{k}_1 = \mathbf{f}(t_0, \mathbf{v}_0) = \mathbf{a}_0 \\ \mathbf{k}_2 = \mathbf{f}\left(t_0 + \dfrac{\mathrm{d}t}{2}, \mathbf{v}_0 + \dfrac{\mathrm{d}t}{2}\mathbf{k}_1\right) = \mathbf{a} \text{ at } 2^{\text{nd}} \text{ increment} = \mathbf{a}_1 . \\ \mathbf{k}_3 = \mathbf{f}\left(t_0 + \dfrac{\mathrm{d}t}{2}, \mathbf{v}_0 + \dfrac{\mathrm{d}t}{2}\mathbf{k}_2\right) = \mathbf{a} \text{ at } 3^{\text{rd}} \text{ increment} = \mathbf{a}_2 \\ \mathbf{k}_4 = \mathbf{f}(t_0 + \mathrm{d}t, \mathbf{v}_0 + \mathrm{d}t \times \mathbf{k}_3) = \mathbf{a} \text{ at } 4^{\text{th}} \text{ increment} = \mathbf{a}_3 \end{cases} \tag{2.26}$$

By the above equations, we can now complete the first iteration.

Table 2.2: Complete form of displacement vector, velocity vector and acceleration vector in first time step of iterations of RK4.

Time: $0 \rightarrow$ h	$\mathbf{u}$	$\mathbf{v}$	$\mathbf{a}$
1st increment	$\mathbf{u}_0$	$\mathbf{v}_0$	$\mathbf{a}_0$
2nd increment	$\mathbf{u}_0 + \dfrac{\mathrm{d}t}{2}\mathbf{m}_1$	$\mathbf{v}_0 + \dfrac{\mathrm{d}t}{2}\mathbf{k}_1$	$\mathbf{a}_1$
3rd increment	$\mathbf{u}_0 + \dfrac{\mathrm{d}t}{2}\mathbf{m}_2$	$\mathbf{v}_0 + \dfrac{\mathrm{d}t}{2}\mathbf{k}_2$	$\mathbf{a}_2$
4th increment	$\mathbf{u}_0 + \mathrm{d}t \times \mathbf{m}_3$	$\mathbf{v}_0 + \mathrm{d}t \times \mathbf{k}_3$	$\mathbf{a}_3$

We have the initial conditions of $\mathbf{u}$ & $\mathbf{v}$, the remaining part is to write down the expression of acceleration at any time and compute it.

Recalling Eq. (2.6) in Chapter 2.1,

$$\ddot{u_n} = -\omega_0^2 u_n + \omega_0^2 R^3 \left[\frac{1}{(a-u_n)^2} - \frac{1}{(a+u_{n+1}-u_n)^2} - \frac{1}{(a+u_n)^2} + \frac{1}{(a+u_n-u_{n-1})^2}\right] - \gamma \dot{u}, \tag{2.27}$$

note that the equation is not exactly the same with Eq. (2.6) as there is a linear damping term in the above equation. By applying the above equation to each of the nanoparticles in the chain, the corresponding acceleration vector $\mathbf{a}$ at any moment can be computed. Also the existence of damping term may help the realization of exceptional point in Chapter 3 as it may lead to certain gain and loss in this system.

Therefore, with a known initial $\mathbf{u}_0$, $\mathbf{v}_0$, and the time dependent acceleration of every single negatively charged electron cloud, one can use RK4 to simulate the $\mathbf{u}$ and $\mathbf{v}$ at any time. Also, taking advantages of $\mathbf{u}$ a vector describing displacement vectors of the centers of mass of the negatively charged electron clouds, the corresponding vector for dipole moment $\mathbf{p}$ can be computed easily by the following equation:

$$\mathbf{p} = -|Q| \cdot \mathbf{u}, \tag{2.28}$$

where Q is describing the total charge in an electron cloud and can be found by rewriting Eq. (2.5):

$$\omega_0^2 R^3 = \frac{(N \cdot q_e)^2}{4\pi\varepsilon_0 (N \cdot m_e)}, \tag{2.29}$$

where N represents the number of electrons in the electron cloud and q_e represents charge of one single electron. As long as we fixed the material in used, a fixed ω_0; the number of electrons in the electron cloud N can be deduced by Eq. (2.29), and so as the total charge $Q = N \cdot q_e$.

Again, we use MATLAB to simulate the solutions by setting the following parameter. We use the configuration (displacement vector of center of mass) of the 4^{th} eigenmode as an initial condition, the factor multiplying on the normalized eigenvector is set by $B = 0.5 \times 10^{-8}\text{m}$, the time step, also known as interval for one iteration in RK-4 is defined by $\text{d}t = 10^{-4}/\omega_0(\text{s})$ and we assume there is no linear damping effect within each of the nanoparticles, i.e. $\gamma = 0.0 \times \omega_0$.

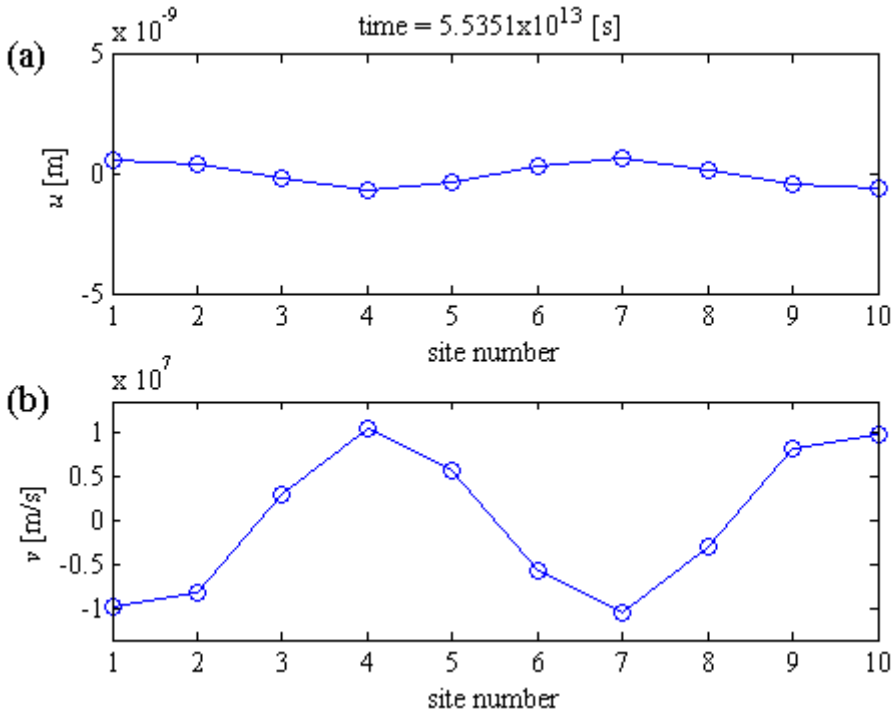

Figure 2.3: (a) The displacement graph, with y-axis being the longitudinal displacement of the center of mass in terms of m and x-axis being the site number representing 10 discrete electron clouds along the one-dimensional plasmonic chain. (b) The velocity graph, with y-axis being the longitudinal velocity of the center of mass in terms of m/s and x-axis being the site number. The above figure is capped when time $= 3000/\omega_0$, i.e. 3×10^7 RK iterations.

With suitable syntax in MATLAB, the program gives a moving figure to show how the displacement vector and velocity vector of n discrete negatively charged electron clouds varies with time, see Fig. 2.3 a snapshot. Also a 3D-surface plot can be generated for the investigation of all the net dipole moments on individual particle sites along the plasmonic chain over time, see Fig. 2.4.

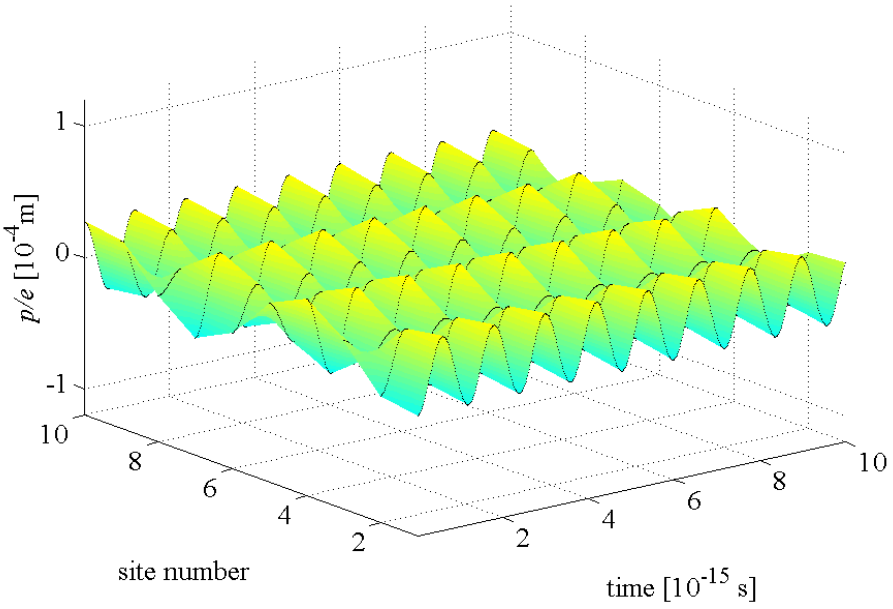

Figure 2.4: (Color online) Time-domain simulation of the net dipole moment, with x-axis being the site number representing 10 discrete electron clouds, y-axis being the time in terms of s and z-axis being the dipole moment normalized by electron charge $e = 1.602 \times 10^{-19}$C. This graph is in the early cutoff of the RK iterations. The small black dots indicate the corresponding dipole strength at each iteration. The colored surface formed by dots is for the purpose of a more distinguishable results along different sites in the chain. The most vigorous oscillation stays in site 1, 4, 7, and 10.

According to the observation of whole process, when $B = 0.5 \times$

10^{-8}m, the system kept oscillating with the form of initial condition, see Fig. 2.3(a), which is similar to the result predicted in Chapter 2.2, we can thus conclude that the system is behaving linearly, and assume it will behave the same as time goes beyond 5.5351×10^{13}s since there is no tendency of such system to run into chaotic behavior. Indeed, the periodicity of such a linear system can be seen clearly in Fig. 2.4.

In the above figure, what we concern is the periodicity. It can be seen that all electron clouds share a high degree of linearity by having a time-translating behavior. In order to have the nonlinear oscillation, some parameters have to be changed.

Theoretically, a lot of parameters can be changed, such as the radius of nanoparticle R, the separation a between them, original driver frequency ω_0, initial displacement vector $\mathbf{u_0}$ in used…etc. Here we choose to change the magnitude of driver, which is denoted as B as shown in Eq. (2.19), since it can be easily done by adjusting the energy input in the system. In order to demonstrate the existence of the nonlinearity in the system, we also compute the net dipole moment-time graph of one particular electron cloud later.

We start the investigation of the net dipole moment-time graph of one particular electron cloud by using an initial value $B = 0.5 \times 10^{-8}$m, and gradually tune up the value of B with investigation on that particular electron cloud repeatedly. Here we randomly picked the 9^{th} electron cloud to study its dipole moment-time graph, i.e. site number $= 9$.

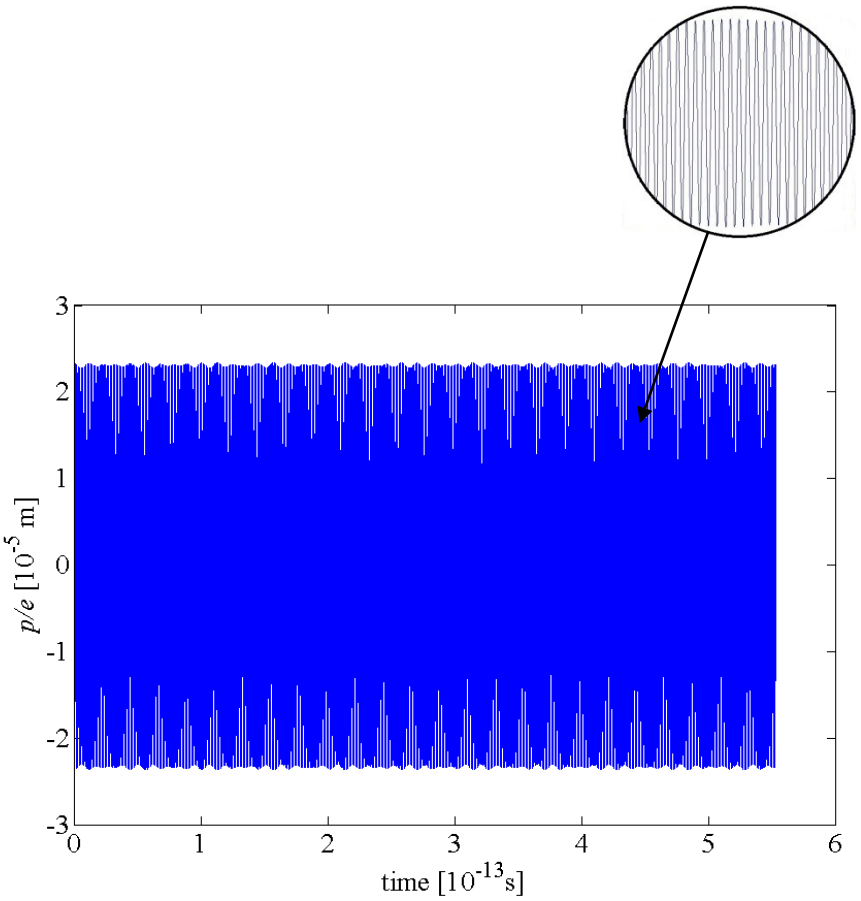

Figure 2.5: (Color online) The net dipole moment-time graph of the 9^{th} electron cloud along the plasmonic chain, i.e. site number = 9, with y-axis being the dipole moment normalized by $e = 1.602 \times 10^{-19}\text{C}$ and x-axis being the time in terms of s. The program executed at around $5.5 \times 10^{-13}\text{s}$ results in an execution of the dipole moment.

Once again, the resulting Fig. 2.5 verifies that the system behave almost linearly. The net dipole moment-time graph of the 9^{th} electron cloud, see Fig. 2.5, shows that the electron cloud is oscillating at a constant frequency and a relatively constant amplitude. Note that the two different colors (dark blue/light blue) found in the graph are meaningless as it indicates the data points are closely packed together, a magnification of

small fraction of the oscillation is shown on the top side of the dipole moment-time graph for clarification.

And by Fig. 2.4, it shows that the whole system (the 10 electron clouds) is oscillating linearly. This can be proved by steady oscillation shown in the spectrum, as it is predictable such that we give the system an initial condition with respect to the 4^{th} eigenfrequency, the energy kept allocating at those sites as the initial condition does if the oscillation stays in linear regime.

Among raising B, in Fig. 2.6(a), we observe the nonlinear part in Eq. (2.27) becomes more significant than the previous case, due to the increase of B, from $0.5 \times 10^{-8}\text{m}$ to $1.25 \times 10^{-8}\text{m}$. Combing the net dipole moment-time graph and the 3D-surface plot in Fig. 2.6(b), it shows a quasi-linear behavior. The quasi-linear behavior is observed through investigation in Fig. 2.6(a), which shows that the starting part ($t = 0\text{s}$ to $t = 1 \times 10^{-13}\text{s}$) and the ending part ($t = 4 \times 10^{-13}\text{s}$ to $t = 5 \times 10^{-13}\text{s}$) are relatively linear while the middle part ($t = 1 \times 10^{-13}\text{s}$ to $t = 4 \times 10^{-13}\text{s}$) shows a vigorous oscillation. Such kind of 'ABA' (A=linear, B=nonlinear) oscillating format is expected to repeat itself as time goes beyond.

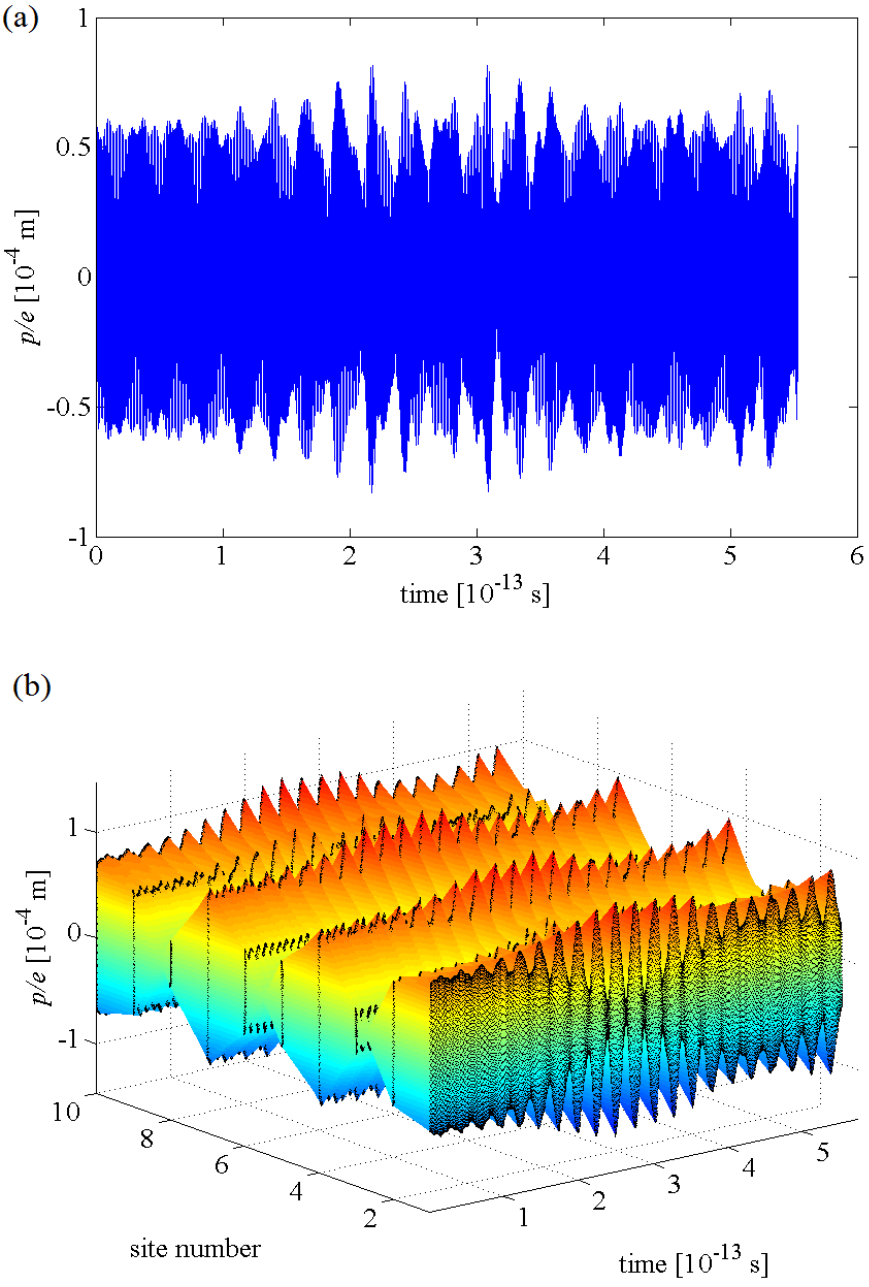

Figure 2.6: (Color online) (a) The net dipole moment-time graph of the 9^{th} electron cloud along the plasmonic chain, with $B = 1.25 \times 10^{-8}$m. Note that the deep blue and light blue color in the graph is meaningless because it is related to a compression of large quantities of data points. (b) Time-domain simulation of the net dipole moment with respect to 10 electron clouds. Through the two figures, a quasi-linear behavior is observed.

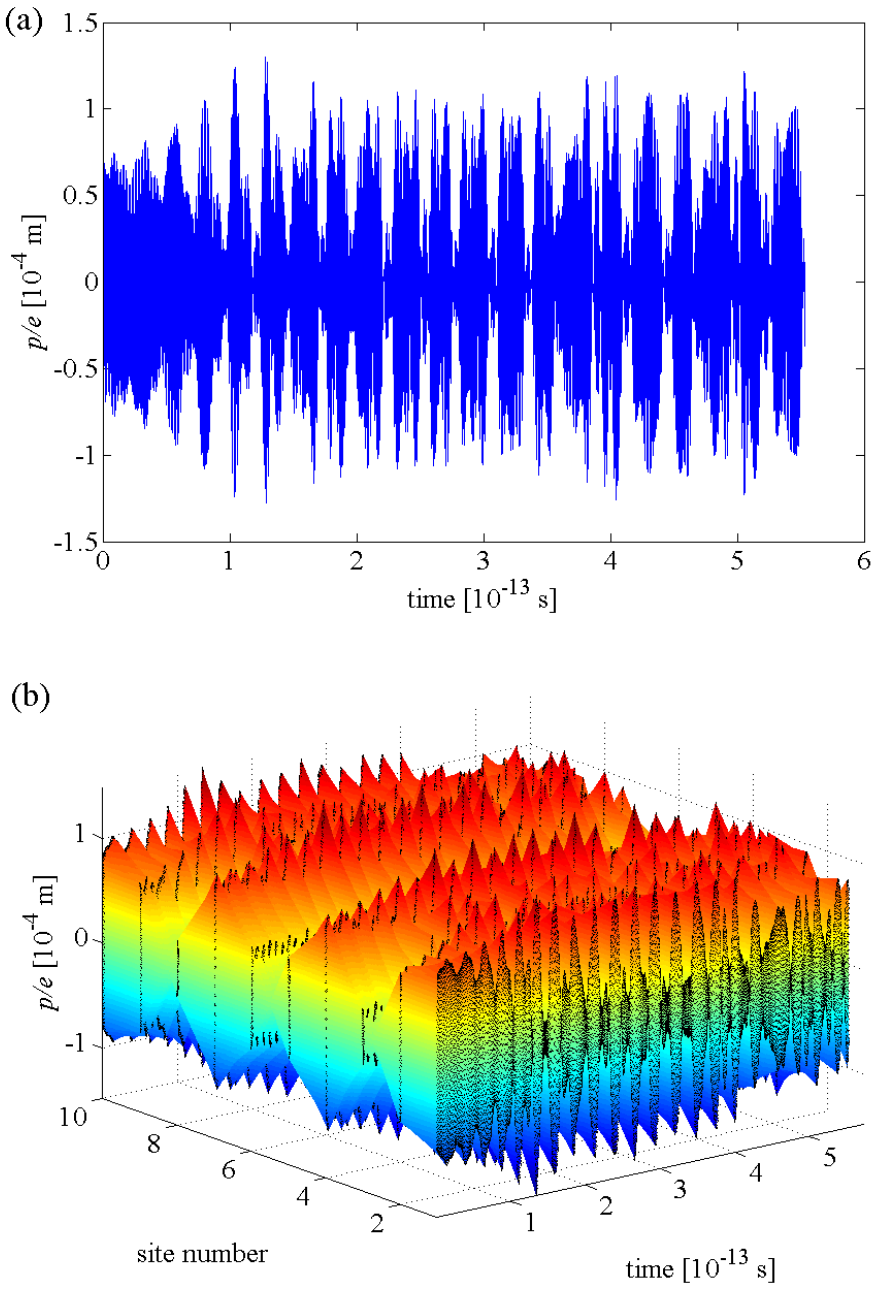

Figure 2.7: (Color online) (a) The net dipole moment-time graph of the 9^{th} electron cloud along the plasmonic chain, with $B = 1.5 \times 10^{-8}$m. (b) Time-domain simulation of the net dipole moment with respect to 10 electron clouds. A nonlinear oscillation is observed after time $t = 1 \times 10^{-13}$s.

Among further increasing the parameter B, from 1.25×10^{-8}m to 1.5×10^{-8}m, the nonlinear terms seems like to become uncontrollable after an approximated time $t = 1 \times 10^{-13}$s, the quasi-linear behaviour turns into a total nonlinear oscillation, for which the nonlinear effect dominates the whole system.

2.4 Hamiltonian and Fourier Analysis

In order to understand the reason behind the quasi-linear behaviour and the total nonlinear behaviour, one way is to look into the Hamiltonian of the system. Recall Eq. (2.10) in Chapter 2.1.

$$\ddot{u_n} = -\omega_0^2 u_n + \omega_0^2 R^3 \left[\frac{1}{(a-u_n)^2} - \frac{1}{(a+u_{n+1}-u_n)^2} - \frac{1}{(a+u_n)^2} + \frac{1}{(a+u_n-u_{n-1})^2}\right],$$

while we generalized it,

$$\ddot{u_n} + f(u) = 0, \tag{2.30}$$

integrate both side, the generalized equation becomes,

$$\dot{u_n}/2 + F(u) = H, \tag{2.31}$$

that is,

$$E_{\mathrm{k}} + E_{\mathrm{p}} = \text{Hamiltonian(Total Energy)}. \tag{2.32}$$

Assume there are 10 sites along the plasmonic chain which gives the expression below:

$$E_{\mathrm{k}} = \sum_{n=1}^{10} \frac{1}{2} v_n^2, \tag{2.33}$$

$$\begin{aligned}&\text{Onsite linear } E_{\mathrm{p}}\\&= E_{\mathrm{p}} \text{ due to the } n^{\mathrm{th}} \text{ positive volume charge}\\&= \text{integrate}[\omega_0^2 u_n] = \sum_{n=1}^{10} \frac{1}{2}\omega_0^2 u_n^2,\end{aligned} \tag{2.34.1}$$

$$\begin{aligned}&\text{Onsite nonlinear } E_{\mathrm{p}}\\&= E_{\mathrm{p}} \text{ due to } (n+1)^{\mathrm{th}} \text{ \& } (n-1)^{\mathrm{th}} \text{ positive charge}\\&= \text{integrate}\left\{\omega_0^2 R^3 \left[\frac{1}{(a+u_n)^2} - \frac{1}{(a-u_n)^2}\right]\right\}\\&= \sum_{n=1}^{10} \omega_0^2 R^3 \left(-\frac{1}{a+u_n} - \frac{1}{a-u_n} + \frac{2}{a}\right),\end{aligned} \tag{2.34.2}$$

$$\begin{aligned}&\text{Coupling } E_{\mathrm{p}}\\&= E_{\mathrm{p}} \text{ due to } (n+1)^{\mathrm{th}} \text{ \& } (n-1)^{\mathrm{th}} \text{ negative charge}\\&= \text{integrate}\left\{\omega_0^2 R^3 \left[\frac{1}{(a+u_{n+1}-u_n)^2} - \frac{1}{(a+u_n-u_{n-1})^2}\right]\right\},\end{aligned}$$

alternatively, we want some expression C for coupling E_{p} such that,

$$\begin{aligned}&\left(\frac{\partial}{\partial u_1} + \frac{\partial}{\partial u_2} + \frac{\partial}{\partial u_3} + \cdots + \frac{\partial}{\partial u_9} + \frac{\partial}{\partial u_{10}}\right) \cdot C\\&\qquad = \omega_0^2 R^3 \left[\frac{1}{(a+u_{n+1}-u_n)^2} - \frac{1}{(a+u_n-u_{n-1})^2}\right],\end{aligned}$$

for $n = 1, 2, \ldots, 10$.

$$\begin{aligned}\therefore C &= \omega_0^2 R^3 \left(\frac{1}{a+u_1} - \frac{1}{a}\right)\\&\quad + \sum_{n=2}^{10} \omega_0^2 R^3 \left(\frac{1}{a+u_n-u_{n-1}} - \frac{1}{a}\right) + \omega_0^2 R^3 \left(\frac{1}{a-u_{10}} - \frac{1}{a}\right).\end{aligned}$$

We will try to verify the expression of C below,

$$\left(\frac{\partial}{\partial u_1}+\frac{\partial}{\partial u_2}+\frac{\partial}{\partial u_3}+\cdots+\frac{\partial}{\partial u_9}+\frac{\partial}{\partial u_{10}}\right)\cdot C$$

$$\begin{aligned}
&= -\omega_0^2R^3\left[\frac{1}{(a+u_1)^2}\right]+\omega_0^2R^3\left[\frac{1}{(a+u_2-u_1)^2}\right]-\omega_0^2R^3\left[\frac{1}{(a+u_2-u_1)^2}\right]\\
&\quad+\omega_0^2R^3\left[\frac{1}{(a+u_3-u_2)^2}\right]-\omega_0^2R^3\left[\frac{1}{(a+u_3-u_2)^2}\right]\\
&\quad+\omega_0^2R^3\left[\frac{1}{(a+u_4-u_3)^2}\right]-\cdots+\cdots\\
&\quad-\omega_0^2R^3\left[\frac{1}{(a+u_9-u_8)^2}\right]+\omega_0^2R^3\left[\frac{1}{(a+u_{10}-u_9)^2}\right]\\
&\quad-\omega_0^2R^3\left[\frac{1}{(a+u_{10}-u_9)^2}\right]+\omega_0^2R^3\left[\frac{1}{(a-u_{10})^2}\right]\\
&= \omega_0^2R^3\left[\frac{1}{(a+u_2-u_1)^2}-\frac{1}{(a+u_1)^2}+\frac{1}{(a+u_3-u_2)^2}-\frac{1}{(a+u_2-u_1)^2}\right.\\
&\quad+\frac{1}{(a+u_4-u_3)^2}-\frac{1}{(a+u_3-u_2)^2}+\cdots+\frac{1}{(a+u_{10}-u_9)^2}\\
&\quad\left.-\frac{1}{(a+u_9-u_8)^2}+\frac{1}{(a-u_{10})^2}-\frac{1}{(a+u_{10}-u_9)^2}\right]\\
&= \sum_{n=1}^{10}\omega_0^2R^3\left[\frac{1}{(a+u_{n+1}-u_n)^2}-\frac{1}{(a+u_n-u_{n-1})^2}\right],
\end{aligned}$$

$$\begin{aligned}
\therefore \text{Coupling } E_{\mathrm{p}} &= \omega_0^2R^3\left(\frac{1}{a+u_1}-\frac{1}{a}\right)\\
&\quad+\sum_{n=2}^{10}\omega_0^2R^3\left(\frac{1}{a+u_n-u_{n-1}}-\frac{1}{a}\right)\\
&\quad+\omega_0^2R^3\left(\frac{1}{a-u_{10}}-\frac{1}{a}\right).
\end{aligned}\tag{2.35}$$

Rewrite Eq. (2.32), we have:

$$\begin{aligned}
&E_{\mathrm{k}}+\text{Onsite linear } E_{\mathrm{p}}+\text{Onsite nonlinear } E_{\mathrm{p}}\\
&\quad+\text{Coupling } E_{\mathrm{p}}\\
&\quad=\text{Hamiltonion(Total Energy)},
\end{aligned}\tag{2.36}$$

Combining Eq. (2.33), Eq. (2.34.1), Eq. (2.34.2), Eq. (2.35), Eq. (2.36), one can compute the total energy-time graph of the system. Normally, since this is a close system, we expect the total energy keeps constant over time, either it is posing a linear oscillation or a nonlinear oscillation. We thus start considering the energy-time analysis on the first case, using $B = 0.5 \times 10^{-8}$m, known as the linear one, see Fig. 2.8.

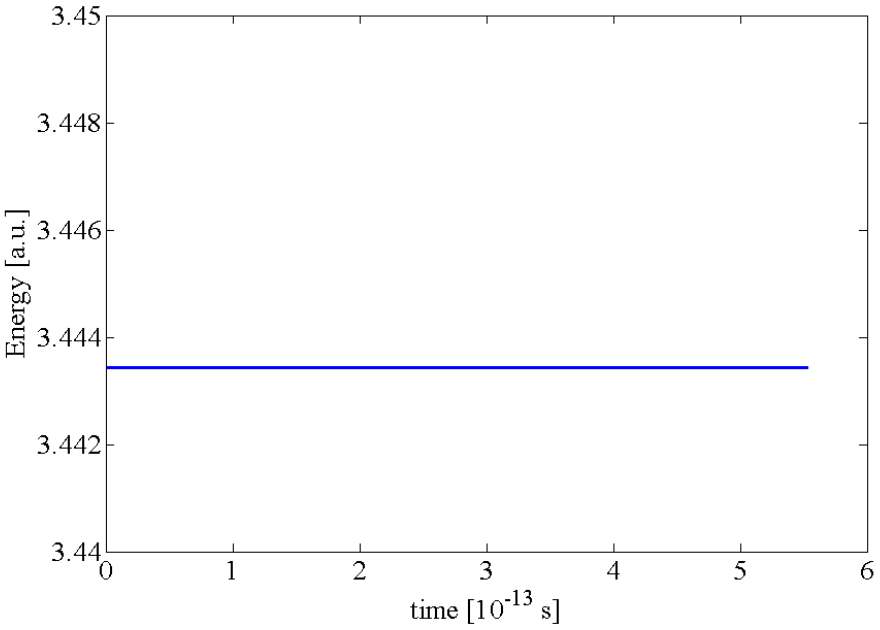

Figure 2.8: The total energy-time graph of the system using initial multiplying parameter $B = 0.5 \times 10^{-8}$m, having 10 sites along the one-dimensional array, using the 4^{th} eigenmode as initial configuration. The program executes at 3×10^{7} RK iterations, i.e. $t = 5.5 \times 10^{-13}$s.

It is obvious that the accuracy of the calculation is verified in Fig. 2.8. Also when the oscillation is subjected to initial condition of 4^{th} eigenfrequency with different values of B, like the example in the previous three distinct sections $B = 0.5 \times 10^{-8}$, 1.25×10^{-8}m and 1.5×10^{-8}m,

their energy-time graphs give the same behavior, a constant-like straight line. It turns out that these 3 models (3 different values of B) are valid under the consideration of Hamiltonian even though two of them are having a comparatively significant nonlinearity. However if initial configuration corresponds to the 8^{th} eigenfrequency is in used, the nonlinearity eventually force the dipole moment of electron clouds being unbounded, results in a ramping in the Hamiltonian. Such a scenario raises another issue, the overlapping of the adjacent charges, either the positive volume charge or the negatively charged electron cloud.

In our formalism, if the displacement of the n^{th} negatively charged electron cloud is being unbounded, it will touch the $(n+1)^{\text{th}}$ or the $(n-1)^{\text{th}}$ boundaries of the charges theoretically. Furthermore, they may overlap with each other. Upon overlapping, the Eq. (2.10) in Chapter 2.1 is no longer valid and will affect the simulation later on since the acceleration vector in the RK iterations is based on Eq. (2.10). Therefore it is essential to check whether there is overlapping happened or not.

There are 2 kinds of overlapping could be happened in the system. The first condition is about the overlapping of the n^{th} negatively charged electron cloud with either the $(n+1)^{\text{th}}$ or the $(n-1)^{\text{th}}$ negatively charged electron cloud, while the second condition is about the overlapping of the n^{th} negatively charged electron cloud with either the $(n+1)^{\text{th}}$ or the $(n-1)^{\text{th}}$ positive volume charge. With a known radius of all nanoparticles being $R = 5\text{nm}$ and a known separation of the sites being $a = 15\text{nm}$, the condition of overlapping are as follow:

$$u_{n+1} - u_n < -5 \times 10^{-9}\text{m}, \quad \text{or}$$
$$u_n - u_{n+1} > 5 \times 10^{-9}\text{m}, \quad \text{or} \qquad (2.37)$$
$$|u_n| > 5 \times 10^{-9}\text{m}.$$

Indeed, after the implementation of the overlapping equations, the results of the original case (eigenvector of the 4^{th} eigenfrequency as initial condition) are quite astonishing. We can see the summarization in the table below.

Table 2.3: Time for the overlapping of electron clouds happened when applying different material, initial eigenmode, (/) denotes no overlapping, (X osc.) denotes after X oscillations, overlapping occurs.

$\omega_0(\text{rad s}^{-1})$	$\omega_0 = 5.420 \times 10^{15}$(Au)	$\omega_0 = 7.982 \times 10^{15}$(Ag)	$\omega_0 = 5.420 \times 10^{15}$(Au)	$\omega_0 = 5.420 \times 10^{15}$(Au)
Initial config.	4^{th} eigenfreq.	4^{th} eigenfreq.	2^{nd} eigenfreq.	5^{th} eigenfreq.
Differrent B (10nm)	0.5(/)	1.075(/)	1.075(/)	0.75(/)
	0.75(/)	1.08(141osc.)	1.08(/)	0.9(/)
	1.07(/)	1.09(24.5osc.)	1.09(/)	0.901(368osc.)
	1.075(/)	1.10(24.5osc.)	1.10(/)	0.902(97osc.)
	1.08(141osc.)	1.11(16.5osc.)	1.15(/)	0.903(97osc.)
	1.09(24.5osc.)	1.12(16.5osc.)	1.20(/)	0.904(97osc.)
	1.10(24.5osc.)	1.13(15.5osc.)	1.30(/)	0.905(97osc.)
	1.11(16.5osc.)	>1.14(0osc.)	1.40(/)	0.906(38.5osc.)
	1.12(16.5osc.)		1.50(/)	0.907(38.5osc.)
	1.13(15.5osc.)			0.907(38.5osc.)
	>1.14(0osc.)			>0.910(0osc.)

From the table above, we can draw into some conclusion. First of all, for the system of one-dimensional plasmonic chain, the nonlinear effect will

not be changed among using different materials, this fact can be seen by investigating the 2 columns in left-hand side of Table 2.3. Even though there are two kinds of material (Au and Ag), a similar response of oscillation can be obtained by applying a same initial condition (eigenvector corresponding to 4^{th} eigenfrequency). Here, the response of oscillation, whether being oscillating vigorously or peacefully, is greatly depending on the initial condition. We observe that for an initial condition from 2^{nd} eigenfrequency, the oscillation is so steady such that the overlapping will never take place. While the initial condition from 5^{th} eigenfrequency behaves so much different such that it will easily overlap. If the easiness of overlapping is proportional to the nonlinearity inside the system, we can somehow assume the following statement be true: The order of eigenmode is proportional to the nonlinearity inside the one-dimensional plasmonic chain.

Yet the most unbelievable part is that if we compare the results from Fig. 2.6 and Fig. 2.7 in Chapter 2.3 with the Table 2.3, for some reason the Hamiltonian remains conserve even though the overlapping of electron clouds happens (This case should not happen as previous example shows that energy should be undergoing a ramp). And if you try tracking the dipole moment-time graph, it is not difficult to find that the Quasi-linear behaviour in Fig. 2.6 and the nonlinear behaviour in Fig. 2.7 happens once there is overlapping, which makes the results having inconsistency.

On behalf of the Hamiltonian evaluation and overlapping effect, we can perform the Fourier transform on the net dipole moment-time graph of

different electron clouds. Fourier transform can sort out the frequency domain in a system, so as to have a better understanding of the nonlinearity in the one-dimensional plasmonic chain. This time, we will study the Fourier transform of one particular electron cloud (9^{th} site in the one-dimensional chain) by using the same normalized eigenvector (4^{th} eigenmode) with different parameter B (0.5×10^{-8}m in Fig. 2.9, 1.0×10^{-8}m in Fig. 2.10). With the previous results, Fig. 2.5, Fig. 2.6, and Fig. 2.7 in Chapter 2.3, we know that the nonlinearity inside the system increased with the parameter B.

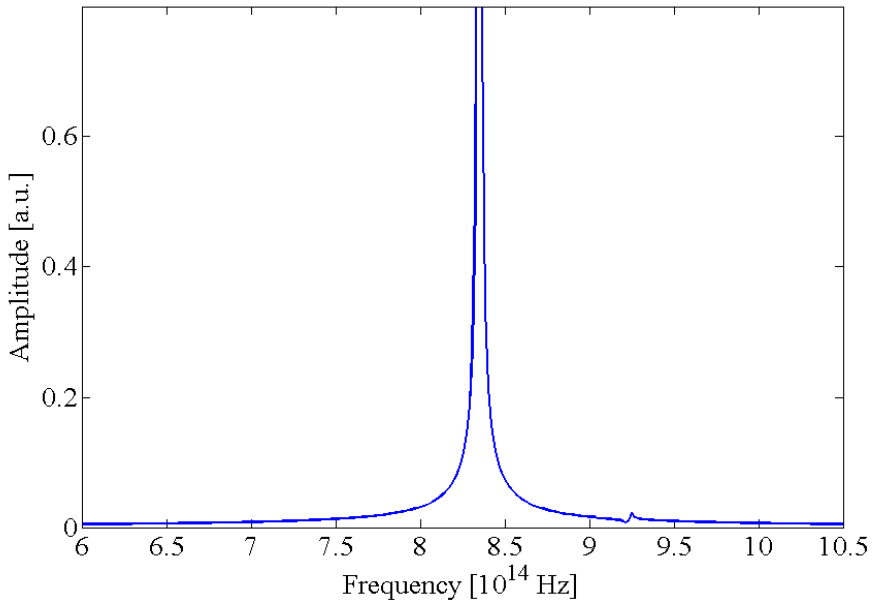

Figure 2.9: Fourier transform of the dipole moment-time data of the 9^{th} electron cloud in the one-dimensional plasmonic chain using initial configuration of eigenvector corresponds to 4^{th} eigenfrequency and an initial multiplying parameter $B = 0.5 \times 10^{-8}$m. At spiky peak at 8.35×10^{14}Hz is observed.

According to the numerical calculation in Fig. 2.9, we can see a peak

eventually located at a frequency of 8.3471×10^{14}Hz. Now if we transform such a value in terms of radian, it equals about $8.3471 \times 10^{14} \times 2\pi = 5.245 \times 10^{15}$rad s^{-1}, which shows the system is oscillating at about this eigenfrequency. And if we compare this result to the theoretical one, the ω_0 we use is 5.420×10^{15}rad s^{-1}, and the 4^{th} eigenfrequency is in used as the initial condition, which is at about $0.9687 \times \omega_0$, the theoretical eigenfrequency in the system is thus denoted by $0.9687 \times 5.420 \times 10^{15} = 5.250 \times 10^{15}$rad s^{-1}. The small error between the numerical experiment and theoretical result may due to a lot of things, like the numerical error in MATLAB, or the nonlinearity in the system. But still, we can judge that the experimental result is supported by the theory. Now if we further look into Fig. 2.9, we can observe a small peak appears at a frequency about 9.25×10^{14}Hz, we could guess this is one kind of results from the nonlinearity in the system at this moment.

In the next part, we start investigating the Fourier-transformed frequency spectrum of the 9^{th} electron cloud again in the one-dimensional plasmonic chain using $B = 1.0 \times 10^{-8}$m, see Fig. 2.10.

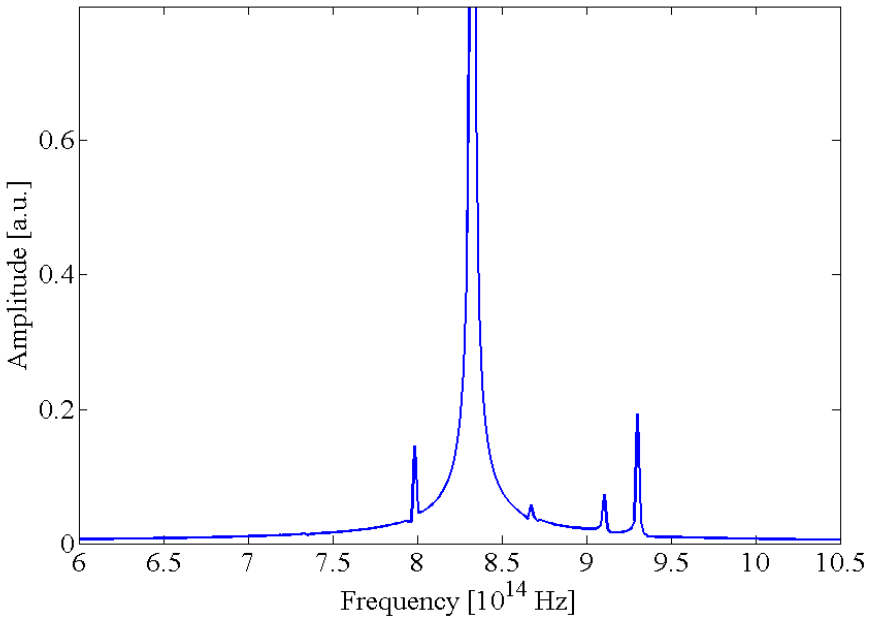

Figure 2.10: Fourier transform of the dipole moment-time data of the 9^{th} electron cloud in the one-dimensional plasmonic chain using initial configuration of eigenvector corresponds to the 4^{th} eigenfrequency and an initial multiplying parameter $B = 1.0 \times 10^{-8}$m. A spiky peak at 8.33×10^{14}Hz is observed with the existence of small peaks from other frequencies.

Like the previous analysis, we start by looking into the highest peak, that is the one located at a frequency of 8.3290×10^{14}Hz. Again we transform such a value in terms of radian, it equals about $8.3290 \times 10^{14} \times 2\pi = 5.233 \times 10^{15}$rad s^{-1}, which is comparatively smaller than the one in Fig. 2.9. We define this spiky peak as 'main frequency'. Indeed, by observing a larger set of B, we found that a bigger B will result in a lower 'main frequency', such frequency conversion is commonly found in nonlinear problem. Not only the lower frequency it brought, but also more 'side frequency' will be brought into the system. We can see that there are four more peaks around the 'main frequency' in which you will not find

them in a linear oscillation. Unfortunately, the design of the one-dimensional plasmonic chain do not support a higher value of B for which the system will literally undergoes overlapping, and makes the Fourier transform analysis became meaningless.

2.5 Energy analysis (FPU-approach)

Now if we look into our one-dimensional plasmonic chain, one can imagine that the negatively charged electron clouds are the masses in FPU-model, and the electrostatic force in between are combined as the nonlinear spring. In that sense, they share a high degree of similarity indeed. This can be verified by the equation of motion in these two systems, like the FPU-one, recall the Eq. (2.6) in Chapter 2.1, the equation of motion is a recurrence equation such that its n^{th} term depends on the $(n-1)^{\text{th}}$, n^{th} and $(n+1)^{\text{th}}$ terms. Under this consideration, there are no difference at all compared to Eq. (1.1) and Eq. (1.2) in Chapter 1.3.

We begin the FPU-approach analysis by lengthening the length of our modelling chain from 10 to 512. Using 512 nanoparticles to form the chain means there will be 512 discrete eigenfrequencies and 512 corresponding normalized eigenvectors. To start with, one important approach is to compute the mode energy indicator-time graph. Since the main idea of FPU model is the energy distribution among different modes in the system, it is important to figure out how is the energy flow.

In order to get the mode energy indicator-time graph in our system,

recall Eq. (2.6) in Chapter 2.1.

$$\ddot{u_n} = -\omega_0^2 u_n + \omega_0^2 R^3 \left[\frac{1}{(a-u_n)^2} - \frac{1}{(a+u_{n+1}-u_n)^2} - \frac{1}{(a+u_n)^2} + \frac{1}{(a+u_n-u_{n-1})^2}\right].$$

We then perform the same procedure in Chapter 2.4, the extraction of Hamiltonian using Eq. (2.30), (2.31),

$$\ddot{u_n} + f(u) = 0,$$

$$\frac{1}{2}\dot{u_n} + F(u) = H,$$

since Hamiltonian is the sum of kinetic energy and potential energy, we can write the following expression:

$$\begin{aligned} E_{u_n}^{\text{kin}} + E_{u_n}^{\text{pot}} = {} & \frac{1}{2}\dot{u_n^2} + \frac{1}{2}\omega_0^2 u_n^2 + \omega_0^2 R^3 \left[-\frac{1}{a+u_n} - \frac{1}{a-u_n} + \frac{2}{a}\right] \\ & + \frac{1}{2}\left\{\omega_0^2 R^3 \left[\frac{1}{a+u_n-u_{n-1}} - \frac{1}{a}\right]\right. \\ & \left. + \omega_0^2 R^3 \left[\frac{1}{a+u_{n+1}-u_n} - \frac{1}{a}\right]\right\}. \end{aligned} \tag{2.38}$$

Note that Eq. (2.38) is a general expression of Hamiltonian including both the linear terms and the nonlinear terms. In the field of FPU, for simplicity, we use linear approximation to approximate the Hamiltonian. On this circumstance, the Hamiltonian is the sum of the energies in the normal modes for the linear system. Eq. (2.38) is thus transformed to:

$$E_{u_n}^{\text{kin}} + E_{u_n}^{\text{pot}} = \frac{1}{2}\dot{u_n^2} + \frac{1}{2}\omega_0^2 u_n^2. \tag{2.39}$$

Next we replace the displacement vector by applying Spatial Fourier Transform on it,

$$\begin{cases} a_k = \sum_{n=1}^{N} u_n \sin\frac{nk\pi}{N+1}, \\ \dot{a_k} = \sum_{n=1}^{N} v_n \sin\frac{nk\pi}{N+1}, \end{cases} \tag{2.40}$$

substitute Eq. (2.40) into Eq. (2.39) yields:

$$E_k^{\text{kin}} + E_k^{\text{pot}} = \frac{1}{2}\dot{a_k^2} + \frac{1}{2}\omega_k^2 a_k^2. \tag{2.41}$$

The above procedure successfully turns the variable n (the site number of electron clouds) in Eq. (2.39) into another variable k (the mode number, from 1 to 512 in our system) in Eq. (2.41). This definition of energy in a normal mode will remain valid provided that the amplitudes of the normal modes remain sufficiently small so that the nonlinear terms in Eq. (2.38) will not become dominated. By using Eq. (2.41), one can now compute the mode energy indicator-time graph to see how energy is distributed among different modes over time.

We start with using eigenvector corresponding to the 1^{st} eigenfrequency (most fundamental mode) to be the initial condition as it is the most easily excited mode. Since the number of sites along the chain has been lengthened from 10 to 512, the normalized eigenvector is greatly diminished compare to that of using 10 nanoparticles, see Fig. 2.11. In order to shorten the simulation time, we input a larger value $B = 3.5 \times 10^{-8}\text{m}$ to have a faster response from the nonlinearity inside the system.

Unlike FPU model, the value of B in our system is not unlimited. The main difference between them is that the FPU one is considering the

oscillation of mass, which would not have the case to overlap, while our case is considering the movable electron cloud interacting with the charges nearby, overlapping is theoretically possible but not favoured. The con of using a larger B is an earlier execution of the program since the results beyond overlapping would require more accurate model.

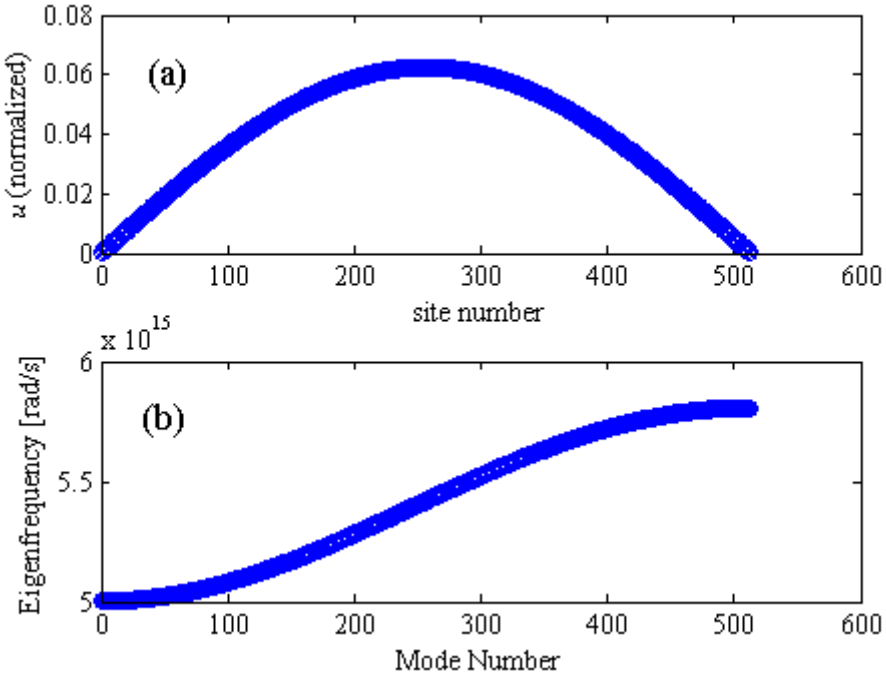

Figure 2.11: (a) The pick off normalized displacement vector, with x-axis being the site number representing 512 discrete electron clouds along the one-dimensional plasmonic chain and y-axis being the normalized longitudinal displacement vector of the center of mass. Here the pick off displacement vector is of the 1^{st} eigenfrequency (fundamental mode). (b) The dispersion band of the 512 discrete eigenfrequencies, with x-axis being the mode number k, and y-axis being the eigenfrequency in terms of rad s^{-1}.

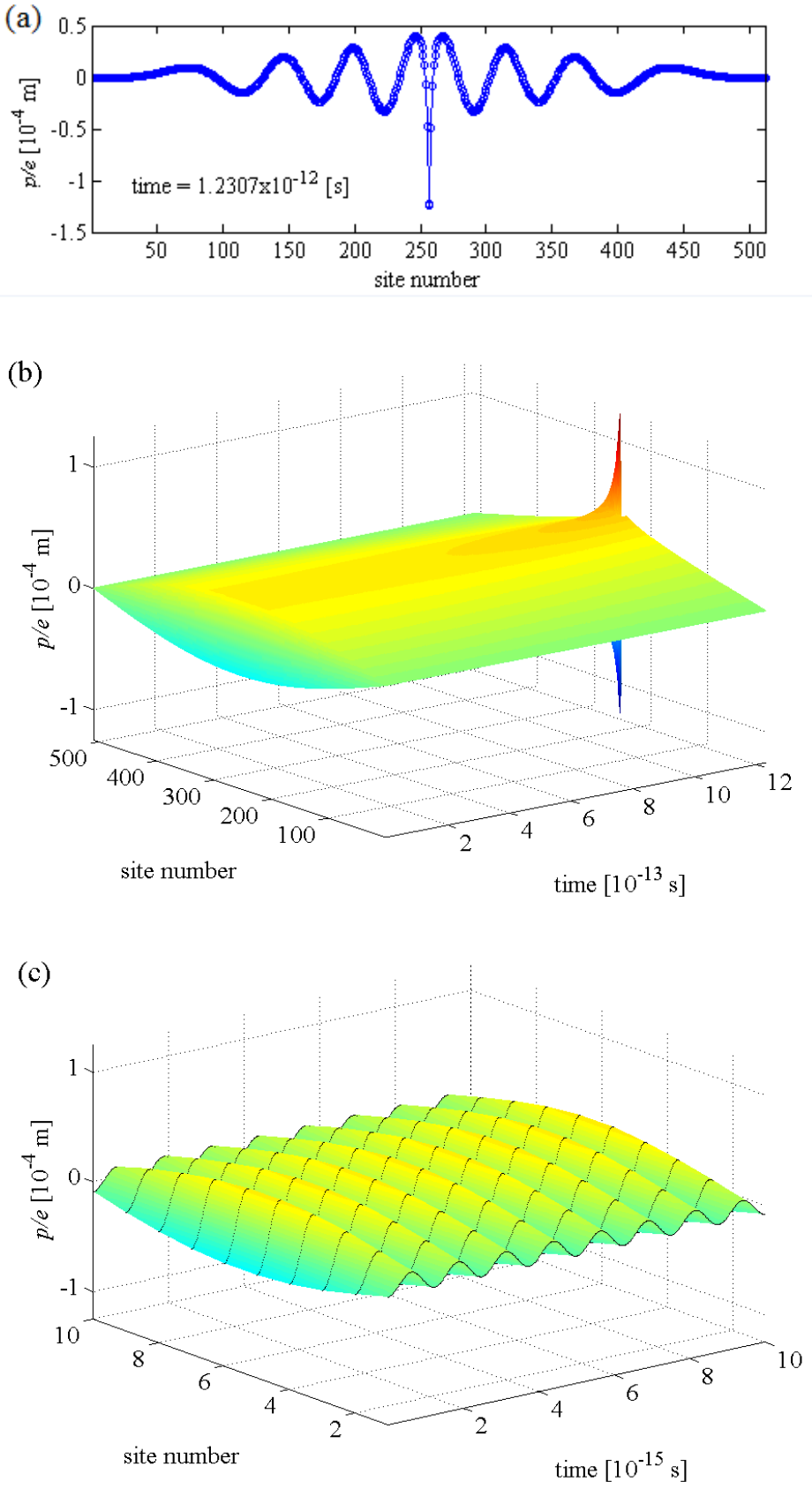

Figure 2.12: (Color online) (a) The net dipole profile right before program execute, with y-axis being the dipole moment normalized by $e = 1.602 \times 10^{-19}\mathrm{C}$ and x-axis

being the site number representing 512 discrete electron clouds; Time-domain simulation of the net dipole moments on individual particle sites in a chain of $N = 512$ particles (b) and in a chain of $N = 10$ particles (c). Both cases are initially excited with the fundamental eigenmode, i.e., all dipole moments are almost in phase; nanoparticle radius $R = 5\text{nm}$; lattice constant $a = 15\text{nm}$; time step for RK-4 $dt = 10^{-4}/\omega_0$ while the displaying time step for the graph $dt' = 0.1/\omega_0$, and the resonance frequency $\omega_0 = 5.420 \times 10^{15}\text{rad s}^{-1}$ (Au). For (c), the black dots indicate the corresponding dipole strength at each iteration. The colored surface formed by dots is for the purpose of a more distinguishable results along different sites in the chain. The data shown here is in an early cut off. While for (b), the dots are omitted and only the surface is displayed. The simulation stops at $t = 1.2307 \times 10^{-12}\text{s}$.

Unlike the numerical calculations done in the previous section, this time with $n = 512$ and $B = 3.5 \times 10^{-8}\text{m}$, the system directly jumps into a nonlinear regime till 1061 oscillations, the executing time, see Fig. 2.12.

From Fig. 2.12(a), we know that the overlapping happens at the site number = 256. For a moment the 256^{th} electron cloud is oscillating vigorously such that it overlaps with the 257^{th} positive volume charge, which is why the program stopped there. One interesting phenomena is that even though the system exhibits nonlinear oscillation, right before overlapping it shows the tendency of energy localization at the middle part of the plasmonic chain such that the dipole strength is greatly enhanced by $|p_{max}|/e = 1.23 \times 10^{-4}\text{m}$, see Fig. 2.12(b). And we notice that such kind of behaviour can only be observed in a long finite chain as shown in Fig. 2.12(b) but not in a short plasmonic nanoparticle chain, i.e. Fig. 2.12(c), as

it is also excited by a similar fundamental mode but posing a linear oscillation with $|p_{max}|/e = 3.21 \times 10^{-5}$m. Indeed, if the above procedure is repeated for several more different initial conditions starting from the lower band of the dispersion band in Fig. 2.11(b), i.e. the 1^{st}, 2^{nd},… eigenmode, before overlapping happens, there is always a tendency of energy localization, such that the extreme-point(s) of the initial eigenvector will always be the localized site(s). We believe the localization of dipole moment in our case is driven by the nonlinearity brought by the Coulomb interactions between charges, as it accounts for most of the unstable factors in our formalism. Given the nonlinear localization can only be found in a much longer plasmonic chain with unit cell $N = 512$ but not in a shorter one, it might be explained by the mode energy transfer [55]. In this final part of Chapter 2, we will look into the mode energy indicator-time graph of the system.

Since we start the program by using eigenvector corresponds to 1^{st} eigenfrequency in the dispersion band as initial condition in Fig. 2.12(b), which implies that initially all energy is allocated in mode 1, as shown in Fig. 2.13. Unlike the results from Fermi [22], instead of staying at the fundamental eigenmode (Mode 1) as found in a short chain in Fig. 2.12(c), the energy distributes to some higher order eigenmodes, and the plasmonic system has quickly drawn into equipartition instead of taking the super-recurrence behaviour. Our system shows a generic ergodicity such that it 'forgets' initial state as time evolved. If one neglects the impact from overlapping, the plasmonic chain might be an answer to the ergodicity since in traditional FPU model, the equipartition will only be happened if the

initial energy is putted into a high frequency mode and with large amplitude.

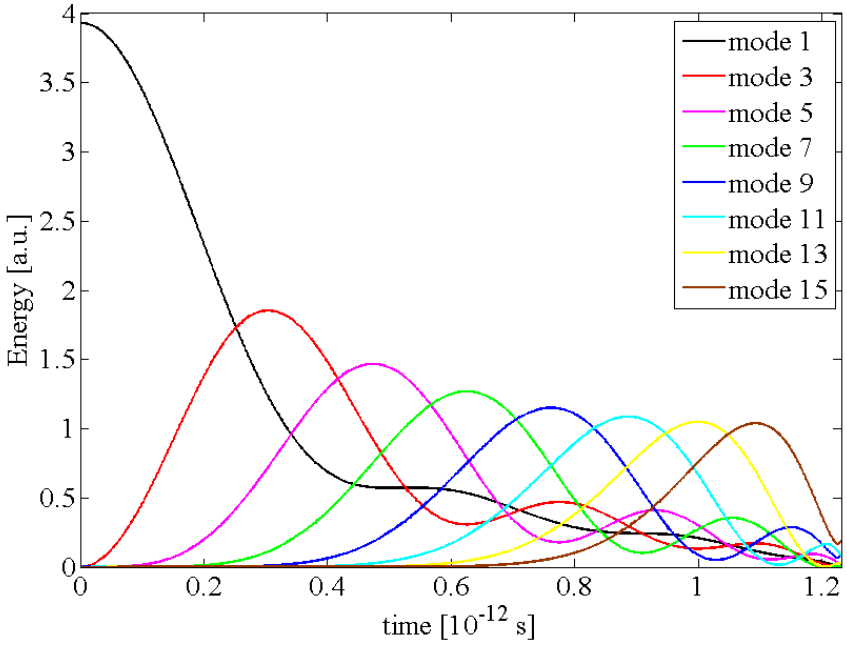

Figure 2.13: (Color online) Energy indicating-time graph of the data set obtained in Fig. 2.12(b). An 'equipartition' is likely to be acquired as energy distributes along modes by symmetry. The energy here is with arbitrary unit as it is a comparative value for modes. Modes 2, 4, 6...etc. cannot be found in the graph as they have a comparatively zero energy with respect to the excited eigenmode.

From Fig. 2.11(a) we know the initial configuration is a half sine wave, the system tends to keep its symmetry since the force acts symmetrically, this explains why the even modes are having comparatively zero energy in the above case. Moreover, in Fig. 2.13, we observe as time evolve, the up-conversion of frequencies lead to raises of different sine functions correspond to different eigenmodes due to the energy distribution among them. This might be able to explain why energy localization happens in Fig. 2.12 as the superposition of different sine functions may form a delta

function which in turn favours the formation of field localization. You can find more results on higher order eigenmodes in Appendix A.

2.6 Conclusion

We presented an overview of ways to analyse the one-dimensional plasmonic chain through the linear and nonlinear aspects by treating the plasmonic nanoparticle a resonator. The nonlinearity in our system basically comes from the Coulomb interaction between charges. Here we adopted methodology of the Runge-Kutta Method and MATLAB was used to perform the RK-iterations to simulate the time-domain behaviour of the one-dimensional plasmonic resonators. The impact of using different initial configurations had been discussed and the Hamiltonian of the system had been evaluated explicitly. By performing the Fourier transform, we found the order of eigenmode and the value of initial multiplying parameter B are directly proportional to the nonlinearity inside the system. Last we performed the FPU-approach energy-analysis by using initial configuration from the first eigenmode, it turns out that the equipartition and the nonlinearity energy localization were mutual interpreted. The equipartition itself also suggested the up-conversion of frequencies takes place, which is commonly found in nonlinear system. In the meanwhile, we do not show any experimental realization on the up-conversion nonlinear localization because of the limitation in fabricating a highly precise long nanoparticle chain, yet the localization is still possible as the dipole oscillation dominates in sub-wavelength system.

Chapter 3 One-dimensional coated diatomic plasmonic chain

3.1 Modelling

To begin with, we first build up the model world by considering a one-dimensional problem like Chapter 2 while the biggest difference is that we do not treat the plasmonic nanoparticle a resonator this time. Instead, we model it as a dispersive metal nanoparticle together with a non-dispersive coated dielectric layer. Since we are considering a diatomic plasmonic chain, the 'building blocks' of the one dimensional chain will consist of two sites, namely A and B. Each site will contain an identical metal nanoparticle with material dielectric function ϵ_1, and is coated by a dielectric layer with permittivity ϵ_2 and ϵ_3 respectively, which are separated by an alternatively changing distances t and $d-t$, see Fig. 3.1. Note that the coated dielectric layers for the two sites in a unit cell are defined by a different permittivity, it is for the simplicity of showing the formulation as they will be regarded as identical in the first part-realization of edge state in diatomic plasmonic chain, and a pair of complex conjugate in the second part-verification of zero extinction in PT-symmetric diatomic plasmonic chain. From Fig. 3.1, the chain contains two nanoparticles in each of its unit cell, therefore regarded as a 'diatomic chain', and is assumed to be embedded in air with vacuum permittivity ϵ_0.

We will start the analogy by considering the classical approach for a

monatomic plasmonic chain as it shares a lot of similarities with our diatomic plasmonic chain, that is, to consider its dispersion relations.

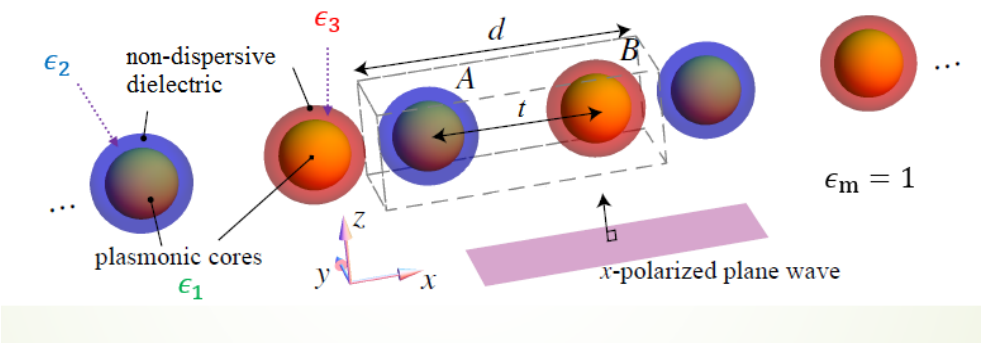

Figure 3.1: Schematic figure of a one-dimensional coated diatomic plasmonic chain for which the above setup is assumed to be duplicated till infinite. There are two spherical dispersive metal nanoparticles with dielectric function ϵ_1 coated with non-dispersive dielectric of different permittivity ϵ_2 and ϵ_3 in one single unit cell having two sites, namely A and B. All coated nanoparticles are of the same size with outer radius b, inner radius a. The length of the unit cells and the separation between site A and site B are denoted as d and t respectively. There is also a dashed-line rectangle showing the unit cell of the one-dimensional diatomic chain. The chain is assumed to be embedded in a medium with relative permittivity $\epsilon_m = 1$.

First of all, we assume the diatomic plasmonic chain is infinitely long and the nanoparticles are denoted by n such that site A is always an even number while site B is an odd number, i.e. site A: $n = \cdots -2, 0, 2, \ldots$; site B: $n = \cdots -1, 1, 3, \ldots$; also an external E-field is incident onto the chain as a stimulate. Instead of using the equations of motion, we model the system by coupled dipole equation this time. It comes from the fact that the coated nanoparticles are not too close together such that the electromagnetic

response of the n^{th} nanoparticle among stimulate can be modelled by the surrounding induced dipole moment and the external E-field incident on it, which is known as the dipole approximation [47]. Here we denote the excited dipole moment on the n^{th} nanoparticle as $\mathbf{p}_n$ while the external E-field experienced by it as $\mathbf{E}_{\text{ext},n}$. And the coupled dipole equation guarantee the following statement describing the behaviour of $\mathbf{p}_n$ to be true:

$$\sum_m (\alpha_n^{-1}\delta_{nm} - \mathbf{G}_{nm})\mathbf{p}_m = \mathbf{E}_{\text{ext},n}, \tag{3.1}$$

where m is a number sweeping the entire sites in the chain, i.e. different n, δ_{nm} is a Kronecker delta function, α_n is known as the quasistatic polarizability with radiation correction of the n^{th} nanoparticle, $\mathbf{G}_{nm}$ is a dyadic Green's function describing the coupling between the dipole moment on n^{th} nanoparticle and the one on m^{th} nanoparticle [48]. Since we are first considering a one-dimensional coated diatomic plasmonic chain with identical nanoparticles in site A and site B, those nanoparticles will therefore share a same polarizability, Eq. (3.1) can be simplified:

$$\alpha^{-1}\mathbf{p}_n = \sum_{m\neq n} \mathbf{G}_{nm}\mathbf{p}_m + \mathbf{E}_{\text{ext},n}. \tag{3.2}$$

Reports have been shown that the quasistatic approximation and nearest neighbour approximation work fine when finding the longitudinal mode [47]. With such simplicity, we are aiming for the solution of longitudinal mode by first considering the explicit Green's function mentioned by J. D. Jackson [48] as follow:

$$\mathbf{E} = \frac{1}{4\pi\epsilon_0}\left\{k^2(\mathbf{n}\times\mathbf{p})\times\mathbf{n}\frac{e^{ikr}}{r} + [3\mathbf{n}(\mathbf{n}\cdot\mathbf{p}) - \mathbf{p}](\frac{1}{r^3} - \frac{ik}{r^2})e^{ikr}\right\}. \tag{3.3}$$

Eq. (3.3) describes the electric dipole field generated by dipole moment $\mathbf{p}$, where $k = \omega/c$ is the wave number, r is the distance between observing point and the point dipole, while $\mathbf{n}$ is a unit vector pointing from the point dipole to the observing point. Indeed, Eq. (3.3) can be plugged into Eq. (3.2) as Eq. (3.2) can be rewrite in this form:

$$\alpha^{-1}\mathbf{p}_n = \sum_{m\neq n} \begin{matrix}\mathbf{E} \text{ experienced by } n^{\text{th}} \text{ nanoparticle} \\ \text{induced by dipole moment } \mathbf{p}_m\end{matrix} + \mathbf{E}_{\text{ext},n}. \quad (3.4)$$

Since we are only interested in the longitudinal mode, Eq. (3.3) can be greatly simplified by considering a 'two-nanoparticles system', see Fig. 3.2. The excited dipole moment in site A and site B are denoted by $\mathbf{p}_1$ and $\mathbf{p}_2$ respectively, and are having direction pointing along the chain axis indicating the solutions are in a longitudinal form by interests. We will first consider the electric dipole field generated by $\mathbf{p}_2$, experienced by $\mathbf{p}_1$, then vice versa. To start with, we write down the vector form of $\mathbf{p}_1$, $\mathbf{p}_2$ and $\mathbf{n}$:

$$\mathbf{p}_1 = \begin{pmatrix} p_1 \\ 0 \\ 0 \end{pmatrix}, \qquad \mathbf{p}_2 = \begin{pmatrix} p_2 \\ 0 \\ 0 \end{pmatrix}, \text{and} \qquad \mathbf{n} = \begin{pmatrix} -1 \\ 0 \\ 0 \end{pmatrix}, \quad (3.5)$$

note that the above equation for $\mathbf{n}$ is valid only when observing E-field generated by $\mathbf{p}_2$ at site A. And Eq. (3.3) gives:

$$\mathbf{E} \text{ at site A} = \frac{1}{4\pi\epsilon_0}\left\{k^2(\mathbf{n}\times\mathbf{p}_2)\times\mathbf{n}\frac{e^{ikr}}{r} + [3\mathbf{n}(\mathbf{n}\cdot\mathbf{p}_2) - \mathbf{p}_2](\frac{1}{r^3} - \frac{ik}{r^2})e^{ikr}\right\}, \quad (3.6)$$

where r denotes the distance between site A and site B. We then evaluate the dot product and cross product in Eq. (3.6) yields:

$$\mathbf{n}\times\mathbf{p}_2 = \begin{vmatrix} \hat{x} & \hat{y} & \hat{z} \\ -1 & 0 & 0 \\ p_2 & 0 & 0 \end{vmatrix} = 0, \qquad \mathbf{n}\cdot\mathbf{p}_2 = -p_2, \quad (3.7)$$

which implies that:

$$\begin{aligned}\mathbf{E}\ \text{at site A} &= \frac{1}{4\pi\epsilon_0}[3\mathbf{n}(\mathbf{n}\cdot\mathbf{p}_2)-\mathbf{p}_2]\left(\frac{1}{r^3}-\frac{ik}{r^2}\right)e^{ikr} \\ &= \frac{1}{4\pi\epsilon_0}\left[2p_2\left(\frac{1}{r^3}-\frac{ik}{r^2}\right)e^{ikr}\right]\hat{x}.\end{aligned} \tag{3.8}$$

And if we repeat the step by considering the electric dipole field generated by $\mathbf{p}_1$, experienced by $\mathbf{p}_2$, it gives:

$$\begin{aligned}\mathbf{E}\ \text{at site B} &= \frac{1}{4\pi\epsilon_0}[3\mathbf{n}(\mathbf{n}\cdot\mathbf{p}_1)-\mathbf{p}_1]\left(\frac{1}{r^3}-\frac{ik}{r^2}\right)e^{ikr} \\ &= \frac{1}{4\pi\epsilon_0}\left[2p_1\left(\frac{1}{r^3}-\frac{ik}{r^2}\right)e^{ikr}\right]\hat{x}.\end{aligned} \tag{3.9}$$

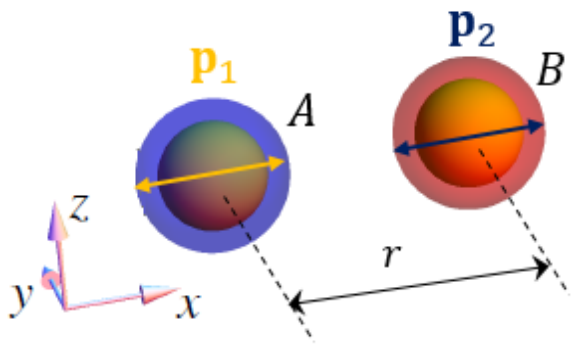

Figure 3.2: Schematic figure of a 'two-nanoparticles system' picking from the unit cell of the diatomic plasmonic chain. The distance between site A and B is denoted as r, site A and site B's nanoparticle is having dipole moment $\mathbf{p}_1$ and $\mathbf{p}_2$ respectively.

Eq. (3.8) & (3.9) suggest that if we are considering a longitudinal mode, the complicated form of Eq. (3.3) could be reduced as follow:

$$\mathbf{E}_{p_m;n} = \frac{1}{4\pi\epsilon_0}\left[2p_m\left(\frac{1}{r^3}-\frac{ik}{r^2}\right)e^{ikr}\right]\hat{x}, \tag{3.10}$$

where $\mathbf{E}_{p_m;n}$ is the electric dipole field generated by dipole moment p_m experienced at some site n, r is the distance between the point dipole p_m and site n.

So if we go back to the model mentioned in Fig. 3.1, combining Eq. (3.4) & (3.10), we have:

$$\alpha^{-1}\mathbf{p}_n = \sum_{m\neq n} \frac{2}{4\pi\epsilon_0}\left[p_m\left(\frac{1}{r_{mn}^3} - \frac{ik}{r_{mn}^2}\right)e^{ikr_{mn}}\right]\hat{x} + \mathbf{E}_{\text{ext},n}, \quad (3.11)$$

which gives us a system of equations of dipole moment $\mathbf{p}$ with size n.

The only left unknown is the quasistatic polarizability α with radiation correction. In this part, the nanoparticles in site A and site B are identical, i.e. $\epsilon_2 = \epsilon_3$, for simplicity, we will use ϵ_2 as the permittivity of the non-dispersive dielectric shell mentioned in Fig. 3.1 for both site A and B. Here we adopt the quasistatic polarizability suggested by Bohren [49] for a perfect coated sphere using the parameters mentioned in Fig. 3.1,

$$\alpha = 4\pi\epsilon_0\epsilon_{\text{m}}b^3\frac{(\epsilon_2-\epsilon_{\text{m}})(\epsilon_1+2\epsilon_2)+f(\epsilon_1-\epsilon_2)(\epsilon_{\text{m}}+2\epsilon_2)}{(\epsilon_2+2\epsilon_{\text{m}})(\epsilon_1+2\epsilon_2)+f(2\epsilon_2-2\epsilon_{\text{m}})(\epsilon_1-\epsilon_2)}, \quad (3.12)$$

where ϵ_0 is the vacuum permittivity, ϵ_{m} is the relative permittivity of the embedded medium, ϵ_2 is a constant relative permittivity of the non-dispersive dielectric shell for sites A and B, ϵ_1 is the dielectric function of the dispersive metal nanoparticles' core using Drude model [47] such that $\epsilon_1(\omega) = 1 - \omega_p^2/\omega(iv_c + \omega)$, b is the outer radius of the coated nanoparticles, f is the volume fraction of the inner sphere towards the outer sphere, i.e. $f = (a/b)^3$ where a is the inner radius. The expression of the dielectric function of the core $\epsilon_1(\omega)$ have ω_p, v_c denoting the plasma frequency and plasma collision frequency (Loss) respectively. Upon adding radiation correction to the polarizability mentioned by Capolino [50], we have:

$$\alpha^{-1}(\omega) = \frac{1}{4\pi\epsilon_0\epsilon_m b^3}\left[\frac{(\epsilon_2+2\epsilon_m)(\epsilon_1+2\epsilon_2)+f(2\epsilon_2-2\epsilon_m)(\epsilon_1-\epsilon_2)}{(\epsilon_2-\epsilon_m)(\epsilon_1+2\epsilon_2)+f(\epsilon_1-\epsilon_2)(\epsilon_m+2\epsilon_2)} - i\frac{2(kb)^3}{3}\right], \quad (3.13)$$

where $k = \omega/c$ is the wave number defined before.

Although Eq. (3.13) looks complicated, it is easier to think the quasistatic polarizability with radiation correction is nothing but a function of ω. With a known form of α^{-1}, Eq. (3.11) could be solved now.

3.2 Dispersion relation, Band gap, topological edge state

Now if one wants to calculate the dispersion relation $\omega(k)$, recalling Eq. (3.11), by putting the external E-field experienced by $\mathbf{p}_n$ to be zero, we have:

$$\alpha^{-1}\mathbf{p}_n = \sum_{m\neq n}\frac{2}{4\pi\epsilon_0}\left[p_m\left(\frac{1}{r_{mn}^3}-\frac{ik}{r_{mn}^2}\right)e^{ikr_{mn}}\right]\hat{x}, \quad (3.14)$$

since it is a longitudinal solution, quasistatic approximation is applicable (i.e. $k \to 0$) in both Eq. (3.14) and Eq. (3.13) describing the quasistatic polarizability with radiation correction which makes the radiation term disappeared literally. Also the nearest neighbor approximation is adopted such that when considering the electromagnetic response of dipole moment $\mathbf{p}_n$ on the n^{th} nanoparticle, only the electric dipole field generated by the dipole moment $\mathbf{p}_{n-1}$ and $\mathbf{p}_{n+1}$ on the respective $(n-1)^{\text{th}}$ and $(n+1)^{\text{th}}$ nanoparticle will be considered. The left-hand side of Eq. (3.14) is having excited dipole moment $\mathbf{p}_n$ in $\hat{x}$-direction, therefore $\hat{x}$ in right-hand side can be omitted. Giving such conditions eventually turn Eq.

(3.14) into a simpler form when plugging into the setup in Fig. 3.1:

$$\begin{cases} \alpha^{-1}p_n = \dfrac{2}{4\pi\epsilon_0}\left[\dfrac{p_{n-1}}{(d-t)^3} + \dfrac{p_{n+1}}{t^3}\right] & \text{for site A nanoparticles,} \\ \alpha^{-1}p_n = \dfrac{2}{4\pi\epsilon_0}\left[\dfrac{p_{n-1}}{t^3} + \dfrac{p_{n+1}}{(d-t)^3}\right] & \text{for site B nanoparticles.} \end{cases} \tag{3.15}$$

From the aforementioned, site A nanoparticles are those denoted by $n = \cdots -2, 0, 2, \ldots$ while site B nanoparticles referred to those denoted by $n = \cdots -1, 1, 3, \ldots$. In finding the dispersion relation, we assume the diatomic chain is infinitely long, due to the periodicity, we can apply the Bloch's theorem, which states the dipole moment can be replaced by:

$$\begin{cases} p_{2m} = p_{\mathrm{A}}e^{ikmd}, \\ p_{2m+1} = p_{\mathrm{B}}e^{ikmd}. \end{cases} \tag{3.16}$$

Substituting Eq. (3.16) into Eq. (3.15) yields:

$$\begin{cases} \alpha^{-1}p_{\mathrm{A}} = \dfrac{2}{4\pi\epsilon_0}\left[\dfrac{p_{\mathrm{B}}e^{-ikd}}{(d-t)^3} + \dfrac{p_{\mathrm{B}}}{t^3}\right], \\ \alpha^{-1}p_{\mathrm{B}} = \dfrac{2}{4\pi\epsilon_0}\left[\dfrac{p_{\mathrm{A}}}{t^3} + \dfrac{p_{\mathrm{A}}e^{ikd}}{(d-t)^3}\right], \end{cases} \tag{3.17}$$

with p_{A} and p_{B} representing dipole moment excited in site A and site B nanoparticles within a unit cell of the diatomic chain, respectively. Rewrite Eq. (3.17) in matrix form:

$$\begin{bmatrix} 0 & \dfrac{2}{4\pi\epsilon_0}\left[\dfrac{e^{-ikd}}{(d-t)^3} + \dfrac{1}{t^3}\right] \\ \dfrac{2}{4\pi\epsilon_0}\left[\dfrac{1}{t^3} + \dfrac{e^{ikd}}{(d-t)^3}\right] & 0 \end{bmatrix} \begin{bmatrix} p_{\mathrm{A}} \\ p_{\mathrm{B}} \end{bmatrix} = \alpha^{-1}\begin{bmatrix} p_{\mathrm{A}} \\ p_{\mathrm{B}} \end{bmatrix}. \tag{3.18}$$

Notice that the 2×2 matrix in left-hand side of the Eq. (3.18), now denoted by $\mathbf{M}_k$, is Hermitian in k space, which will guarantee real eigenvalues such that the eigenvalues equal to the quasistatic polarizability,

a function in terms of ω:

$$\alpha^{-1}(\omega) = \text{Eigenvalues of } \mathbf{M}_k.$$

With the above relation, the dispersion relation can be computed once the configuration of the system is well defined. Knowing the fact that a monatomic plasmonic chain will give no band gap when considering its dispersion relation using quasistatic Green's function and quasistatic polarizability in the formalism [44], i.e. $t = d/2$, a natural starting point is in considering a diatomic plasmonic chain, i.e. $t \neq d/2$. C. W. Ling [44] has verified that for a diatomic plasmonic chain with individuals being pure metal nanoparticles described by Drude model can have two non-degenerated longitudinal bands when considering the dispersion relation, and a topological edge state can be sustained in the diatomic chain if certain requirements are being acquired. We will try to verify it in our one-dimensional coated diatomic plasmonic chain.

Using the configuration mentioned in Fig. 3.1, we first set the coated metal nanoparticles having outer radius $b = 10\text{nm}$, for simplicity all other spatial parameters are in ratio of this term. The inner radius $a = 10 \times \frac{0.125}{0.175} = 7.143\text{nm}$. The core of the coated metal nanoparticles are having dielectric function described by lossless-Drude model, i.e. $\epsilon_1 = 1 - (\omega_p/\omega)^2$ with plasma frequency $\omega_p = 2\pi \times 1.6 \times 10^{15} = 1.01 \times 10^{16}\text{rad s}^{-1}$, which is a reasonable value for silver (Ag). The coated layers are assumed to be non-dispersive with a constant relative permittivity $\epsilon_2 = 1.5$. The embedded medium is assumed to be air with vacuum permittivity $\epsilon_0 = 8.85 \times 10^{-12}\text{F m}^{-1}$. The separation between coated nanoparticles,

which are governed by length of the unit cell and inner separation between site A and site B within the unit cell, are defined by $d = \frac{10}{0.175} = 57.1\text{nm}$ and $t = 10 \times \frac{0.6}{0.175} = 34.3\text{nm}$ respectively. Note that $t \neq d/2$ implies that the chain is a diatomic chain. Plugging in all the parameters mentioned above into Eq. (3.18), the dispersion relation $\omega(k)$ can be solved numerically using Wolfram Mathematica, one of the most extensive mathematics resource when handling alphabetical problems, through the eigenvalue problem mentioned above, see Fig. 3.3.

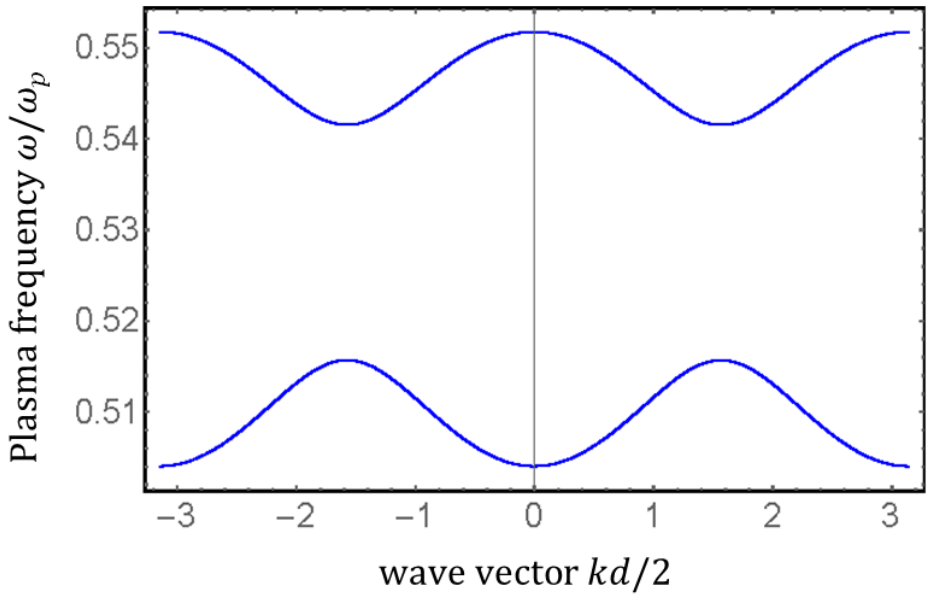

Figure 3.3: Band dispersion of a 1-D diatomic plasmonic chain using identical coated metal nanoparticles for both site A and site B, with x-axis being the wave vector $kd/2$ covering both the 1^{st} and 2^{nd} Brillouin zone, y-axis being the normalized plasma frequency ω/ω_p. It shows the longitudinal dispersion relation of the diatomic chain with $d = 57.1\text{nm}$, $t = 34.3\text{nm}$. Since there are two coated metal nanoparticles in one unit cell, two non-degenerated longitudinal bands are observed. A band gap ranging from $0.515\omega_p$ to $0.542\omega_p$ is observed as $t \neq d/2$ for a diatomic chain.

Here the two non-degenerated longitudinal band in the dispersion figure is given by two kinds of coupling between the adjacent nanoparticles as there are two coated metal nanoparticles in one unit cell, see Fig. 3.3. Also, similar to the case of using purely metal nanoparticles, the diatomic configuration of the plasmonic chain opens a band gap in between the range of $0.515\omega_p < \omega < 0.542\omega_p$, which will not be found in the case of monatomic chain.

Among opening the band gap in the dispersion relation of calculating the longitudinal band in a one-dimensional diatomic chain using coated metal nanoparticles, next part we will aim for verifying the edge state in such a system, i.e. $d = \frac{10}{0.175} = 57.1\text{nm}$ and $t = 10 \times \frac{0.6}{0.175} = 34.3\text{nm}$, as the topological edge state is commonly found in between band gap. Furthermore, to verify the existence of the edge state, we cannot premeditate an infinitely long chain as the edge state is expected to be localized at the interface between two topological different configurations. In this sense, we expect a finite one-dimensional diatomic chain with identical coated metal nanoparticles allocated in site A and site B as mentioned in Fig. 3.1 will allow an edge state to sustain for which the field will be localized in two edges of the diatomic chain. This prediction is based on the fact that the surrounding medium: air with vacuum permittivity $\epsilon_0 = 8.85 \times 10^{-12}\text{F m}^{-1}$ is already a kind of topological different configuration with respect to the finite one-dimensional diatomic chain. Therefore, in between the interface of these two configurations, the two edges of the finite one-dimensional diatomic chain, will be favorable for the sustain of a

localized edge state. We will try to verify this edge state in an analytical approach in Chapter 3.2, and will try to verify it in a numerical approach through simulation in Chapter 3.3.

To consider the finite one-dimensional diatomic chain, the Bloch's theorem is no longer applicable since it is only valid when the chain is infinitely long, which makes the substitution in using Eq. (3.16) failed. A natural starting point for the finite diatomic chain is to get back to the Eq. (3.14), which gives us an explicit electromagnetic response of the longitudinal dipole moment $\mathbf{p}_n$ on the n^{th} nanoparticle among considering the influences of electric dipole field induced by other dipole moment $\mathbf{p}_m$ such that $m \neq n$. Without the presence of an external oscillating electric field $\mathbf{E}_{\text{ext}}$, that is:

$$\alpha^{-1} p_n = \sum_{m \neq n} \frac{2}{4\pi\epsilon_0} \left[p_m \left(\frac{1}{r_{mn}^3} - \frac{ik}{r_{mn}^2} \right) e^{ikr_{mn}} \right]. \tag{3.19}$$

For simplicity, we directly cancel the $\hat{x}$ on right-hand side as all vectors are lying on the direction of chain axis $\hat{x}$. Also, note that the expression of quasistatic polarizability with radiation loss in Eq. (3.13) can be used normally as it has no assumption with the Bloch's Theorem.

Eq. (3.19) is an important starting point for all the analytic analysis on the longitudinal behavior as it is a response function using dynamic Green's function when considering the coupling between dipole moment. Later on, for the purpose of comparison, results will be computed under two aspects: one is with quasistatic approximation (i.e. $k \to 0$) on the Green's

function and the quasistatic polarizability having radiation correction mentioned in Eq. (3.13), the core of nanoparticles are having dielectric function governed by lossless-Drude model, together with the nearest neighbour approximation on the Green's function; while the other one will keep using the exact form of Eq. (3.19) without doing any approximation on both the Green's function and the quasistatic polarizability having radiation correction, a Drude model having small damping term is used to describe the dielectric function of the core of the coated metal nanoparticles.

Once again, we are using the configuration mentioned in Fig. 3.1, a one-dimensional diatomic chain with identical coated metal nanoparticles, i.e. non-dispersive dielectric shell having identical permittivity $\epsilon_2 = \epsilon_3$ for site A and site B, for simplicity, we use ϵ_2 to describe the constant permittivity of all the shells. While unlike Chapter 3.1, the chain is not infinitely long but with a finite length this time. We first study a finite diatomic chain with total chain length $N = 32$, i.e. 32 coated metal nanoparticles, for which the nanoparticles are denoted by n such that it is ranging from 0 to 31, site A nanoparticles are defined by $n = 0, 2, \dots, 30$, while site B nanoparticles are defined by $n = 1, 3, \dots, 31$.

In the first set of computation, a quasistatic approximation and nearest neighbour approximation are applied to the dynamic Green's function mentioned in Eq. (3.19), which gives a set of equations:

$$\begin{cases} \alpha^{-1}p_0 = \dfrac{2}{4\pi\epsilon_0}\left[\dfrac{p_1}{t^3}\right], \\ \alpha^{-1}p_n = \dfrac{2}{4\pi\epsilon_0}\left[\dfrac{p_{n-1}}{(d-t)^3} + \dfrac{p_{n+1}}{t^3}\right] \quad \text{for } n = 2,4,\dots,30, \\ \alpha^{-1}p_n = \dfrac{2}{4\pi\epsilon_0}\left[\dfrac{p_{n-1}}{t^3} + \dfrac{p_{n+1}}{(d-t)^3}\right] \quad \text{for } n = 1,3,\dots,29, \\ \alpha^{-1}p_{31} = \dfrac{2}{4\pi\epsilon_0}\left[\dfrac{p_{30}}{t^3}\right]. \end{cases} \tag{3.20}$$

Note that the first and the last equations in Eq. (3.20) are identified separately owing to the fact that they are describing the electromagnetic response of the dipole moments in the edge sites of the one-dimensional diatomic chain. Also, quasistatic approximation is adopted for the explicit polarizability states in Eq. (3.13), which eventually makes the radiation correction term disappeared, with the core of the coated metal nanoparticles described by lossless-Drude model, i.e. $\epsilon_1 = 1 - (\omega_p/\omega)^2$. Now, rewrite Eq. (3.20) in a matrix form yields:

$$\begin{bmatrix} 0 & \frac{2}{4\pi\epsilon_0}\frac{1}{t^3} & 0 & \cdots & 0 \\ \frac{2}{4\pi\epsilon_0}\frac{1}{t^3} & 0 & \frac{2}{4\pi\epsilon_0}\frac{1}{(d-t)^3} & \cdots & 0 \\ 0 & \frac{2}{4\pi\epsilon_0}\frac{1}{(d-t)^3} & 0 & \cdots & 0 \\ \vdots & \ddots & \ddots & \ddots & \vdots \\ 0 & 0 & \cdots & \frac{2}{4\pi\epsilon_0}\frac{1}{t^3} & 0 \end{bmatrix} \begin{bmatrix} p_0 \\ p_1 \\ p_2 \\ \vdots \\ p_{31} \end{bmatrix} = \alpha^{-1}\begin{bmatrix} p_0 \\ p_1 \\ p_2 \\ \vdots \\ p_{31} \end{bmatrix}. \tag{3.21}$$

Eq. (3.21) looks very much similar to the eigenvalue problem mentioned in Eq. (3.18) when we were considering the infinitely long chain using Bloch's Theorem previously. Yet the biggest difference is that the

matrix on the left-hand side is no longer a 2×2 matrix, instead it is a 32×32 matrix, denoted by $\mathbf{M}_N$, which is already generalized as an $N \times N$ matrix having its size depends on the chain length N. Knowing the fact that the diatomic plasmonic chain is with finite length, Bloch's Theorem is no longer applicable thereby implies that $\mathbf{M}_N$ is not in k space, dispersion relation cannot be obtained. In spite of this, one can plot the coupled longitudinal modes supported by the diatomic chain in frequency-domain through the formalism below, rewrite Eq. (3.21), we have:

$$\begin{bmatrix} \alpha^{-1} & \frac{-2}{4\pi\epsilon_0}\frac{1}{t^3} & 0 & \cdots & 0 \\ \frac{-2}{4\pi\epsilon_0}\frac{1}{t^3} & \alpha^{-1} & \frac{-2}{4\pi\epsilon_0}\frac{1}{(d-t)^3} & \cdots & 0 \\ 0 & \frac{-2}{4\pi\epsilon_0}\frac{1}{(d-t)^3} & \alpha^{-1} & \cdots & 0 \\ \vdots & \ddots & \ddots & \ddots & \vdots \\ 0 & 0 & \cdots & \frac{-2}{4\pi\epsilon_0}\frac{1}{t^3} & \alpha^{-1} \end{bmatrix} \begin{bmatrix} p_0 \\ p_1 \\ p_2 \\ \vdots \\ p_{31} \end{bmatrix} = 0. \tag{3.22}$$

We regard the 32×32 matrix in the left-hand side of Eq. (3.22) a modified $\mathbf{M}_{32}$, denoted by $\mathbf{M}_{32,\text{modified}}$, that is,

$$\mathbf{M}_{32,\text{modified}} p_n = 0, \tag{3.23}$$

where,

$$\mathbf{M}_{32,\text{modified}} = \begin{bmatrix} \alpha^{-1} & \frac{-2}{4\pi\epsilon_0}\frac{1}{t^3} & 0 & \cdots & 0 \\ \frac{-2}{4\pi\epsilon_0}\frac{1}{t^3} & \alpha^{-1} & \frac{-2}{4\pi\epsilon_0}\frac{1}{(d-t)^3} & \cdots & 0 \\ 0 & \frac{-2}{4\pi\epsilon_0}\frac{1}{(d-t)^3} & \alpha^{-1} & \cdots & 0 \\ \vdots & \ddots & \ddots & \ddots & \vdots \\ 0 & 0 & \cdots & \frac{-2}{4\pi\epsilon_0}\frac{1}{t^3} & \alpha^{-1} \end{bmatrix}. \tag{3.24}$$

In order to have a non-trivial solution, determinant of $\mathbf{M}_{32,\text{modified}}$ must be zero. Recall the formalism of the quasistatic polarizability in Eq. (3.13), we know it is indeed a function of ω, which tells us that the $\mathbf{M}_{32,\text{modified}}$ is also a function of ω. Generally, as the chain under consideration is not always sufficiently short or with a simple expression, which in turn gives us a big complicated matrix $\mathbf{M}_{N,\text{modified}}(\omega)$, where N = Chain length. It is usually hard to search the root directly for the equation $\det\left|\mathbf{M}_{N,\text{modified}}(\omega)\right| = 0$ in locating the resonant states supported by the plasmonic chain. An alternatively way in doing this is to do the density plot on the quantity $1/\det\left|\mathbf{M}_{N,\text{modified}}(\omega)\right|$ against ω as it consumes much less computational power [7]. By sweeping the ω within certain range, the quantity $1/\det\left|\mathbf{M}_{N,\text{modified}}(\omega)\right|$ will give a big value whenever there is a supported plasmon mode, hence resonant states can be located easily. Furthermore, each distinct sweeping frequency ω will imply the matrix $\mathbf{M}_{N,\text{modified}}(\omega)$ having N eigenvalues together with N eigenvectors. By definition, $\det\left|\mathbf{M}_{N,\text{modified}}(\omega)\right| = \prod_i^N \lambda_i$, which equals to the product of all eigenvalues of $\mathbf{M}_{N,\text{modified}}(\omega)$ at that specified frequency. Now if we consider a particular frequency where resonant states should be found, obviously at that particular frequency $\det\left|\mathbf{M}_{N,\text{modified}}(\omega)\right| = 0$, or we can justify there exist one eigenvalue, or some eigenvalues λ_i of $\mathbf{M}_{N,\text{modified}}(\omega)$ vanished at that particular frequency. In this way, plotting $1/\det\left|\mathbf{M}_{N,\text{modified}}(\omega)\right|$ or $1/\min|\lambda|$ against ω are literally the same, both of them will give a huge quantity at the resonant states of coupled plasmon mode where $\min|\lambda| =$ the minimum eigenvalue of $\mathbf{M}_{N,\text{modified}}(\omega)$ after taking the absolute sign.

Like the aforesaid, we will analyze the coupled longitudinal mode supported in the one-dimensional diatomic chain by plotting the $1/\min|\lambda|$ against ω using Eq. (3.24), see Fig. 3.4. The results are obtained using previous setup in calculating band gap (see Fig. 3.3) except chain length $N = 32$ for this time.

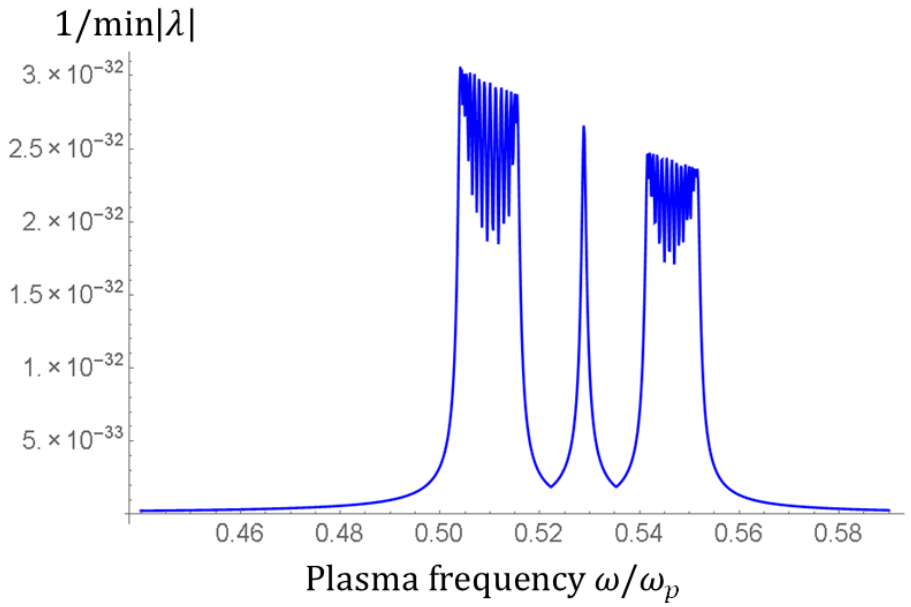

Figure 3.4: Plotting of $1/\min|\lambda|$ against normalized plasma frequency ω/ω_p for a one-dimensional diatomic plasmonic chain using identical coated metal nanoparticles for both site A and site B, with chain length $N = 32$. Results are obtained using quasistatic approximation and nearest neighbor approximation on Green's function, a quasistatic polarizability with core of coated nanoparticle described by lossless-Drude model. It shows the coupled longitudinal modes supported in the diatomic chain whenever a large quantity of $1/\min|\lambda|$ appears. The diatomic chain is with $d = 57.1\text{nm}$, $t = 34.3\text{nm}$. A band gap is observed in between $0.515\omega_p$ and $0.542\omega_p$, also a supported longitudinal mode is found in between the band gap at about $0.529\omega_p$, which should be the topological edge state as expected.

From Fig. 3.4, we confirm that there is a band gap in between $0.515\omega_p$ and $0.542\omega_p$ when considering a one-dimensional diatomic chain with chain length $N = 32$, which shows an exact conformity to the results obtained from an infinitely long diatomic chain, see Fig. 3.3. This result is predictable as in both case, quasistatic approximation and nearest neighbor approximation are in used. Moreover, Fig. 3.4 states that there is a state exist within the band gap at about $0.529\omega_p$, which should be the topological edge state with fields localized at the two edges of the finite diatomic chain.

In order to verify the existence of the edge state in the diatomic chain, we look into the magnitude profile of the dipole moments at different eigenstates. Here, we can compute the dipole moment if there is an external electric field exists so that Eq. (3.11) is valid, combining with Eq. (3.22):

$$\begin{bmatrix} \alpha^{-1} & \frac{-2}{4\pi\epsilon_0}\frac{1}{t^3} & 0 & \cdots & 0 \\ \frac{-2}{4\pi\epsilon_0}\frac{1}{t^3} & \alpha^{-1} & \frac{-2}{4\pi\epsilon_0}\frac{1}{(d-t)^3} & \cdots & 0 \\ 0 & \frac{-2}{4\pi\epsilon_0}\frac{1}{(d-t)^3} & \alpha^{-1} & \cdots & 0 \\ \vdots & \ddots & \ddots & \ddots & \vdots \\ 0 & 0 & \cdots & \frac{-2}{4\pi\epsilon_0}\frac{1}{t^3} & \alpha^{-1} \end{bmatrix} \begin{bmatrix} p_0 \\ p_1 \\ p_2 \\ \vdots \\ p_{31} \end{bmatrix} = \begin{bmatrix} E_{\text{ext},0} \\ E_{\text{ext},1} \\ E_{\text{ext},2} \\ \vdots \\ E_{\text{ext},31} \end{bmatrix}, \quad (3.25)$$

where $E_{\text{ext},n} =$ external electric field experienced by the coated nanoparticle denoted by n. For simplicity, we assume all the nanoparticles

in the finite diatomic chain experiencing an identical arbitrary electric field $E_{\text{ext},n} = 1$ for $n = 0,1,2,\dots,31$. Therefore the dipole moment p can be easily determined:

$$\begin{bmatrix} p_0 \\ p_1 \\ p_2 \\ \vdots \\ p_{31} \end{bmatrix} = \text{Inverse}\left[\mathbf{M}_{32,\text{modified}}(\omega)\right] \cdot \begin{bmatrix} 1 \\ 1 \\ 1 \\ \vdots \\ 1 \end{bmatrix}, \tag{3.26}$$

Using the results in Fig. 3.4, we know the eigenstates supported by the diatomic chain in certain frequency (Lower band, upper band, a state within band gap). Putting the corresponding ω into Eq. (3.26), dipole moments along the chain can be plotted, see Fig. 3.5. As the band gap is ranging from $0.515\omega_p < \omega < 0.542\omega_p$, the magnitude profile of real part and complex part of the dipole moment p_n for $n = 0,1,\dots,31$ is plotted for eigenstates right below band gap at around $\omega = 0.515\omega_p$, within the band gap at $\omega = 0.529\omega_p$ and above the band gap at $\omega = 0.545\omega_p$ in Fig. 3.5(a), (b) and (c) respectively. Notice that Fig. 3.5(b) is showing the magnitude profile of the eigenstate located within the band gap, which we suspect it is an edge state with fields localized in two edges of the diatomic chain, is being verified now as the dipole moments at two edges of the diatomic chain posing a strong magnitude and is decaying among going inwards of the diatomic chain.

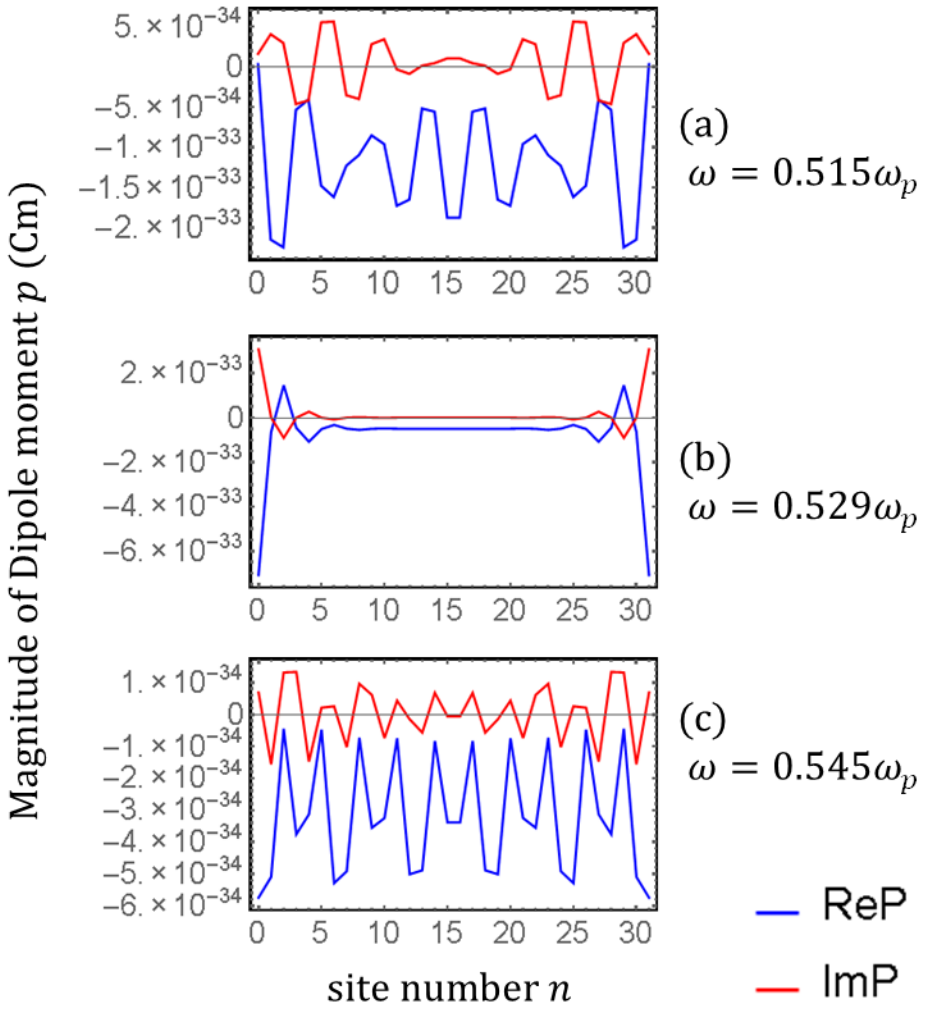

Figure 3.5: (Color online) Plotting of magnitude of the dipole moment p_n along the finite one-dimensional diatomic chain at three eigenstates suggested in Fig. 3.4. (a) Eigenstate below the band gap for $\omega = 0.515\omega_p$; (b) Eigenstate in between the band gap for $\omega = 0.529\omega_p$; (c) Eigenstate above the band gap for $\omega = 0.545\omega_p$; The blue line represents real part of the magnitude of the dipole moment, the orange line represents complex part. Fig. 3.5(b) verifies the supported mode found in between the band gap in Fig. 3.4 is an edge state having fields localized in two edges of the diatomic chain.

It seems there are a lot of approximation in the above calculation,

the core of the identical coated metal nanoparticles are so ideal that they do not have any loss. While in this part, we will repeat the calculation on a finite chain with a similar setup, yet without using quasistatic approximation and nearest neighbor approximation on both the Green's function and polarizability, also the core of the coated metal nanoparticles is described by a commonly used Drude model.

Since we are not going to use the approximation this time, we have to get back to Eq. (3.11), that is:

$$\alpha^{-1}p_n = \sum_{m\neq n}\frac{2}{4\pi\epsilon_0}\left[p_m\left(\frac{1}{r_{mn}^3}-\frac{ik}{r_{mn}^2}\right)e^{ikr_{\mathrm{mn}}}\right]+E_{\mathrm{ext},n}. \qquad (3.27)$$

Note that the $\hat{x}$ term is directly canceled in right-hand side of Eq. (3.11) for simplicity. Luckily, with all the calculation done previously, this time we will directly aim for the expression on $1/\min|\lambda|$ so that we can do the sweeping on frequency ω in identifying the coupled longitudinal plasmon mode supported by the diatomic chain. To find the expression of $1/\min|\lambda|$, we first omit the external electric field, rewrite Eq. (3.27) in the format of Eq. (3.22), we have:

$$\begin{bmatrix} \alpha^{-1} & \frac{-2}{4\pi\epsilon_0}\left(\frac{1}{r_{1,0}^3}-\frac{ik}{r_{1,0}^2}\right)e^{ikr_{1,0}} & \cdots & \frac{-2}{4\pi\epsilon_0}\left(\frac{1}{r_{31,0}^3}-\frac{ik}{r_{31,0}^2}\right)e^{ikr_{31,0}} \\ \frac{-2}{4\pi\epsilon_0}\left(\frac{1}{r_{0,1}^3}-\frac{ik}{r_{0,1}^2}\right)e^{ikr_{0,1}} & \alpha^{-1} & \cdots & \frac{-2}{4\pi\epsilon_0}\left(\frac{1}{r_{31,1}^3}-\frac{ik}{r_{31,1}^2}\right)e^{ikr_{31,1}} \\ \frac{-2}{4\pi\epsilon_0}\left(\frac{1}{r_{0,2}^3}-\frac{ik}{r_{0,2}^2}\right)e^{ikr_{0,1}} & \frac{-2}{4\pi\epsilon_0}\left(\frac{1}{r_{1,2}^3}-\frac{ik}{r_{1,2}^2}\right)e^{ikr_{0,1}} & \cdots & \frac{-2}{4\pi\epsilon_0}\left(\frac{1}{r_{31,2}^3}-\frac{ik}{r_{31,2}^2}\right)e^{ikr_{31,2}} \\ \vdots & \ddots & \ddots & \vdots \\ \frac{-2}{4\pi\epsilon_0}\left(\frac{1}{r_{0,31}^3}-\frac{ik}{r_{0,31}^2}\right)e^{ikr_{0,31}} & \cdots & \frac{-2}{4\pi\epsilon_0}\left(\frac{1}{r_{30,31}^3}-\frac{ik}{r_{30,31}^2}\right)e^{ikr_{30,31}} & \alpha^{-1} \end{bmatrix}\begin{bmatrix} p_0 \\ p_1 \\ p_2 \\ \vdots \\ p_{31} \end{bmatrix} = 0, \qquad (3.28)$$

where $r_{m,n}$ is the distance between the sites denoted by m and n in the

one-dimensional diatomic chain, k is a wave number and can be replaced by $k = \omega/c$. Here we denote the 32×32 matrix in the left-hand side of Eq. (3.28) by $\mathbf{M}_{32,\text{precise}}$, which gives:

$$\mathbf{M}_{32,\text{precise}} p_n = 0. \tag{3.29}$$

Also, by replacing wave number k with ω/c, the 32×32 matrix $\mathbf{M}_{32,\text{precise}}$ can be once again became a function of ω, as long as the wave number found in the explicit expression of the quasistatic polarizability having radiation loss in Eq. (3.13) has been replaced with ω/c, since it exists this time as there is no quasistatic approximation working on it.

So far, the concepts of finding roots (supported eigenstates) using $\det|\mathbf{M}_{32,\text{precise}}(\omega)| = 0$, plotting $1/\det|\mathbf{M}_{32,\text{precise}}(\omega)|$ or $1/\min|\lambda|$ against ω show no contradiction without using quasistatic approximation and nearest neighbor approximation. Therefore we may plot the $1/\min|\lambda|$ against ω using Eq. (3.28) such that $\min|\lambda| =$ the minimum eigenvalue of $\mathbf{M}_{32,\text{precise}}(\omega)$ after taking the absolute sign, see Fig. 3.6. The results are obtained using previous configuration mentioned in Fig. 3.4 except core described by a common Drude model $\epsilon_1 = 1 - \omega_p^2/\omega(i\nu_c + \omega)$ with plasma frequency $\omega_p = 2\pi \times 1.6 \times 10^{15} = 1.01 \times 10^{16}\text{rad s}^{-1}$, plasma collision frequency (Loss) $\nu_c = 0.0001 \times \omega_p = 1.01 \times 10^{12}\text{rad s}^{-1}$.

Although we are considering a system without using the approximation, from Fig. 3.6, we notice the range of band gap is almost exactly the same with the one using approximation, which is also ranging from $0.515\omega_p$ to $0.542\omega_p$. A longitudinal coupled plasmon mode is found

in the band gap at about $0.529\omega_p$ in both of the case. Comparing the results of Fig. (3.4) and (3.6), the nearest neighbor approximation and quasistatic approximation is good enough in our system. Nevertheless, we still take a closer look on the dipole moments of the supported eigenstates.

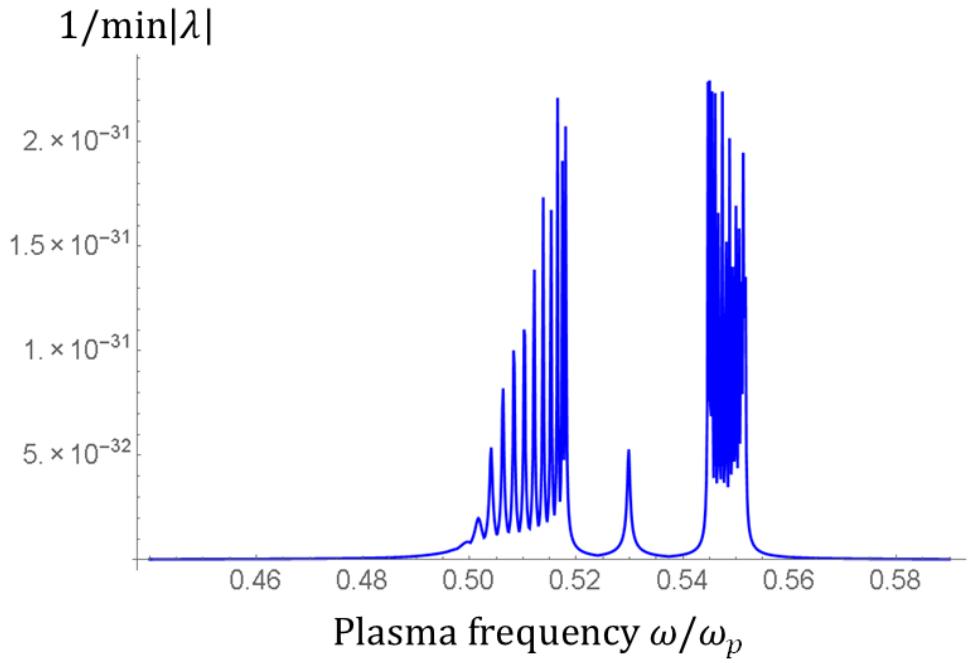

Figure 3.6: Plotting of $1/\min|\lambda|$ against normalized plasma frequency ω/ω_p for a one-dimensional diatomic plasmonic chain using identical coated metal nanoparticles for both site A and site B, with chain length $N = 32$. Results are obtained without using quasistatic approximation and nearest neighbor approximation on Green's function, a quasistatic polarizability with core of coated nanoparticle described by Drude model having loss $= 0.0001 \times \omega_p$. It shows the coupled longitudinal modes supported in the diatomic chain whenever a large quantity of $1/\min|\lambda|$ appears. The diatomic chain is with $d = 57.1\text{nm}$, $t = 34.3\text{nm}$. A band gap is observed in between $0.515\omega_p$ and $0.542\omega_p$, also a supported longitudinal mode is found in between the band gap at about $0.529\omega_p$, which should be the topological edge state as expected.

Following Eq. (3.25), combining with Eq. (3.27), we have:

$$\mathbf{M}_{32,\text{precise}} \begin{bmatrix} p_0 \\ p_1 \\ p_2 \\ \vdots \\ p_{31} \end{bmatrix} = \begin{bmatrix} E_{\text{ext},0} \\ E_{\text{ext},1} \\ E_{\text{ext},2} \\ \vdots \\ E_{\text{ext},31} \end{bmatrix}, \tag{3.30}$$

for which $\mathbf{M}_{32,\text{precise}}$ is a complicated matrix with size 32×32. Assuming an arbitrary external incidents electric field $E_{\text{ext},n} = 1$ for $n = 0,1,2,\dots,31$, dipole moments can be calculated by:

$$\begin{bmatrix} p_0 \\ p_1 \\ p_2 \\ \vdots \\ p_{31} \end{bmatrix} = \left[\mathbf{M}_{32,\text{precise}}(\omega)\right]^{-1} \cdot \begin{bmatrix} 1 \\ 1 \\ 1 \\ \vdots \\ 1 \end{bmatrix}. \tag{3.31}$$

Similiar to Fig. 3.5, we pick three eigenstates to plot in Fig. 3.7(a), (b), and (c) respectively. That is, the eigenstate right below band gap at $\omega = 0.515\omega_p$, within the band gap at $\omega = 0.529\omega_p$, and above the band gap at $\omega = 0.545\omega_p$. Among comparing the results with Fig. 3.5(a), (b), and (c), the magnitude profile of the dipole moment p_n does not vary much as expected. If we further look into the eigenstates located within band gap, see Fig. 3.5 (b) and Fig. 3.7(b), although the dipole moments flip from real plane to complex plane, still, it is strongly localized in two edges of the diatomic chain, which tells that there is a longitudinal edge mode supported in the chain within the band gap range.

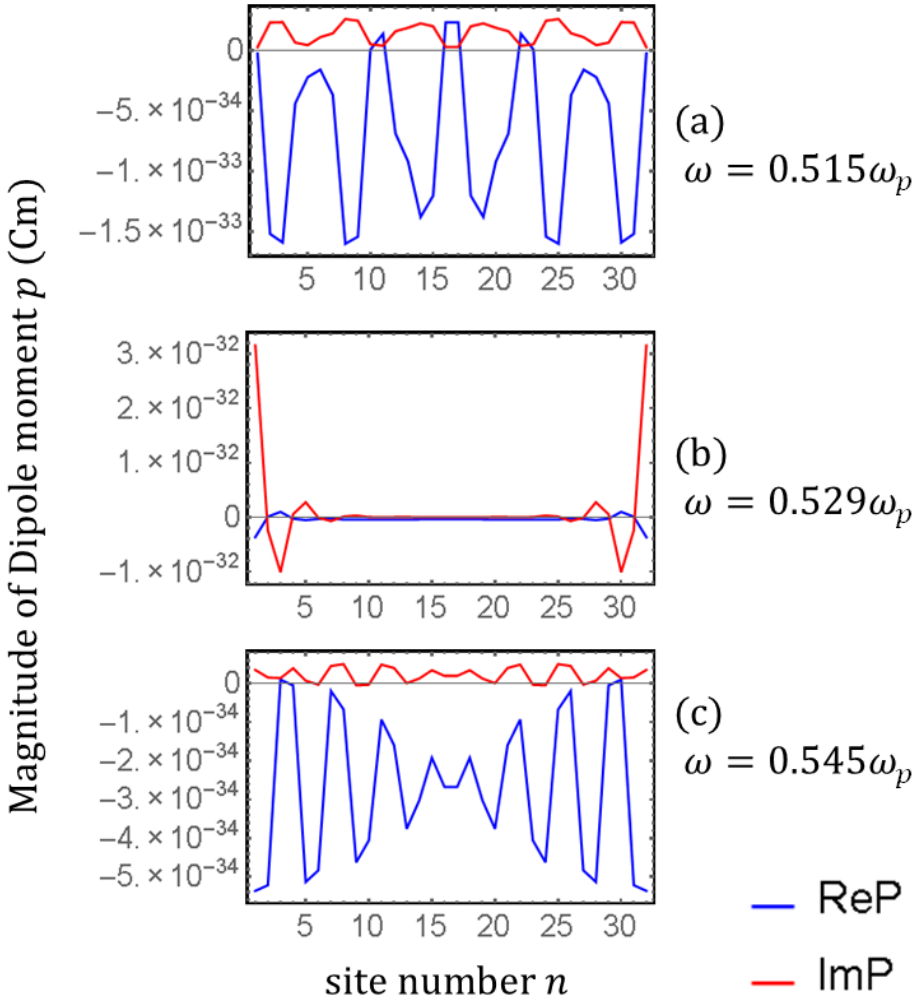

Figure 3.7: (Color online) Plotting of magnitude of the dipole moment p_n along the finite one-dimensional diatomic chain at three eigenstates suggested in Fig. 3.6. (a) Eigenstate below the band gap for $\omega = 0.515\omega_p$; (b) Eigenstate in between the band gap for $\omega = 0.529\omega_p$; (c) Eigenstate above the band gap for $\omega = 0.545\omega_p$; The blue line represents real part of the magnitude of the dipole moment, the orange line represents complex part. Fig. 3.7(b) verifies the supported mode found in between the band gap in Fig. 3.6 is an edge state having fields localized in two edges of the diatomic chain.

3.3 Extinction cross section

In this part, we would like to verify the existence of edge state in a finite one-dimensional diatomic chain with identical coated metal nanoparticles in site A and site B embedded in air with vacuum permittivity $\epsilon_0 = 8.85 \times 10^{-12}\text{F m}^{-1}$, see Fig. 3.1, using a powerful 3D Maxwell solver named Finite-difference time-domain [51] to perform the simulations.

To do this, we first consider a one-dimensional diatomic chain using the setup mentioned in Fig. 3.1. In order to excite the longitudinal dipole moments, a plane wave acts as a stimulate by doing the job of $\mathbf{E}_{\text{ext},n}$ in Eq. (3.11) such that it propagates in a direction perpendicular to the chain axis while polarized along the chain axis. Instead of defining a plane wave source in Lumerical FDTD, we use an advanced source called Total-field scattered-field (TFSF), see Fig. 3.8. The TFSF source is often used to study scattering from small particles, owing to its ability to separate the computation region into two distinct region. Upon defining a TFSF source, the source itself has a box-like structure, inside the box it contains the total field (i.e. sum of the incident field and scattered field), while outside the box it only contains the scattered field. The incident field is simulated as a plane wave having its wave vector perpendicular to the injection plane. The main advantage of using the TFSF source is that the absorption cross section C_{abs} and scattering cross section C_{sca} can be obtained easily by adding a built-in analysis box named 'cross_section' inside and outside the TFSF source (box-like) respectively. With a known absorption cross section and

scattering cross section, the extinction cross section C_{ext} can be calculated manually using $C_{\text{ext}} = C_{\text{abs}} + C_{\text{sca}}$. The reason of why having the observation on extinction cross section helps identifying edge states will be explained below, also the formulation will lead us to calculate an analytic extinction spectrum, which can also be used to compare to simulation results in FDTD.

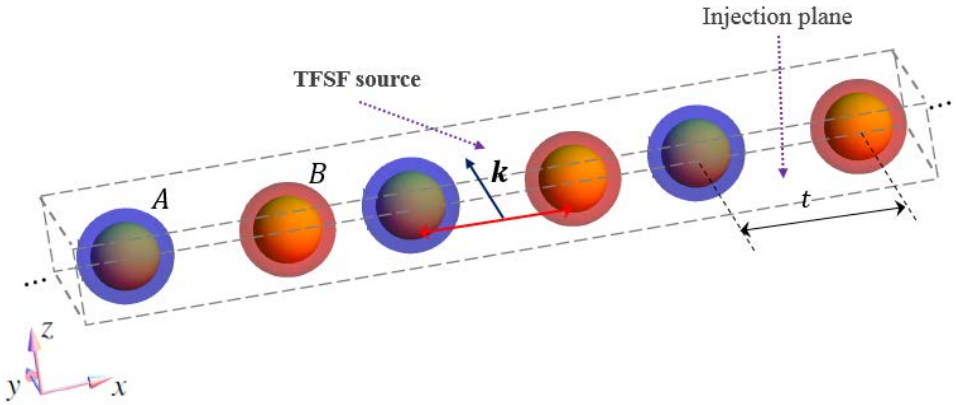

Figure 3.8: Illustration of the setup in FDTD simulation. We can see the diatomic chain is with configuration mentioned in Fig. 3.1. The two short dotted lines in the edge of the chain simply means you can pad the chain with more unit cells. The box with grey-colored dash-line denotes the TFSF source and must cover the entire chain. Inside the box it calculates the total field, while only scattered field will be calculated outside the box. The red arrow denotes the polarization direction (i.e. electric field oscillating along) and the blue arrow denotes the propagating direction.

We begin with the exact solution of the extinction cross section expressed by J. D. Jackson [48], using the configuration of Fig. 3.9:

$$C_{\text{ext}} = \frac{4\pi}{k}\,\text{Im}\left[\frac{\mathbf{E}_0^*}{|\mathbf{E}_0|}\cdot\frac{\mathbf{F}(\mathbf{n}=\mathbf{n}_0)}{|\mathbf{E}_0|}\right], \tag{3.32}$$

where $\mathbf{E}_0 =$ external plane wave, $\mathbf{F} =$ scattering amplitude, $\mathbf{n} = \hat{\mathbf{R}}$, $\mathbf{n}_0 = \hat{\mathbf{k}}_0$, if the observing point is placed infinitely far away, we have:

$$\left|\mathbf{R} - \mathbf{r}_j\right| \approx R - \mathbf{r}_j \cdot \mathbf{n} \rightarrow \quad \mathbf{n}_j = \frac{\mathbf{R} - \mathbf{r}_j}{\left|\mathbf{R} - \mathbf{r}_j\right|} \approx \mathbf{n}, \tag{3.33}$$

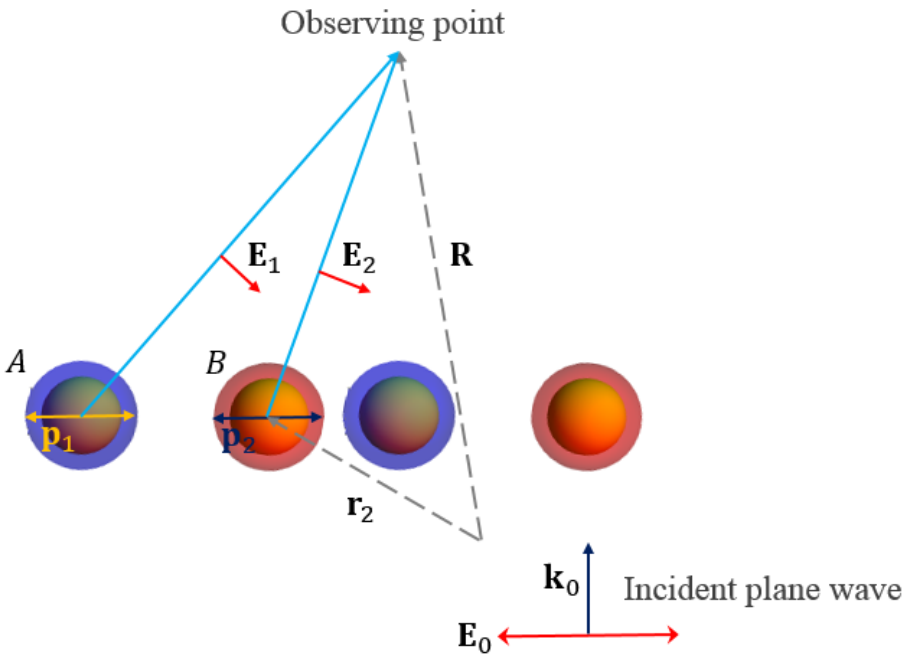

Figure 3.9: Illustration of a general setup in calculating the extinction cross section of a cluster of scatters. The incident electric field is polarized along the chain axis, and propagates in the $\mathbf{k}_0$ direction. There will be excited dipole moment $\mathbf{p}_j$ on the j^{th} nanoparticles which having distance $\mathbf{r}_j$ from origin. The observing point has displacement $\mathbf{R}$ from origin and experiences the dipole electric field $\mathbf{E}_j$ generated by $\mathbf{p}_j$. From the figure, we know $\mathbf{n}_0 \cdot \mathbf{p}_j = 0$, $\mathbf{n}_0 \cdot \mathbf{r}_j =$ constant, $\mathbf{E}_0^* \cdot \mathbf{p}_j = E_0 p_j$.

If we want to calculate the scattering amplitude $\mathbf{F}$, we have to first consider the scattered electric field generated by dipole moment $\mathbf{p}_j$, using the expressions given by [48], combining with Eq. (3.33) yields:

$$\mathbf{E}_j \approx \frac{k^2}{4\pi\epsilon_0}\left(\mathbf{p}_j - \left(\mathbf{n} \cdot \mathbf{p}_j\right)\mathbf{n}\right)e^{-ik\mathbf{n}\cdot\mathbf{r}_j}\frac{e^{-ikR}}{R}. \tag{3.34}$$

And the total scattered electric field is just summing all the scattered electric field generated by all dipole moments, which gives:

$$\mathbf{E}_s = \sum_j \mathbf{E}_j = \mathbf{F}(\mathbf{n})\frac{e^{-ikR}}{R} \quad \rightarrow$$
$$\mathbf{F}(\mathbf{n}) = \frac{k^2}{4\pi\epsilon_0}\sum_j (\mathbf{p}_j - (\mathbf{n}\cdot\mathbf{p}_j)\mathbf{n})e^{-ik\mathbf{n}\cdot\mathbf{r}_j}. \tag{3.35}$$

Notice that $\mathbf{F}(\mathbf{n})$ is the scattering vector amplitude we want, substituting the expression of $\mathbf{F}(\mathbf{n})$ in Eq. (3.35) into Eq. (3.32) using the relation concluded from Fig. 3.9,

$$C_{\text{ext}} = \frac{k}{\epsilon_0|\mathbf{E}_0|}\,\text{Im}\sum_j p_j, \tag{3.36}$$

Eq. (3.36) basically tells an important information, that is the extinction cross section is obviously a variable in frequency domain and is greatly depends on the imaginary part of the magnitude of all the dipole moments in the chain. In the previous section, we successfully calculated the magnitude of the excited dipole moment throughout the chain, if one carefully looks at Fig. 3.7(b), a magnitude profile of dipole moments for the edge state when considering a one-dimensional diatomic chain with no quasistatic approximation and nearest neighbor approximation, you can see that the imaginary part of the dipole moments at the edge will give a significant value, while Eq. (3.36) tells you that if this is the case, then the extinction spectrum of that particular frequency for the edge state to sustain will also pose a large value. Therefore, from the analytic aspect, doing observation on the extinction spectrum will definitely help locating the edge state, especially for Lumerical FDTD as it already turns the output data into frequency domain using Fourier transform automatically.

Unlike the previous section, due to the limitations on computational power, we consider a finite one-dimensional diatomic chain using the setup mentioned previously in Fig. 3.6 except we consider chain length $N = 8$ instead of 32 this time.

Using the above framework, results are obtained in two approaches: the analytic one using dynamic Green's function without nearest neighbor approximation and a quasistatic polarizability with radiation corrections, a plotting of $1/\min|\lambda|$ against normalized plasma frequency ω/ω_p to locate the band gap and edge state as shown in Fig. 3.10, and the analytic extinction cross section C_{ext} against normalized plasma frequency ω/ω_p is plotted using Eq. (3.36) such that we treat $|\mathbf{E}_0| = 1$, see Fig. 3.11; while the setup mentioned in Fig. 3.8 is conducted by FDTD in the numerical approach with the source being a pulse having frequency ranging from $0.45\omega_p$ to $0.51\omega_p$ and amplitude $= 1$. Note that Lumerical FDTD is a time-domain solver, thus gives results in frequency-domain ranging from $0.45\omega_p$ to $0.51\omega_p$, a simulated extinction cross section C_{ext}, together with absorption and scattering cross section C_{abs} & C_{sca}, is plotted against frequency-domain to compare with the analytic one, see Fig. 3.12.

In Fig. 3.10, as the size of the one-dimensional diatomic chain is significantly reduced from $N = 32$ to $N = 8$, which results in less supported modes within the diatomic chain. From the previous results, we know the difference between applying quasistatic approximation/nearest neighbor approximation and using dynamic Green's function is little in comparing Fig. 3.4 and Fig. 3.6, therefore we can deduce the range of band

gap should also be around $0.515\omega_0$ to $0.546\omega_0$ this time and the peak at around $0.530\omega_0$ should be the edge state we aim for. By further substituting the external electric driving field has amplitude $= 1$, we can calculate the dipole moments in frequency domain, which will eventually help us get the extinction spectrum through Eq. (3.36), see Fig. 3.11.

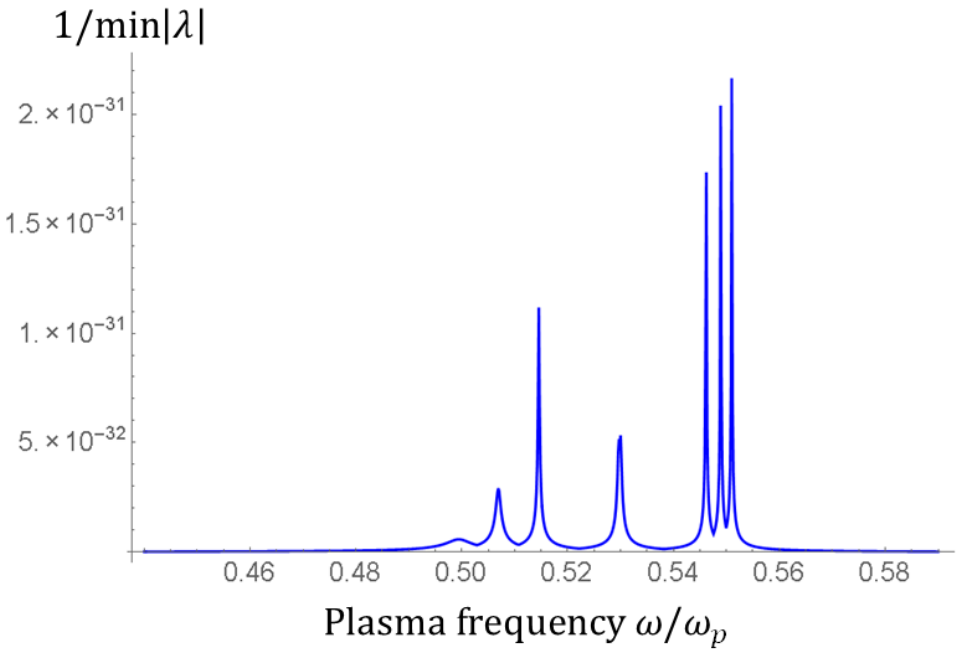

Figure 3.10: Plotting of $1/\min|\lambda|$ against normalized plasma frequency ω/ω_p for a one-dimensional diatomic plasmonic chain using identical coated metal nanoparticles for both site A and site B, with chain length $N = 8$. Results are obtained using dynamic Green's function without nearest neighbor approximation, a quasistatic polarizability with core of coated nanoparticle described by Drude model having loss $= 0.0001 \times \omega_p$. It shows the coupled longitudinal modes supported in the diatomic chain whenever a large quantity of $1/\min|\lambda|$ appears. The diatomic chain is with $d = 57.1\text{nm}$, $t = 34.3\text{nm}$. The supported mode in the middle is at about $0.530\omega_p$, which is in between two other supported mode at about $0.515\omega_p$ and $0.546\omega_p$, are presumed to be the edge state and the range of band gap, respectively.

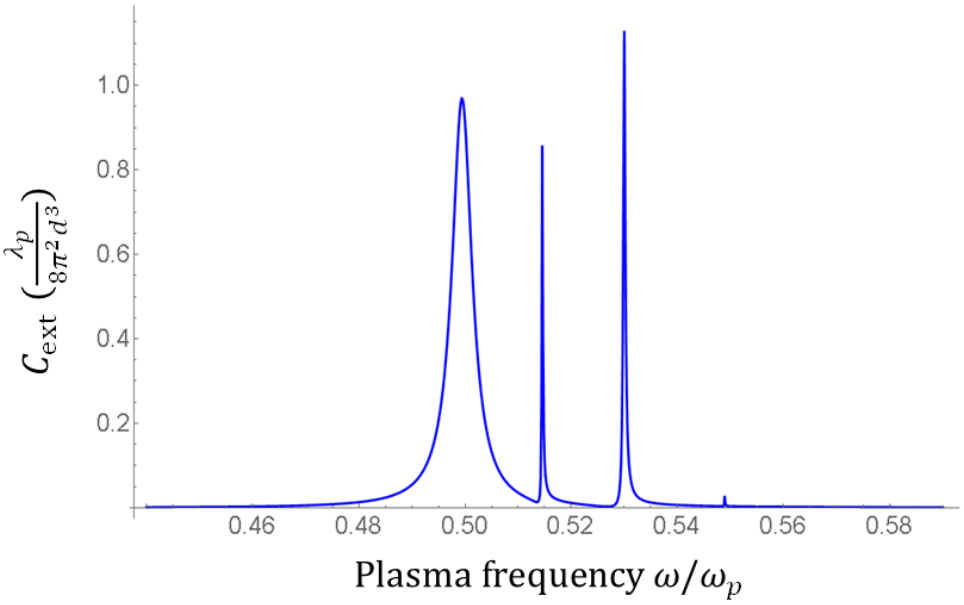

Figure 3.11: Analytic extinction cross section (in unit of $\lambda_p/8\pi^2 d^3$) of the one-dimensional diatomic plasmonic chain using identical coated metal nanoparticles for both site A and site B mentioned in Fig. 3.1, with chain length $N = 8$, against normalized plasma frequency ω/ω_p. The three peaks are at around $0.499\omega_p$, $0.515\omega_p$ and $0.530\omega_p$ such that they are all supported mode shown in Fig. 3.10 and are presumed to be coming from the lower band for the $0.499\omega_p$ and the $0.515\omega_p$ one, and an edge state for the $0.530\omega_p$ one. This figure tells the actual response of the diatomic chain among various frequencies.

In Fig. 3.11, the extinction cross section is plotted in unit of $\lambda_p/8\pi^2 d^3$ such that λ_p is the plasma wavelength and d is the length of a unit cell mentioned in Fig. 3.1. The changing of unit comes from the fact that the wave number k in Eq. (3.36) can be replaced by $k = \frac{\omega/\omega_p}{c/\omega_p} = \frac{\omega/\omega_p}{\lambda_p} 2\pi$ in the purpose of easier reading. By definition, the extinction spectrum tells whether extinction of fields will occur or not at different frequencies, an actual response of the system. We can see there are three

significant peaks at around $0.499\omega_p$, $0.515\omega_p$ and $0.530\omega_p$ such that they are all supported modes within the diatomic chain stated in Fig. 3.10. If we compare the frequency domain in Fig. 3.10 and 3.11, the edge state should be the one with most spiky peak at around $0.530\omega_p$.

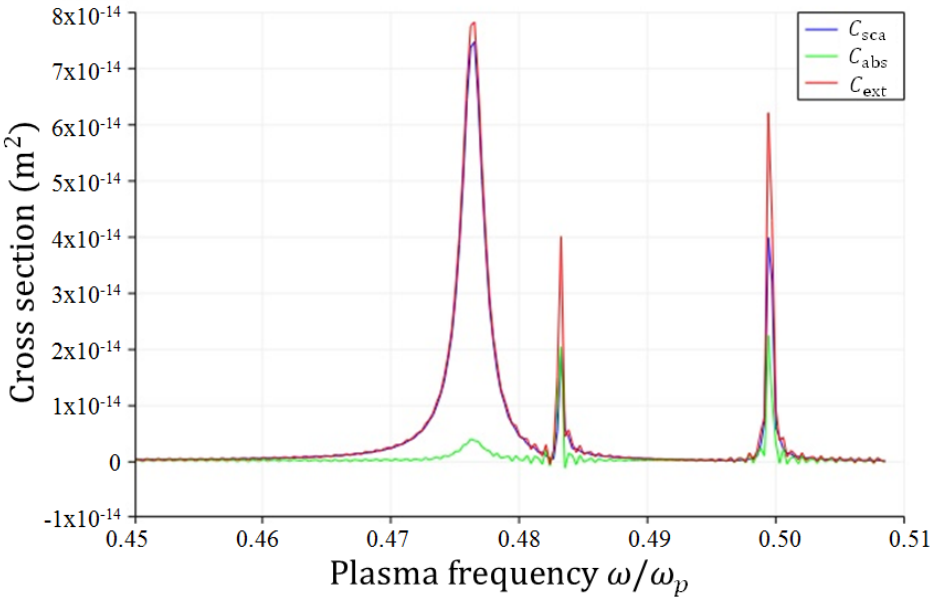

Figure 3.12: (Color online) Cross sections (in unit of m^2) of the one-dimensional diatomic plasmonic chain using identical coated metal nanoparticles for both site A and site B mentioned in Fig. 3.1 using setup explained in Fig. 3.8, with chain length $N = 8$, against normalized plasma frequency ω/ω_p. The mesh in use is 1.5nm within the TFSF source and the simulation time is long enough for a relevant Fourier-transform to take place. Extinction, absorption and scattering cross sections are plotted in different color. The three peaks are at around $0.476\omega_p$, $0.483\omega_p$ and $0.499\omega_p$ such that they are presumed to be the three excited mode shown in Fig 3.11 with slightly shifted frequencies coming from the lower band and the edge state.

Now if we compare the results obtained in using the Lumerical

FDTD as shown in Fig. 3.12, the extinction cross section (red line) shows a lot of conformities with the analytic one, i.e. both of them have three sharp peaks with a broaden one in the most left-hand side...etc., except the peaks are all shifted to a slightly lower frequencies. This looks relevant as the FDTD performs simulations based on the actual parameters and integration through meshes, when we solve the equations analytically, we always treat the sites as point dipole like the coated nanoparticles having electron distribution in phase throughout it while it might not be the case in the actual simulations. If the core of the nanoparticles experiences electron dipole force having phase slightly behind the coated layer, this may result in a decrease in the restoring force, hence the resonance frequencies as shown in Fig. 3.12. In this sense, the peak at the most right-hand side at around $0.499\omega_p$ should be the edge state in our analytic calculation.

To verify this, a 2D field-profile monitor on xy-plane (y the propagating direction of the plane wave) is set to monitor the magnitude of the electric field along the direction of the chain axis E_x throughout the entire spatial distribution in the FDTD simulations. As the results are in frequency-domain, the field patterns of the particular frequencies for the three peaks to take place in Fig. 3.12 will be plotted in Fig. 3.13(b) to compare with Fig. 3.13(a), the magnitude profile of the dipole moments calculated analytically with respect to the resonant frequencies obtained in extinction spectrum in Fig. 3.11, see Fig. 3.13.

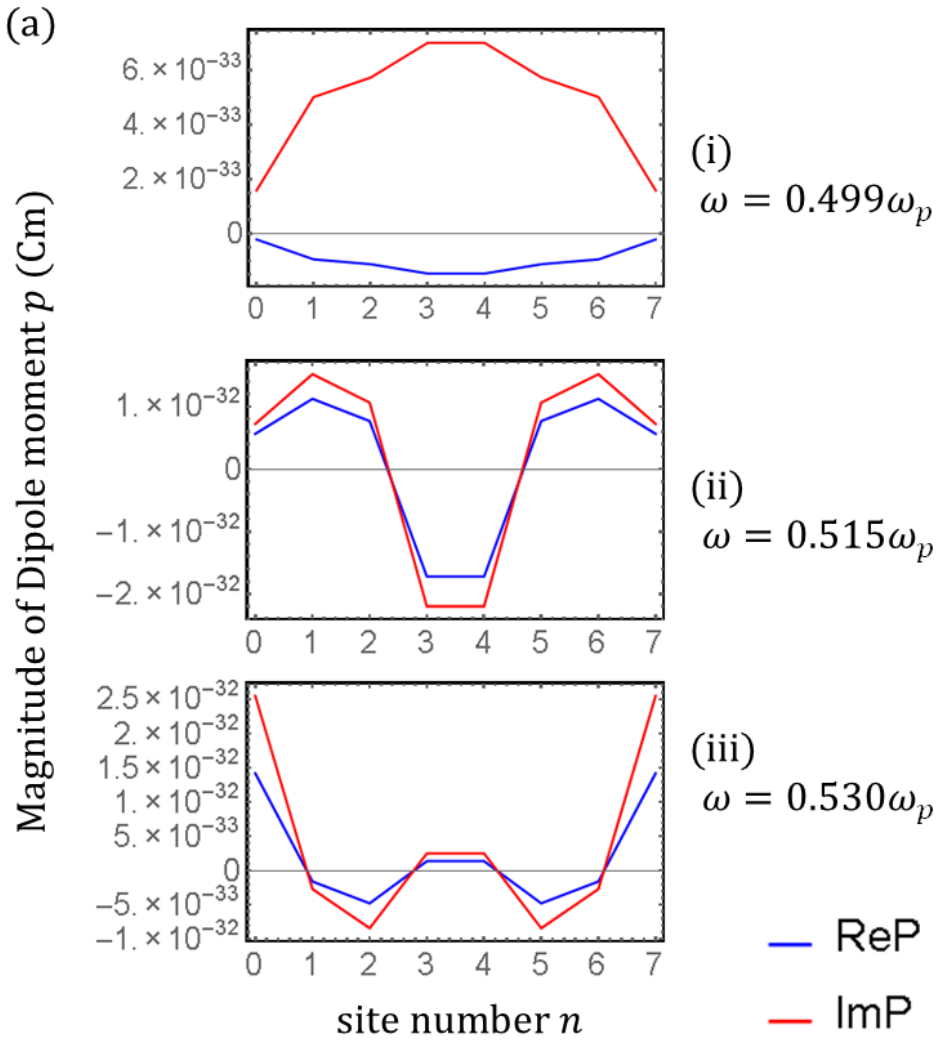
(a)
Magnitude of Dipole moment p (Cm)
$6.\times10^{-33}$
$4.\times10^{-33}$
$2.\times10^{-33}$
0
0 1 2 3 4 5 6 7
(i)
$\omega = 0.499\omega_p$
$1.\times10^{-32}$
0
$-1.\times10^{-32}$
$-2.\times10^{-32}$
0 1 2 3 4 5 6 7
(ii)
$\omega = 0.515\omega_p$
2.5×10^{-32}
$2.\times10^{-32}$
1.5×10^{-32}
$1.\times10^{-32}$
$5.\times10^{-33}$
0
$-5.\times10^{-33}$
$-1.\times10^{-32}$
0 1 2 3 4 5 6 7
(iii)
$\omega = 0.530\omega_p$
site number n
ReP
ImP

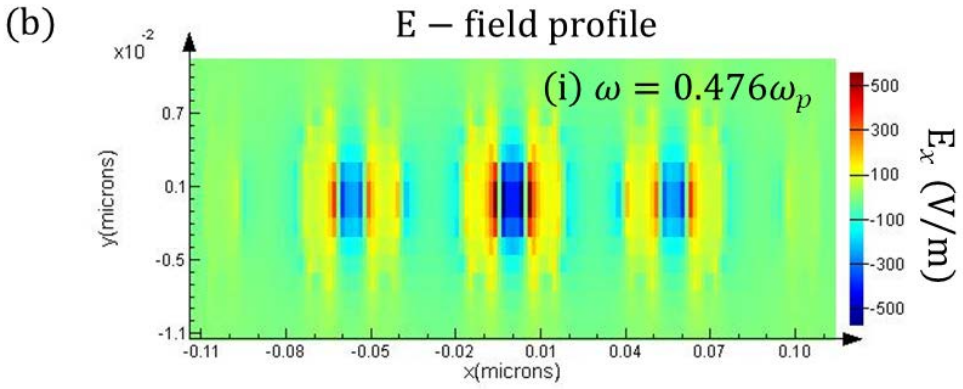
(b)
E − field profile
(i) $\omega = 0.476\omega_p$
x10^-2
0.7
0.1
-0.5
-1.1
y(microns)
-0.11 -0.08 -0.05 -0.02 0.01 0.04 0.07 0.10
x(microns)
500
300
100
-100
-300
-500
E_x (V/m)

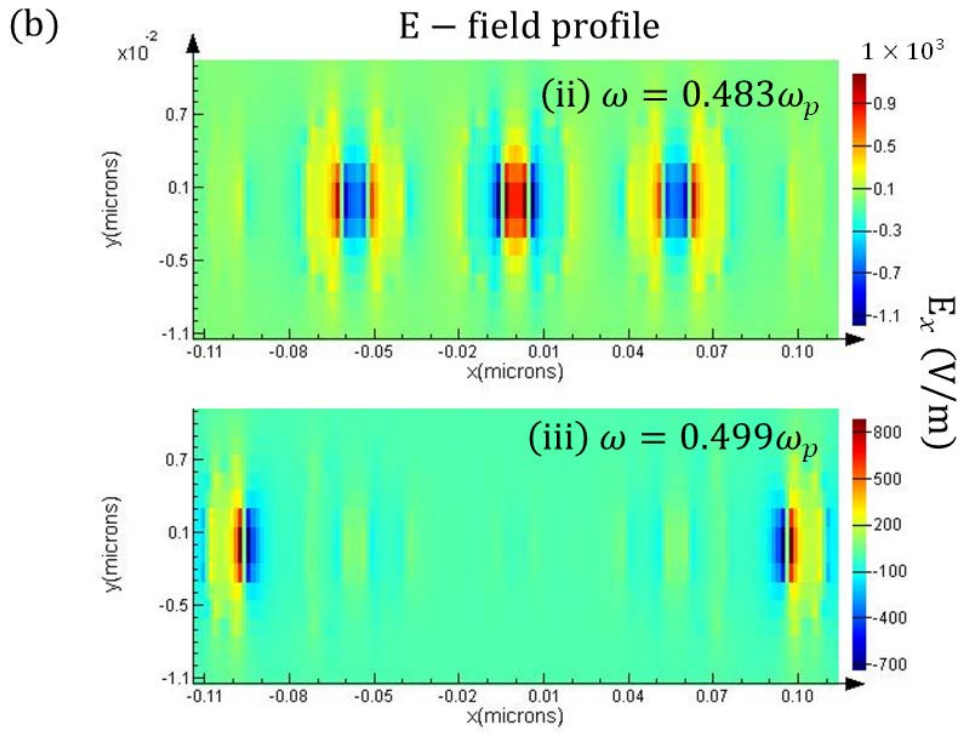

Figure 3.13: (Color online) (a) The spatial magnitude profile of the dipole moments calculated analytically in the one-dimensional diatomic plasmonic chain with identical coated metal nanoparticles being the individuals, having chain length $N = 8$, at three different picked off frequencies described in Fig. 3.11, (i) $\omega = 0.499\omega_p$, (ii) $\omega = 0.515\omega_p$, (iii) $\omega = 0.530\omega_p$ such that it corresponds to the edge state. (b) The electric field profile obtained by setting the similar setup in FDTD using 2D field monitor to record the magnitude of E_x throughout the entire spatial distribution of the setup at three different picked off frequencies described in Fig. 3.12, (i) $\omega = 0.476\omega_p$, (ii) $\omega = 0.483\omega_p$, (iii) $\omega = 0.499\omega_p$. The mesh in use is 1.5nm. By comparing the magnitude of the dipole moments in (a) with the electric field profile in (b), one can justify the three peaks mentioned in Fig. 3.11 match those mentioned in Fig. 3.12 with Fig. 3.13(a.iii) and Fig. 3.13(b.iii) being the edge state.

As we presume the resonant frequencies obtained in the cross section plotting in Fig. 3.12 using FDTD simulations are decreased compare

to those obtained in the calculated extinction spectrum in Fig. 3.11, Fig. 3.13 shows agreement with our prediction. For the most left-hand side broaden peaks found in Fig. 3.11 and Fig. 3.12, Fig. 3.13(a.i) tells the dipole moments in the middle part of the chain will have strongest magnitude, results in a strong field localization in the middle of the diatomic chain which decays on moving outward, is being verified in Fig. 3.13(b.i). For the middle spiky peaks observed in Fig. 3.11 and Fig. 3.12, Fig. 3.13(a.ii and b.ii) gives agreement of their dipole moments magnitude and the spatial distribution of the electric field E_x. While for the most right-hand side peaks found in Fig. 3.11 and Fig. 3.12, we expect it is an edge state as Fig. 3.10 predicts that particular supported mode inside the diatomic chain is allocated in between band gap, is being proofed in Fig. 3.13(a.iii and b.iii), as you can see the dipole moments in the edge is of significant magnitude compare to others and the electric field profile suggested that the fields are localized in the edges of the diatomic chain. Going through the results aforesaid once, we can justify that the topological protected edge state do exists in a one-dimensional diatomic chain with identical coated nanoparticles in both the analytic approach and numerical simulations.

3.4 PT-symmetry in diatomic chain

In this last part of Chapter 3, we are going to consider the effect brought by PT-symmetry in the one-dimensional diatomic chain mentioned in Fig. 3.1. The unit cell of the diatomic chain consist of two sites denoted by A and B. Both sites contain a coated metal nanoparticle with core described by dispersive material dielectric function ϵ_1, and is coated by a

non-dispersive dielectric layer with permittivity ϵ_2 and $\epsilon_3 = \epsilon_2^*$ respectively, with an alternatively changing spatial separation t and $d - t$ between sites, see Fig. 3.14.

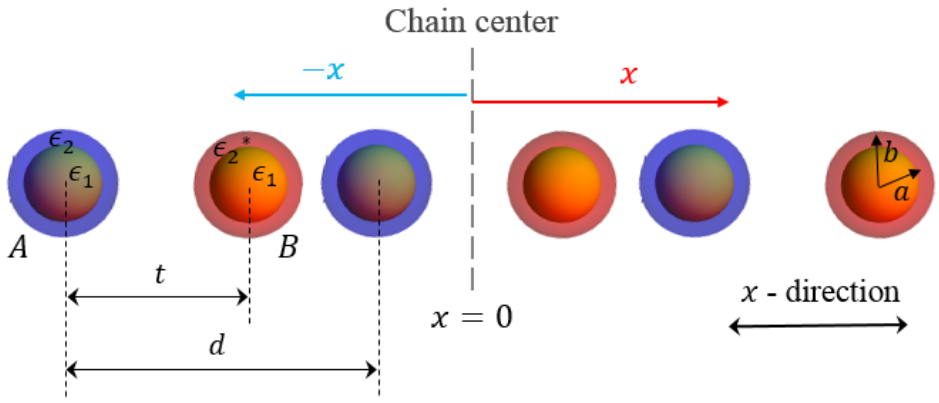

Figure 3.14: Schematic figure of a PT-symmetric one-dimensional coated diatomic plasmonic chain. There are two spherical dispersive metal nanoparticles with dielectric function ϵ_1 coated with non-dispersive dielectrics of different permittivity ϵ_2 and $\epsilon_3 = \epsilon_2^*$ in one single unit cell having two sites, namely A and B. All coated nanoparticles are of the same size with outer radius b, inner radius a. The length of the unit cells and the separation between site A and site B are denoted as d and t respectively. The chain is assumed to be embedded in a medium with relative permittivity ϵ_m = 1. Also an illustration of defining origin in the diatomic chain having number of unit cells an odd number is shown.

To verify the diatomic chain is PT-symmetric, a one dimension coordinate system is plugged in along the x-direction (direction of the chain axis), the origin $x = 0$ is assumed to be in the middle of site A and site B of the $[(U + 1)/2]^{\text{th}}$ unit cell where U is the total number of unit cell in the diatomic chain and is an odd number, or in the middle of site B of

the $(U/2)^{\text{th}}$ unit cell and site A of the $(U/2+1)^{\text{th}}$ unit cell if U is an even number. The right-hand side is denoted as positive x direction and vice versa. Recalling Eq. (1.10) in Chapter 1.5.1, it states that light will undergoes a PT-symmetric potential if the real part of the permittivity is an even function of position x while the imaginary part is an odd function, which can be satisfied using the above mentioned coordinating system. Since the coated dielectric layer of site A and site B have their permittivity formed a complex conjugate pair, which is like implementing a balanced gain/loss into the dielectric shells in site A and site B separately. Such a balanced gain/loss in the spatial configuration breaks the P-symmetry and T-symmetry, but makes the system PT-symmetric.

As the phenomena of obtaining zero extinction cross section at the frequency of topological protected edge state takes place reported by C. W. Ling [46] can be easily observed once the system is PT-symmetric, one may try computing the extinction cross section before optimization. For simplicity and easiness of comparison, we first consider a finite PT-symmetric one-dimensional diatomic chain having chain length $N = 8$ using the setup mentioned in Fig. 3.14, such that the coated metal nanoparticles are slightly different for site A and site B by having a complex conjugate pair for the coated layer permittivity i.e. $\epsilon_2 = 1.5 + 0.01i$ (loss) and $\epsilon_2^* = 1.5 - 0.01i$ (gain), while all are having outer radius $b = 10\text{nm}$, inner radius $a = 10 \times \frac{0.125}{0.175} = 7.143\text{nm}$, core described by Drude model $\epsilon_1 = 1 - \omega_p^2/\omega(i\nu_c + \omega)$ with plasma frequency $\omega_p = 2\pi \times 1.6 \times 10^{15} = 1.01 \times 10^{16}\text{rad s}^{-1}$, plasma collision frequency (Loss) $\nu_c =$

$0.0001 \times \omega_p = 1.01 \times 10^{12}\text{rad s}^{-1}$ and is denoted by $n = 0,1,2,\dots,7$; with embedded medium permittivity $\epsilon_0 = 8.85 \times 10^{-12}\text{F m}^{-1}$, length of unit cell $d = \frac{10}{0.175} = 57.1\text{nm}$, separation between site A and site B $t = 10 \times \frac{0.6}{0.175} = 34.3\text{nm}$. Here the chain center (origin) is in the middle of site B of the 2^{nd} unit cell and site A of the 3^{rd} unit cell, upon using this spatial configuration, $\epsilon^*(-x) = \epsilon(x)$ is satisfied, which implies the system is PT-symmetric. Dynamic Green's function without nearest neighbor approximation together with quasistatic polarizability with radiation corrections are used, employing the form of Eq. (3.31) by assuming an arbitrary external electric field $E_{\text{ext},n} = 1$ for $n = 0,1,2,\dots,7$ incidents on all the coated nanoparticles, dipole moments in frequency-domain can be calculated by:

$$\begin{bmatrix} p_0 \\ p_1 \\ p_2 \\ \vdots \\ p_7 \end{bmatrix} = \left[\mathbf{M}_{8,\text{PT}-\text{symmetric}}(\omega)\right]^{-1} \cdot \begin{bmatrix} 1 \\ 1 \\ 1 \\ \vdots \\ 1 \end{bmatrix}. \tag{3.37}$$

Note that if we generalize the problem to write the matrix in terms of chain length N, the matrix mentioned here, which is denoted by $\mathbf{M}_{N,\text{PT}-\text{symmetric}}$, is having a little difference when compare to the one mentioned in Eq. (3.31) denoted by $\mathbf{M}_{N,\text{precise}}$. By replacing the diagonal terms an identical quasistatic polarizability (with radiation correction) to two kinds of polarizabilities having gain/loss coated dielectric layer alternatively using Eq. (3.13), $\mathbf{M}_{N,\text{precise}}$ can eventually turn into $\mathbf{M}_{N,\text{PT}-\text{symmetric}}$. Among obtaining the expressions of dipole moments, one can repeat the steps of applying Eq. (3.36) to find the extinction cross

section in frequency-domain.

In Fig. 3.15, the analytic extinction cross section C_{ext} against normalized plasma frequency ω/ω_p for (a) diatomic chain with coated nanoparticles having dielectric shell permittivity $\epsilon_2 = 1.5 + 0.00i$ (NOT PT-symmetric); and (b) with dielectric shell permittivity $\epsilon_2 = 1.5 + 0.01i$ (PT-symmetric), are plotted for comparison. From Fig. 3.15(a), we can see the most right-hand side peak describing the resonant of the edge state having edge state frequency $\omega = 0.530\omega_p$, as aforesaid in Fig. 3.11, is reduced and almost vanished once the system switches into PT-symmetric regime in Fig. 3.15(b), thus gives the zero extinction property of the edge state in PT-symmetric diatomic chain. In order to study what is happening, among considering a PT-symmetric diatomic chain, we plot the magnitude profile of real part and complex part of the dipole moment p_n for $n = 0,1,\dots,7$ at the edge state frequency $\omega = 0.530\omega_p$ having zero extinction using Eq. (3.37), see Fig. 3.16. From Fig. 3.16, we can see that the edge state will still be excited yet it gives a zero extinction in the extinction spectrum, such a property can be explained by observing the imaginary part of the excited dipole moments at the edge state frequency $\omega = 0.530\omega_p$. By formulation in Eq. (3.36), we know the extinction cross section depends on the summation of all the imaginary part of the excited dipole moments in the diatomic chain, while the edge state frequency for a PT-symmetric diatomic chain implies the $\text{Im}(p(x))$ being an odd function, results in a zero extinction property at the edge state frequency.

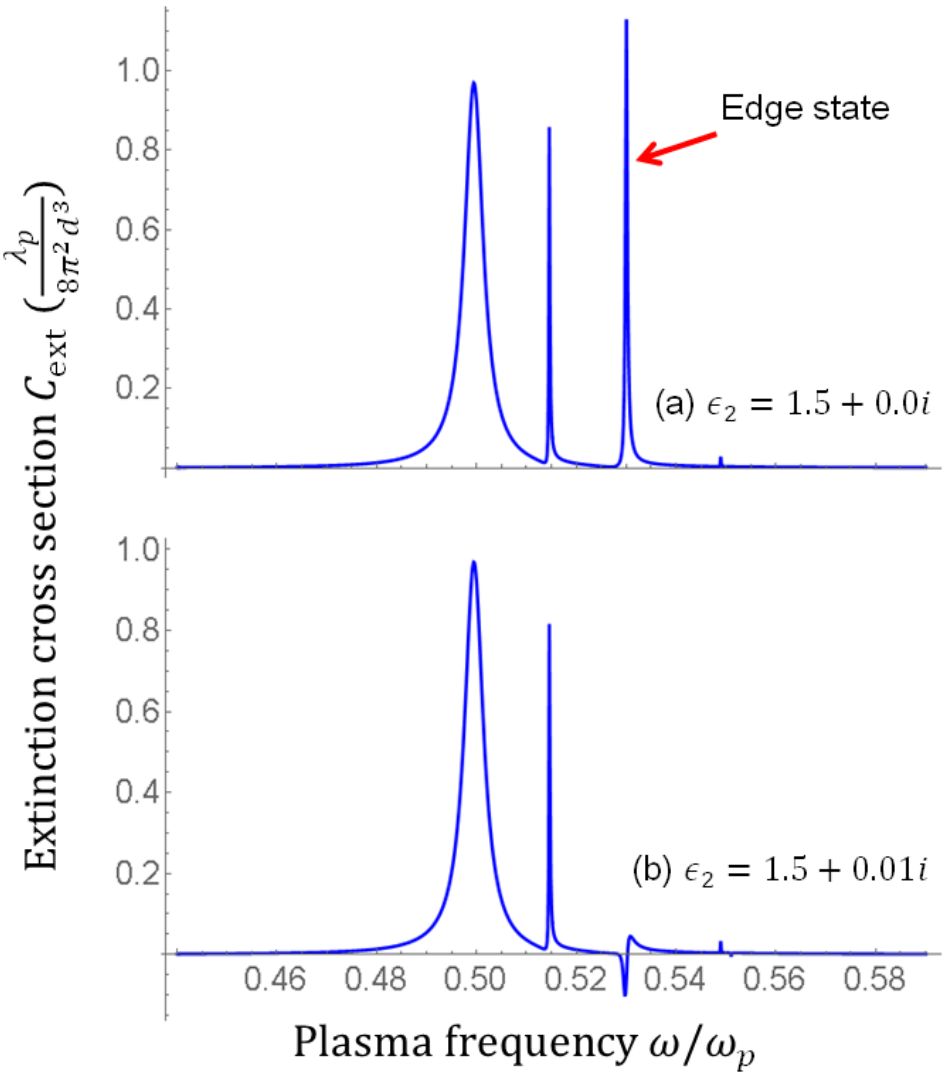

Figure 3.15: Analytic extinction cross section (in unit of $\lambda_p/8\pi^2 d^3$) of the diatomic plasmonic chain using (a) identical coated metal nanoparticles and (b) coated nanoparticles with gain/loss dielectric shells alternatively, PT-symmetric; against normalized plasma frequency ω/ω_p are plotted for comparison. The two diatomic chains have chain length $N = 8$, with $d = 57.1\text{nm}$, $t = 34.3\text{nm}$, $b = 10\text{nm}$, $a = 7.14\text{nm}$, plasma collision frequencies for the cores are set to be $v_c = 0.0001\omega_p$. By comparing Fig. 3.15(a) and (b), we can see that at the edge state frequency $\omega = 0.530\omega_p$, the extinction cross section C_{ext} is significantly reduced and almost vanished when the system switches from a non-PT-symmetric one to a PT-symmetric one.

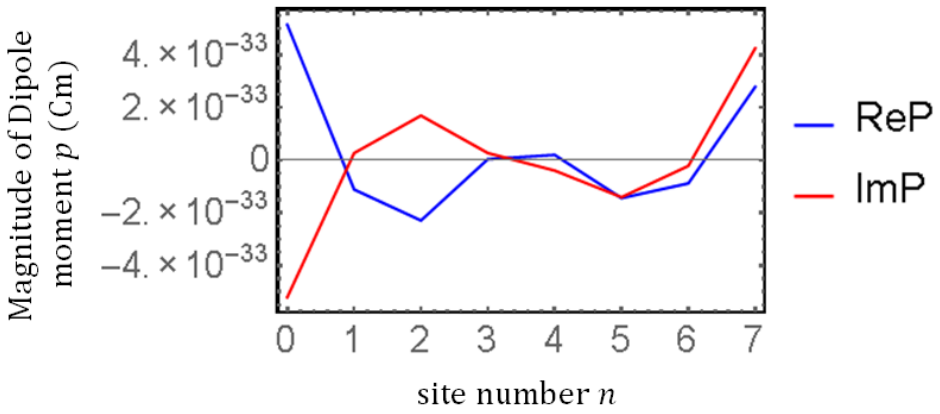

Figure 3.16: (Color online) The spatial magnitude profile of the excited dipole moments calculated analytically in the PT-symmetric diatomic plasmonic chain having chain length $N = 8$, at the edge state frequency $\omega = 0.530\omega_p$ found in non-PT-symmetric diatomic chain, see Fig. 3.11. The blue and orange line represent real and imaginary part of the excited dipole moments, respectively. The real part of the magnitude forms an even function of x while the imaginary part forms an odd function of x, most likely.

Since the analytic results using dynamic Green's function without nearest neighbor approximation together with quasistatic polarizability with radiation corrections successfully verify the existence of zero extinction property of the edge state frequency in PT-symmetric diatomic chain, in this part we will aim for the verification in Lumerical FDTD through setting up a compatible simulation. Once again we consider a diatomic plasmonic chain using the setup mentioned in Fig. 3.14, with configuration taken from Fig. 3.15(b). The chain is PT-symmetric as $\epsilon^*(-x) = \epsilon(x)$ is satisfied as previous stated. The TFSF source mentioned in Fig. 3.8 acts as an external longitudinal stimulate to excite the dipole moments within the PT-symmetric diatomic chain, the source itself is once again a pulse having

frequency ranging from $0.45\omega_p$ to $0.51\omega_p$ and amplitude $= 1$, which will return the cross sections in frequency-domain. A 2D field-profile monitor on xy-plane (y the propagating direction of the plane wave) is set simultaneously to give the field profile of E_x this time, so that the results can be used to compare with the analytic one.

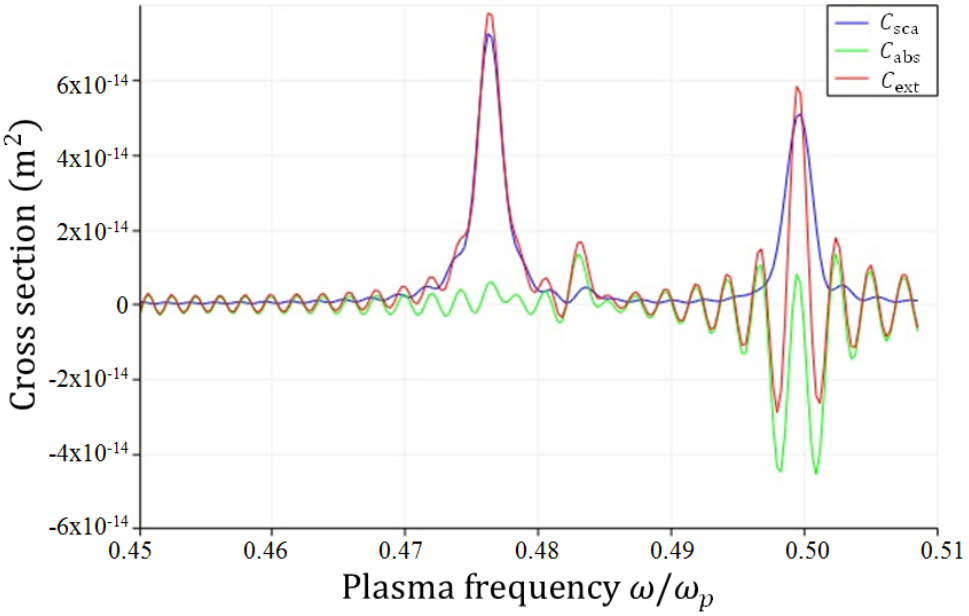

Figure 3.17: (Color online) Cross sections (in unit of m^2) of the PT-symmetric diatomic plasmonic chain using coated metal nanoparticles with setup mentioned in Fig. 3.14, with chain length $N = 8$, against normalized plasma frequency ω/ω_p. The mesh in use is 1.5nm within the TFSF source and the simulation time is short due to the divergence of electric field. Extinction, absorption and scattering cross sections are plotted in red, blue and green color respectively. The three peaks are at around $0.476\omega_p$, $0.483\omega_p$ and $0.499\omega_p$ such that they are presumed to be the three excited mode mentioned in Fig 3.15(b) with slightly shifted frequencies. The most right-hand side peak corresponds to the edge state and is of great fluctuation. The fluctuation mainly comes from the Fourier-transform as the simulation time is not long enough.

In Fig. 3.17, like the previous simulation results, the absorption cross section (green-line) and scattering cross section (blue-line) are plotted against the frequency-domain, and the extinction cross section is obtained by $C_{\text{ext}} = C_{\text{abs}} + C_{\text{sca}}$. While looking into the extinction cross section, there are approximately three peaks at around $0.476\omega_p$, $0.483\omega_p$ and $0.499\omega_p$ with the last one presumed to be the resonant of the edge state in the PT-symmetric diatomic chain. This shows conformity to the FDTD results of the non-PT-symmetric diatomic chain using identical coated metal nanoparticles as shown in Fig. 3.12 if we only consider the frequency-domain but not the magnitude, this makes sense as the analytic solutions for the non-PT-symmetric one also have similar resonant frequencies with the PT-symmetric one if we compare Fig. 3.15(a) and (b). To further verify this, the analytic magnitude profile of the excited dipole moments at the resonant peaks (include the 'vanished peaks' with edge state frequency) shown in Fig. 3.15(b) together with the simulated field-pattern for those resonant peaks obtained in Fig. 3.17 using FDTD are plotted in Fig. 3.18(a) and (b) respectively. By comparing Fig. 3.18(a.i) and (b.i), (a.ii) and (b.ii), the sites where a large magnitude of dipole moment is observed posing a relatively strong field localization, which suggests the peaks mentioned in Fig. 3.15(b) from the analytic approach is coherent to those obtained through FDTD in Fig. 3.17. For the resonant edge state having zero extinction property in Fig. 3.15(b), the magnitude profile of the dipole moments in Fig. 3.18(a.iii) implies the field is localized in the edges, yet this time the system is not that PT-symmetric due to the slightly imbalance of permittivity with a lossy plasmonic core within each nanoparticle when it comes to actual simulation using FDTD, therefore the localized fields stay

in the gain side to balance the excessive lose, results in an asymmetric field-pattern observed in Fig. 3.18(b.iii).

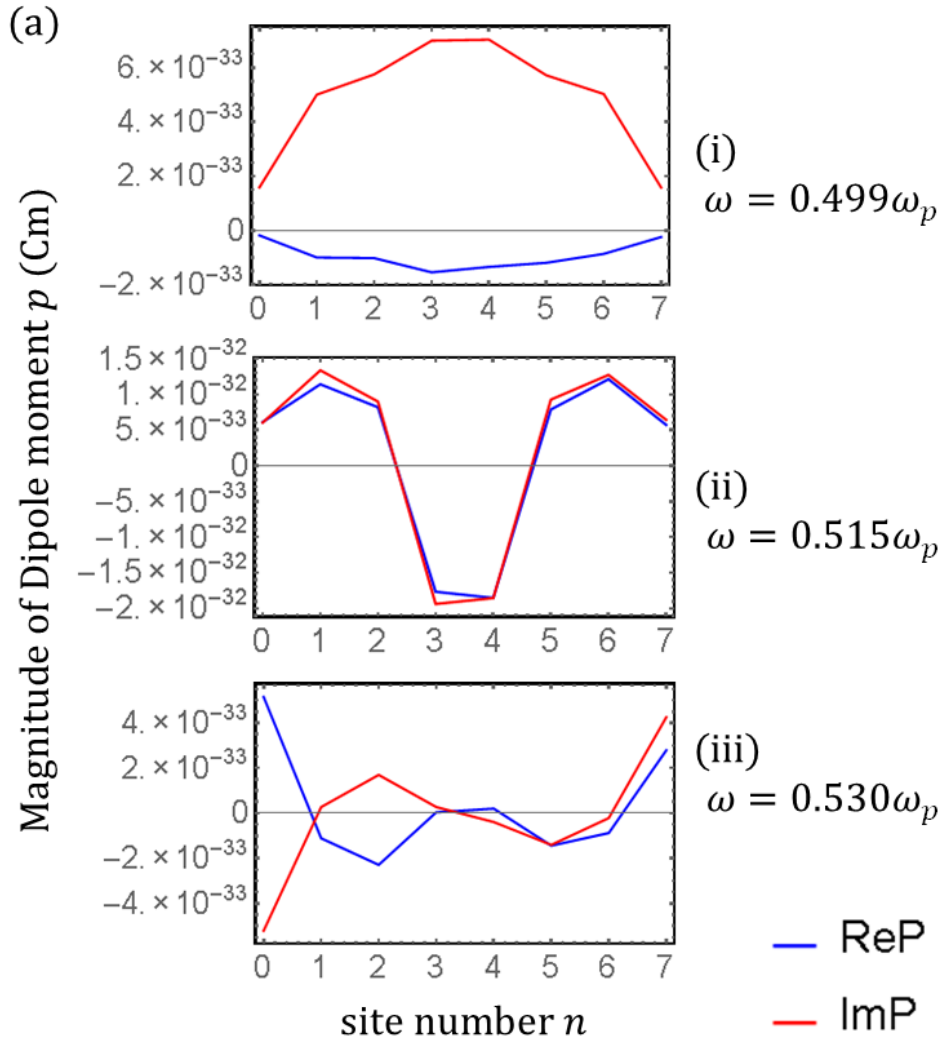

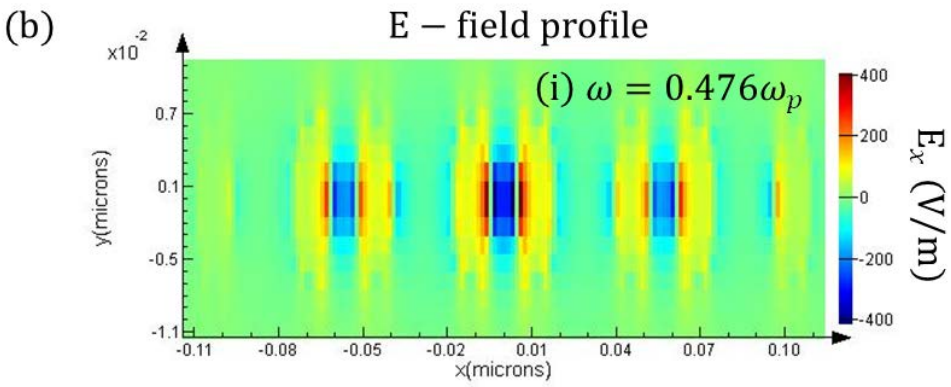

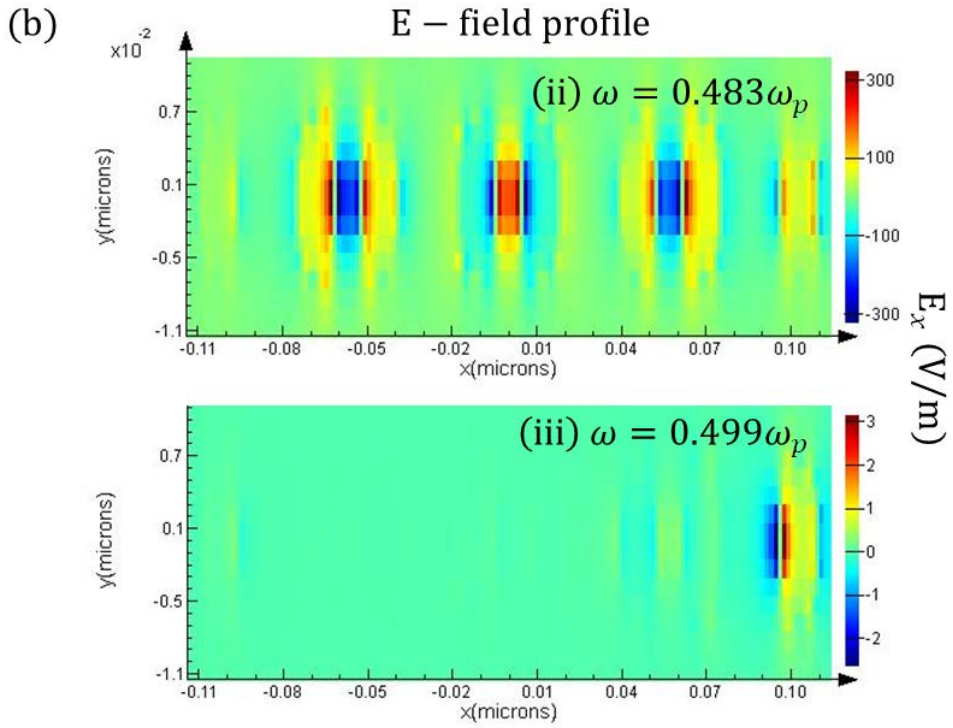

Figure 3.18: (Color online) (a) The spatial magnitude profile of the dipole moments calculated analytically in the PT-symmetric diatomic plasmonic chain with coated metal nanoparticles having setup mentioned in Fig. 3.14, adopting chain length $N = 8$, at three different picked off frequencies described in Fig. 3.15(b), (i) $\omega = 0.499\omega_p$, (ii) $\omega = 0.515\omega_p$, (iii) $\omega = 0.530\omega_p$ such that it corresponds to the edge state. (b) The electric field profile obtained by setting the similar setup in FDTD using 2D field monitor to record the magnitude of E_x throughout the entire spatial distribution of the setup at three different picked off frequencies described in Fig. 3.17, (i) $\omega = 0.476\omega_p$, (ii) $\omega = 0.483\omega_p$, (iii) $\omega = 0.499\omega_p$. The mesh in use is 1.5nm. By comparing the magnitude of the dipole moments in (a) with the electric field profile in (b), one can justify the three peaks mentioned in Fig. 3.15(b) match those mentioned in Fig. 3.17 with Fig. 3.18 (a.iii) and (b.iii) being the edge state with vanished extinction.

If we focus back to Fig. 3.17, the so called 'zero extinction property'

we expect to happen at the edge state frequency $\omega = 0.499\omega_p$ can not be observed since the magnitude of the extinction cross section around that range is fluctuating vigorously, we can only deduce there is a downward trend for the absorption cross section around. Knowing the fact that the fluctuation comes from the Fourier-transform, one natural approach is to extend the simulation time to obtain more data points. Unluckily, this time we are doing the simulations with gain media, enabling a large simulating time will significantly increase the probability of the electric field to be diverged, which will eventually make the results unreasonable. But still, we try to evaluate the cross sections by using a longer simulation time and the results are astonishing as shown in Fig. 3.19(a).

In Fig. 3.19(a), we plot the cross sections (absorption, scattering and extinction) against frequency domain of the PT-symmetric diatomic chain using TFSF source as stimulate. Having more than double the simulation time when compare to that obtained in Fig. 3.17, we can see that the edge mode becomes the only dominated resonant state within the diatomic chain by gaining a huge magnitude in both the absorption cross section and scattering cross section. Note that the absorption cross section C_{abs} has a negative peak, which seems like a total opposite of the scattering cross section C_{sca}, if one flips the sign to plot the negative value of absorption cross section $-C_{\text{abs}}$ as shown in Fig. 3.19(b), they look very much similar such that $-C_{\text{abs}} = C_{\text{sca}}$ at frequencies around the edge state of the PT-symmetric diatomic chain. Recalling the definition of extinction cross section $C_{\text{ext}} = C_{\text{abs}} + C_{\text{sca}}$, if $-C_{\text{abs}} = C_{\text{sca}}$ is really the case around edge state frequency $\omega = 0.530\omega_p$, it literally means the $C_{\text{ext}} = 0$ which

implies the prediction we verified previously, that is, a 'zero extinction property' at the edge state frequency of a PT-symmetric diatomic chain.

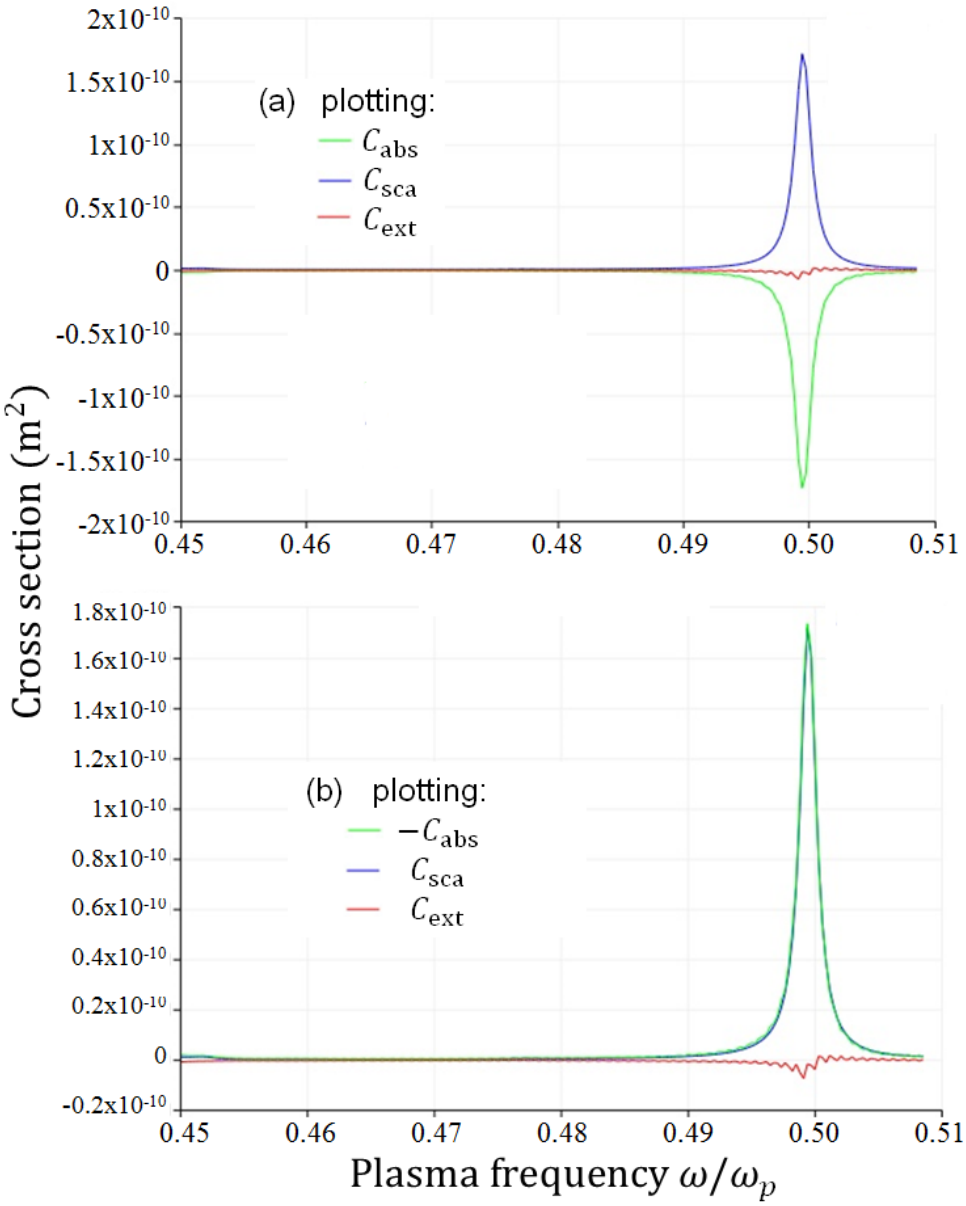

Figure 3.19: (Color online) (a) Cross sections (in unit of m^2) of the PT-symmetric diatomic plasmonic chain using coated metal nanoparticles with setup mentioned in Fig. 3.14, with chain length $N = 8$, against normalized plasma frequency ω/ω_p. The mesh in use is 1.5nm within the TFSF source. The simulation time is doubled compare to the results obtained in Fig. 3.17. The field diverges as the peak at the

resonant frequency of the edge state is having magnitude over 100times bigger than that in Fig. 3.17. The absorption cross section and scattering cross section seems like about to cancel each other to obtain a zero extinction cross section. (b) Plotting of the cross sections with the absorption cross section having a flipped sign, i.e. $-C_{\mathrm{abs}}$, it shows that the negative absorption cross section is almost the same as the scattering cross section, i.e. $-C_{\mathrm{abs}} = C_{\mathrm{sca}}$, and supposes to give a zero extinction at the edge state frequency $\omega = 0.499\omega_p$.

Yet in FDTD simulation, there is a little numerical error which makes the absorption cross section and scattering cross section cannot be perfectly canceled at the edge state frequency, and because the simulation time is long enough for the fields to diverge, the magnitude of the cross sections of that particular resonant state having fields localized in the gain coated nanoparticle has already became over one hundred times compare to those normal resonant peaks mentioned in Fig. 3.17. If one can overcome the numerical error to have perfect cancelation around edge state frequency so as to make 'zero extinction' happens, we should be able to observe those two resonant peaks on the left-hand side as shown in Fig. 3.17.

Finally, in this last part of Chapter 3, I will try to verify the 'zero extinction property' of the edge state in PT-symmetric diatomic plasmonic chain using a method called multiple scattering theory, also known as MST, which is highly precise numerically for spherical objects. The MST basically consider the EM fields expanded by adopting vector spherical harmonics, and the accuracy can be increased by increasing the truncating number (L), which represents the angular momentum in the multipole

expansion. The MST formulation for a finite number of nanoparticles can be found in several publication [52-54], which will not be discussed here, and we will focus on the resulting extinction spectrum here, see Fig. 3.20. Fig. 3.20(b) is plotted by adopting the exact configuration mentioned in Fig. 3.15(b) for the finite PT-symmetric diatomic chain, also a similar setup by using identical coated nanoparticles having dielectric shell permittivity $\epsilon_2 = 1.5$ is plotted in Fig. 3.20(a) for comparison.

In Fig. 3.20(a) and (b), both the absorption, scattering and extinction cross sections are plotted in a normalized scale against the normalized plasma frequency ω/ω_p using red-dashed line, blue-dashed line and dark line, respectively. Although using MST is much more complicated, the main advantage is that the absorption and scattering behavior can be computed instead of only formulating the extinction cross section when considering the coupled dipole equation. Like the results obtained in using coupled dipole equation and Lumerical FDTD, the MST verifies three spiky peaks in a non-PT-symmetric diatomic chain which are around $0.493\omega_p$, $0.508\omega_p$ and $0.525\omega_p$; and verifies the existence of the 'zero extinction property' in a PT-symmetric diatomic chain by showing a greatly diminished peak at the resonant frequency of the edge state $\omega = 0.525\omega_p$ among comparing Fig. 3.20(a) and (b). Also from Fig. 3.20(b), it suggests that the zero extinction property is given by the simultaneous cancelation of the scattering and absorption cross sections. This gives support to our results obtained through Lumerical FDTD simulations as shown in Fig. 3.18(a) and (b), which we predict the zero extinction cross section is caused by the perfect cancelation of the scattering and absorption cross sections.

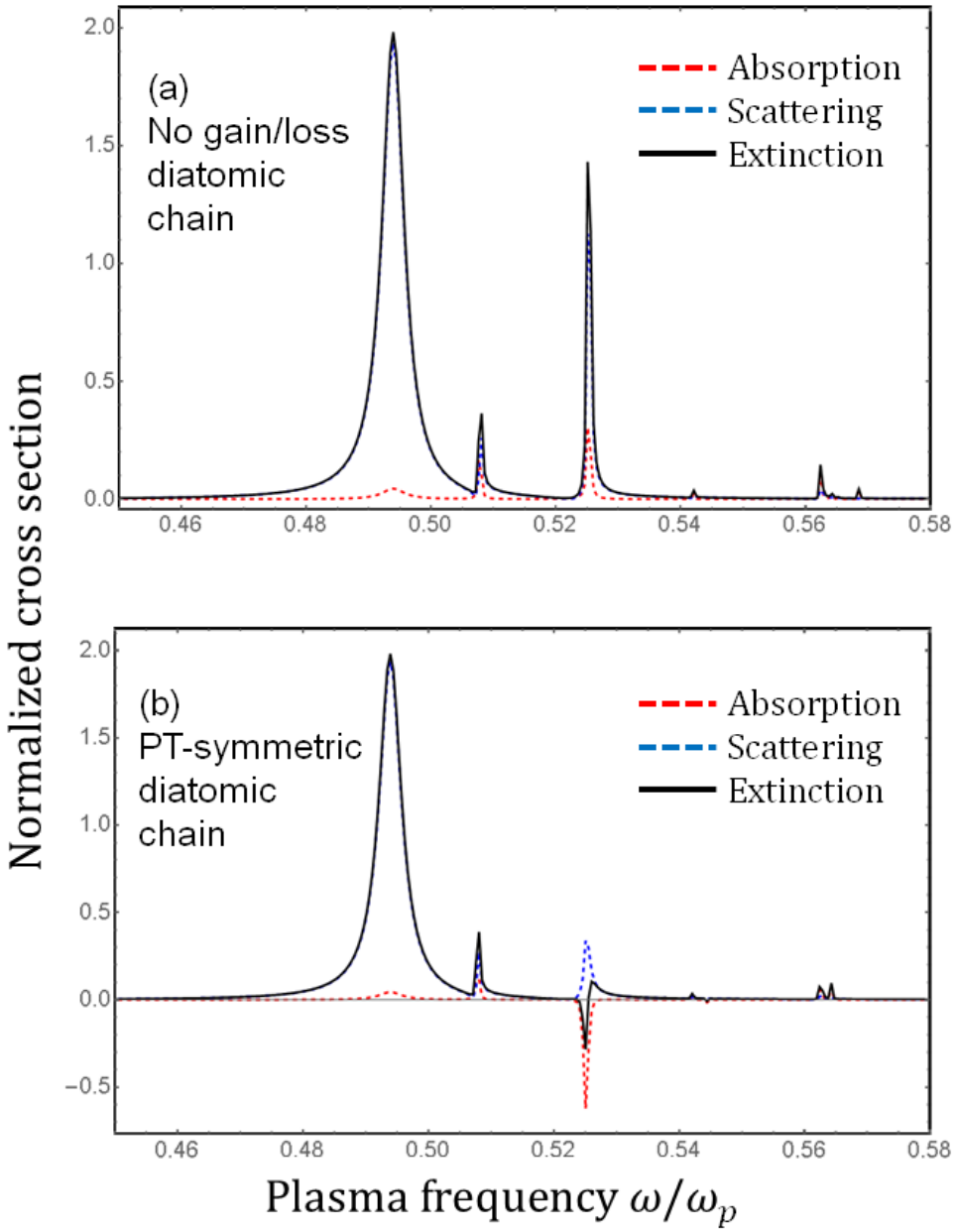

Figure 3.20: (Color online) Normalized cross sections of the diatomic plasmonic chain using (a) identical coated nanoparticles with no gain/loss in its dielectric shell, (b) coated nanoparticles with gain/loss dielectric shells alternatively, therefore PT-symmetric, against normalized plasma frequency ω/ω_p. The diatomic chain has chain length $N = 8$, with $d = 57.1\text{nm}$, $t = 34.3\text{nm}$, $b = 10\text{nm}$, $a = 7.14\text{nm}$, plasma collision frequencies for the cores are set to be $v_c = 0.0001\omega_p$. Absorption, scattering and extinction cross sections are plotted using red-dashed line, blue-dashed line and dark line respectively. The three peaks (include the 'vanished peak') is at

around $0.493\omega_p$, $0.508\omega_p$ and $0.525\omega_p$. The non-PT-symmetric chain shares same resonant frequencies with the PT-symmetric one, which is of expected. Looking into the 'vanished extinction' of resonant state at the edge state frequency, it shows the cancelation effect of the absorption and scattering cross sections.

3.5 Conclusion

In this Chapter, we provided number of ways to analyse the one-dimensional diatomic plasmonic chain through theoretical aspects and numerical simulations. We first considered a one-dimensional diatomic chain having individuals an identical coated metal nanoparticle. The analogy was started by considering the governing equations using coupled dipole equation and quasistatic polarizability with radiation corrections. By considering the longitudinal solutions only, formulations were shown to be greatly simplified. The dispersion relation $\omega(k)$ had been discussed by applying Bloch's Theorem to the coupled dipole equation, and among opening a band gap in the dispersion relation when considering a diatomic chain, topological protected edge state is favoured once the chain became finite. Upon considering a finite diatomic chain, methods in finding the edge state and the corresponding dipole moments were discussed in both conditions: using quasistatic Green's function and polarizability with nearest neighbour approximation, and with dynamic Green's function without using nearest neighbour approximation. Results showed that the two conditions do not differ much when considering longitudinal solutions. Extinction cross section had also been evaluated explicitly and was used to help finding the edge state. Here we used Lumerical FDTD to verify the existence of edge

state as cross sections could be easily computed and the results were not disappointed as it showed conformity to the analytic one. Last, we considered a PT-symmetric diatomic chain by inserting balanced gain/loss into the system, and we tried to verify the 'zero extinction property' of the edge state frequency by using coupled dipole equation, Lumerical FDTD simulations and also the multiple scattering theory, it turns out that three of them shared quite a conformity and suggest that the 'zero extinction property' is came from the cancelation of the scattering and absorbing behaviour of the PT-symmetric diatomic system. Unluckily the FDTD one was posing certain numerical error in computing the extinction cross section such that a perfect cancelation of scattering and absorption cross section cannot be achieved.

Chapter 4 Summary

In this thesis, the nonlinear and non-Hermitian electrodynamics in chains of plasmonic nanoparticles were studied and presented.

In Chapter 2, we built a model for the one-dimensional nonlinear plasmonic chain for which its nonlinearity comes from the Coulomb interaction of charges using Nearest Neighbour Approximation (NNA). Upon using linearization and rewriting the equations in the form of eigenvalue problem, we were able to obtain the initial configuration of different eigenmodes. By numerical calculation using the Runge-Kutta Method, an iteration skill to deal with differential equations without doing integrations, together with the use of MATLAB, we obtained the data set describing how the system behave in a long term consideration such that adjusting the initial configuration would give us different responses. Knowing the fact that the system is nonlinear in nature, the inconsistent results were explained by an explicit evaluation on the Hamiltonian which tells the electron clouds start to overlap. Also analysis on Fourier-transform was performed and we found the order of eigenmode and the value of initial multiplying parameter B are directly proportional to the nonlinearity inside the system, which gives rise to the shifting of 'main frequency' and the appearance of 'side frequencies'. To explain this phenomena, we considered the classical FPU-model by doing the mode energy analysis, upon using initial configuration from the first eigenmode and the observation on the mode energy-indicator diagram, the frequency conversion phenomena was

understood by the sharing of energy among different eigenmodes, also known as the 'Equipartition'. It turns out that the equipartition and the nonlinearity energy localization were being explained by each other.

In Chapter 3, we switched our focus to the one-dimensional diatomic chain by setting up the model through 'dimerization' in traditional plasmonic chain, i.e. adding one more nanoparticle in a unit cell along the chain. We first considered a diatomic chain with unit cell having two identical coated metal nanoparticles. The governing equation we picked is the coupled dipole equation since it works good when the nanoparticles are small enough by treating the individual along the chain as a point scatter and can couple to each other to support plasmon mode propagation. By adopting a quasistatic approximation and nearest neighbour approximation in considering the Green's function together with a quasistatic polarizability, the dispersion relation $\omega(k)$ was computed using Bloch's Theorem together with rewriting equations in form of eigenvalue problem. Since the special spatial configuration of diatomic plasmonic chain would lead to an opening of band gap, it is natural to predict an edge state would be favoured once the diatomic chain became finite. As Bloch's Theorem is no longer applicable in finite system, we presented another way of computing $1/\min|\lambda|$ by sweeping the frequency ω to locate the band gap and the resonant state supported by the finite diatomic chain. Both the analytical results obtained by plotting the excited dipole moments using Mathematica and the numerical results obtained by setting up simulations in FDTD verified the existence of edge state in a finite diatomic chain. Extinction spectrum was computed in both analytic regime and in simulations of

FDTD as it helped locating the resonant frequency of edge state. In the late Chapter 3, the influences brought by PT-symmetry on diatomic chain had been discussed. We first reformulated the equations so that the model had switched into a PT-symmetric diatomic chain by implementing balanced gain/loss to the coated dielectric shell of the corresponding nanoparticles such that they satisfied the relation $\varepsilon^*(-\hat{x}) = \varepsilon(\hat{x})$. By doing so we tried to verify the 'zero extinction property' found at resonant frequency of the edge state in the diatomic chain through different aspects. Here, results were mainly expressed in the form of extinction spectrum, magnitude profile of the dipole moments and the electric field profile at resonant state. It turns out that the coupled dipole equation formalisms, Lumerical FDTD simulations and also the analytic calculations of adopting multiple scattering theory give quite a conformal answer that the 'zero extinction property' is given by the cancelation of the scattering and absorbing behaviour of the PT-symmetric diatomic system.

Overall, we have studied the one-dimensional plasmonic chain by treating the metal nanoparticle a resonator, and also the plasmonic chain with diatomic configuration using various methodology such as eigenvalue problem, coupled dipole equation, Runge-Kutta iterations...etc. It is an interesting topic to study as it might favor many plausible applications, such as nonlinear optics and subwavelength waveguiding.

Appendix A

We continue discussing the nonlinear plasmonic chain mentioned in Chapter 2 with 512 entries along the chain in this Appendix. The analysis on using eigenvector corresponds to 2^{nd} eigenfrequency in the dispersion band in Fig. 2.11(b) in Chapter 2 as initial conditions will be skipped since it behaves almost the same with the 1^{st} eigenfrequency. They both start by a nonlinear oscillation, but this time end up with energy localized on two extreme-points in the initial configuration instead of one, the energy indicator-time graph shows the energy is dispersed by symmetry from mode 2 to mode 6, 10, 14, 18…etc. The equipartition is also acquired this time.

A.1 3^{rd} eigenfrequency

What makes the system interesting to study comes from the next part, the initial configuration dedicated by eigenvector corresponds to 3^{rd} eigenfrequency. From the previous case, we will easily assume equipartition happens within the lower dispersion band yet the outcome is quite against the conjectured conclusion this time. We start by looking into the energy indicator-time graph directly, see Fig. A.1. The initial eigenvector is taken from the 3^{rd} eigenfrequency and parameter $B = 2.0 \times 10^{-8}\mathrm{m}$, it is tuned to be lower than the previous case to prevent an early overlapping.

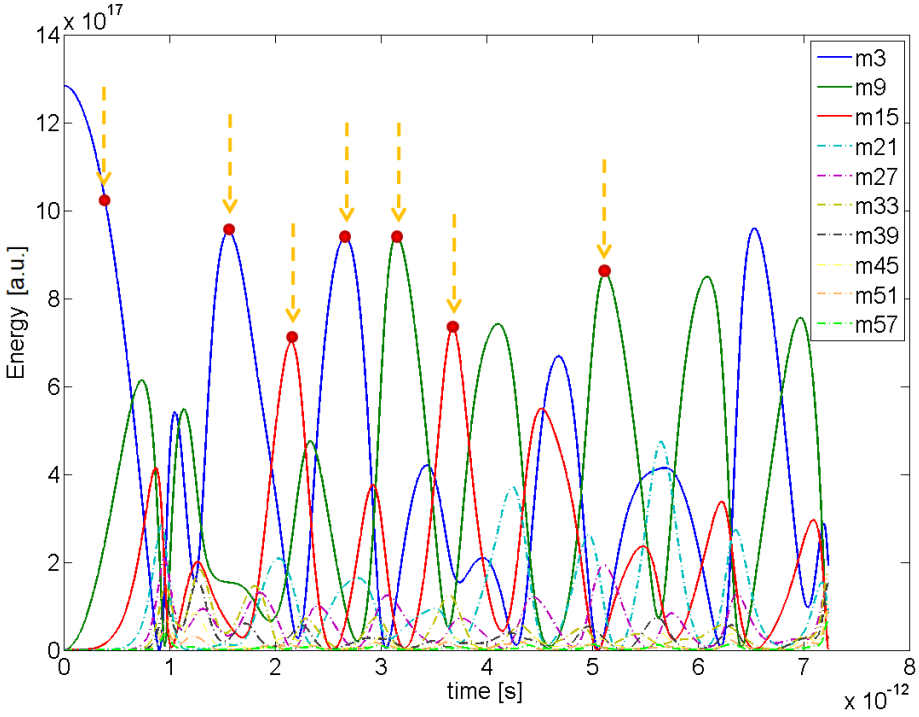

Figure A.1: (Color online) Energy indicator-time graph of several modes, with y-axis being the energy-level indicator and the x-axis being the time. The plot stops at 6238 oscillations. Note that there does not have the plot of modes 1, 2, 4, 5, 6…etc. because those modes have comparatively zero energy with respect to the excited one. Also other than modes $3, 9, 15$, others are plotted with doted lines as they are not of interests. The denoted red spots pointed by yellow doted arrows are points picked, such that at those particular time, a specified mode is somewhat dominated. From left to right, we denotes the marked point as point $1, 2, 3 \ldots 7$ as it will be useful later.

Since the picked points in Fig. A.1 are chosen for some particular described mode (either mode 3, 9, 15) to be dominated, if the system is subjected to oscillation by an initial condition of 3^{rd} eigenmode, when we look into the system at a certain time, say point 1 for which mode 3 is dominated, we will expect the system oscillates in a frequency either equal to or close to the 3^{rd} eigenfrequency in the dispersion band in Fig. 2.11(b) in Chapter 2 (The dispersion band is unchanged with a changing initial

condition, as Fig. 2.11(a) depends on the applied initial eigenfrequency while Fig. 2.11(b) is unchanged, it is fixed for the system.) To verify this, we pick out 3 particular electron clouds, the 128^{th}, 170^{th} and 256^{th} electron clouds along the chain, see Fig. A.2, examine their dipole moment-time graph, perform the Fourier Transform and take out the 'main frequency' mentioned in Chapter 2.4, compare it with the dominated frequency mentioned in Fig. A.1 to see the difference.

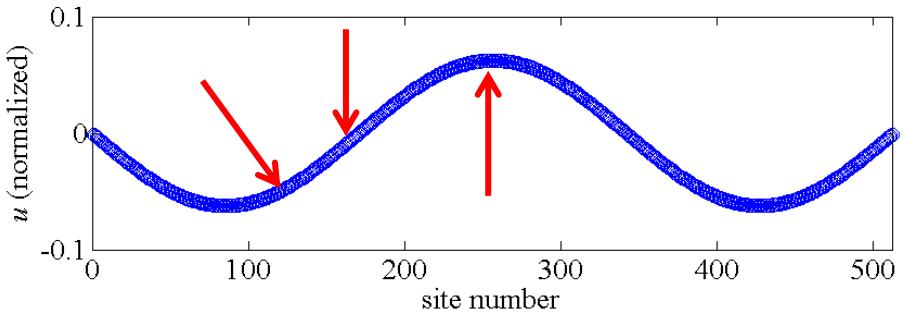

Figure A.2: The initial configuration of the normalized displacement vector corresponding to the 3^{rd} eigenmode, with x-axis being the site number representing 512 discrete electron clouds, y-axis being the normalized u. The 3 red arrows point at the 3 picked particular sites, which is the 128^{th}, 170^{th} and the 256^{th} one.

The table below gives the exact value of the eigenfrequencies in the dispersion band:

Table A.1: The exact value of the eigenfrequencies for 3 picked mode $k = 3, 9, 15$. Used in comparison of main frequencies in Fig. 2.14 and Table 2.5.

Mode number	3	9	15
Eigenfrequency(Hz)	$7.9617\text{x}10^{14}$	$7.9627\text{x}10^{14}$	$7.9645\text{x}10^{14}$

Table A.2: The main frequency for the Fourier transform of the 3 picked electron clouds ($128^{th}, 170^{th}, 256^{th}$) at different stopping time (7 points denoted in Fig. A.1) with the information of dominated eigenmode found in Fig. A.1 at those 7 stopped time. (*) denotes extremely dominated eigenmode at that particular time.

Particles / Point	128	170	256	Dominated
	Main freq. (Hz)	Main freq. (Hz)	Main freq. (Hz)	Eigenmode in Fig. 2.14
1	7.9596×10^{14}	7.9596×10^{14}	7.9596×10^{14}	Mode 3
2	7.9590×10^{14}	7.9590×10^{14}	7.9462×10^{14}	Mode 3*
3	7.9590×10^{14}	7.9636×10^{14}	7.9450×10^{14}	Mode 15
4	7.9589×10^{14}	7.9627×10^{14}	7.9439×10^{14}	Mode 3*
5	7.9589×10^{14}	7.9621×10^{14}	7.9462×10^{14}	Mode 9*
6	7.9589×10^{14}	7.9616×10^{14}	7.9453×10^{14}	Mode 15
7	7.9589×10^{14}	7.9569×10^{14}	7.9472×10^{14}	Mode 9

The point 1, 2, 3…7 also indicate another kind of time evolvement since those represented point are picked from left to right in Fig. A.1. We will start by first looking into the behaviour of the 128^{th} electron cloud in Table A.2. We can see that among time evolvement, although the dominated eigenmode keeps changing, the 'main frequency' of the 128^{th} electron cloud remains almost the same, only a small deviation is found at point 1 yet data of point 1 are not that reliable normally since the time duration from the beginning to point 1 is very short, which makes the Fourier transform meaningless as it gains accuracy from a larger time scale. This is quite astonishing as we initially assumed that when the system is subjected

to nonlinear oscillation, the nonlinearity will spread to the entire system, such nonlinearity would be found everywhere. And the results from the 128^{th} electron cloud tell a different story, it shows contradiction with the conjectured assumption such that there are some sites in the plasmonic chain remain relatively stable even if the system is subjected into certain nonlinearity. Note that we despite the 'side frequencies' here and only concern about the 'main frequency'.

Next, we will look into the behaviour of the 170^{th} electron cloud. From Fig. A.2, we can see that the 170^{th} electron cloud is located at around zero displacement in the initial configuration. Theoretically it should be one of the most stable sites as it will remain at zero displacement if the system is allowed to oscillate linearly. Yet the results show contradiction once again, with 128^{th} electron cloud being the stable site instead, the 170^{th} electron cloud shows a nearest results with the dominated eigenmode defined in Fig. A.1, especially at the points with extremely dominated mode, i.e. point 2, 4 and 5. Upon comparing the 'main frequency' obtained from Fourier transform of the dipole moment-time graph of the 170^{th} electron cloud, we can see that at point 2, the experimental result 7.9590×10^{14}Hz compares to the theoretical result 7.9617×10^{14}Hz; at point 4, the experimental result 7.9617×10^{14}Hz compares to the theoretical result 7.9617×10^{14}Hz; at point 5, the experimental result 7.9621×10^{14}Hz compares to the theoretical result 7.9627×10^{14}Hz; three sets of data show a small deviation between experimental results and theoretical results, which suggest that the energy transfer between modes could be an answer to the shifting of 'main frequency' or creation of peaks – 'side frequencies' in

Fourier transform. With a suitable configuration, we expect the energy indicator-time graph can explain the Fourier diagram well.

We will end up the analysis on the 3^{rd} eigenmode by considering the behaviour of the 256^{th} electron cloud. It can be clearly shown in Fig. A.2 that the 256^{th} electron cloud represents one of the three extreme-points in the initial configuration. By the assumption from the previous cases in this section, we do expect energy localization will take place here before the system comes to an execution by overlapping of electron clouds. Here we recall the conjecture conclusion in the last part of Chapter 2.4, that is, using a larger initial multiplying parameter B will result in a lower 'main frequency'. It is not difficult to find that the data of 256^{th} electron cloud in Table A.2 is comparatively smaller than the 128^{th} one and the 170^{th} one. If one tries to explain this phenomena and map the conclusion above, one possible guess is the energy localization. Since localization of energy will amplify the oscillation amplitude on that particular site, it is by means the same with using a larger initial multiplying parameter B, which results in a lower 'main frequency', as you can see the 'main frequencies' of 256^{th} electron cloud is significantly lower than that of the others now.

Among examining this set of Eigen parameter, we confirm that the nonlinearity in one-dimensional plasmonic chain is strongly depending on the localization of energy in the chain. In our case (512 entries along the chain), the 128^{th} entries is a relatively stable site, the 170^{th} entries shares a relatively similar behaviour with the energy indicator-time graph in

mode-energy analysis, while the 256^{th} entries is obviously the site where energy localization take place.

A.2 Selection Rules (Lower band)

With the few sets of data discussed previously, one can draw the selection rules for lower band as it will describe what mode would be excited for some initial condition. And after discussing this we will start looking at some initial conditions with shorter wavelength (higher frequency) obtained in the dispersion diagram in Fig. 2.11(b) in Chapter 2. Basically, if k denotes the eigenmode to be applied initially to the one-dimensional plasmonic chain, eigenmodes denoted by $k + 2ak$ would be subjected to excitation lately for $\text{a} = 0,1,2,3$ ....

We do not clearly define the range of lower band since we only know it works for $k = 1, 2, 3$ currently and assume it will work for initial conditions started with a lower dispersion eigenfrequency.

A.3 128^{th} & 384^{th} eigenfrequency

We combine the analysis of these two sets of Eigen parameters because they are symmetrically opposite in Fig. 2.11(b) in Chapter 2. We expect two systems share some degrees of similarity. You can find the energy indicator-time graph of using eigenvector corresponds to 128^{th} eigenfrequency and 384^{th} eigenfrequency as initial condition in Fig. A.3(a) and (b) respectively, both using same $B = 3.0 \times 10^{-8}\text{m}$.

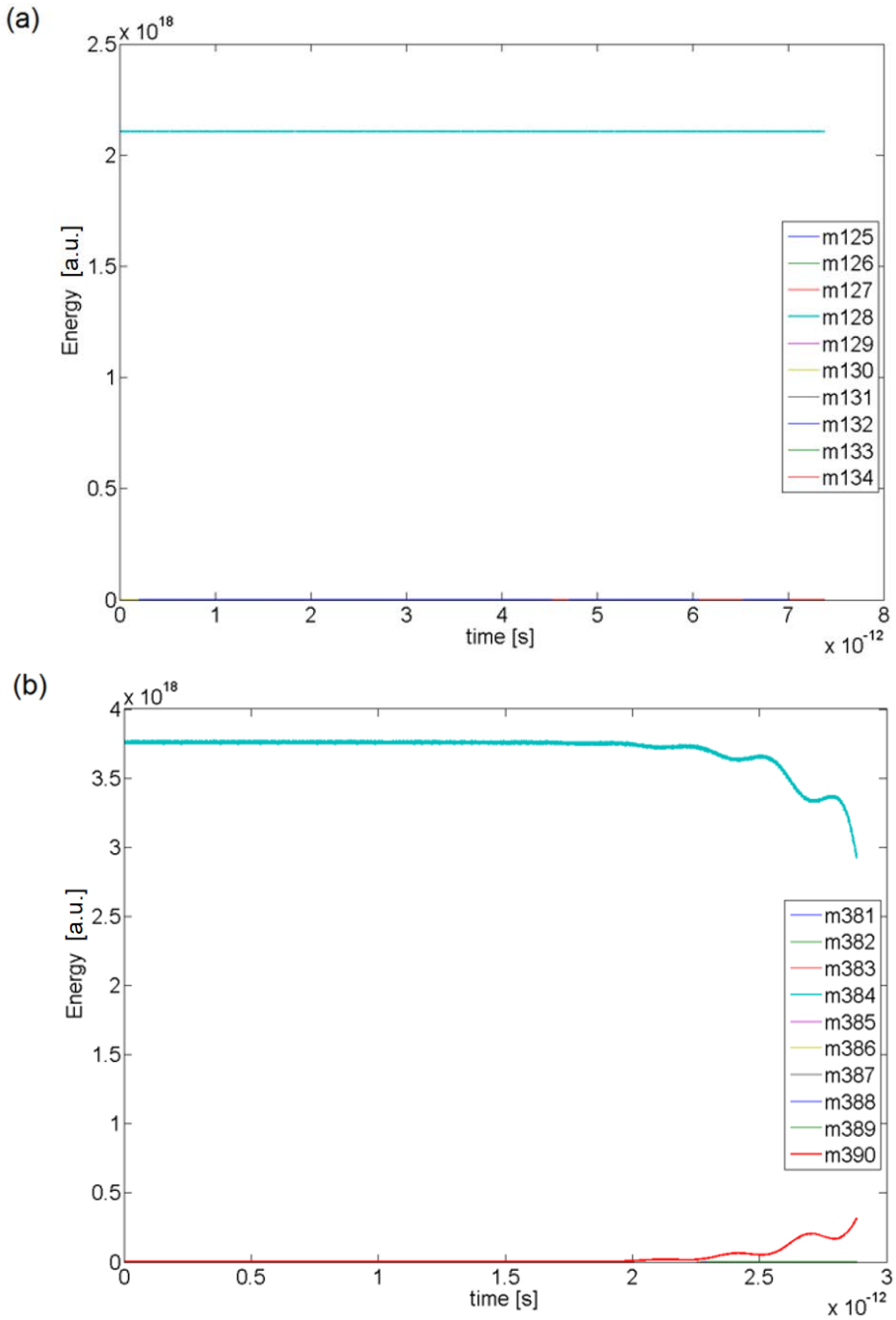

Figure A.3: (Color online) (a) Using the 128^{th} eigenmode as the initial configuration, the energy indicator-time graph of several modes, with y-axis being the energy-level indicator and x-axis being the time, this system does not have the overlapping of electron clouds within the simulation time. (b) Using the 384^{th} eigenmode as the initial configuration, the energy indicator-time graph of several modes, with y-axis being the energy-level indicator and the x-axis being the time, the plot stops at 2487 oscillations as overlapping happens.

Basically, these two data sets show a high degree of similarity at the beginning. The energy is almost 100% maintained in the mode they initially putted in. The energy stored in 384^{th} eigenmode is comparatively less stable to that of the 128^{th} one, as you can see the energy indicating line of 384^{th} eigenmode is thicker because of some small oscillation over time. Such a small difference leads them behave totally different later. The energy stored in 128^{th} one keep constant till the end, which explains why the system do not overlap as there does not have energy distribution, the system is oscillating almost linearly. Yet on the other side the energy stored in 384^{th} one starts to fade before overlapping happens (the plot stops at 2487 oscillations because of overlapping). In Fig. A.3(b), we can only see the eigenmode 390 is being excited while there should be some other eigenmode is being excited too. It is interesting to study why there is similarity and difference coexist between two symmetrically opposite eigenmode.

A.4 256^{th} eigenfrequency

The analysis with an initial condition of eigenvector corresponds to 256^{th} eigenfrequency will be meaningful as it is located in the middle of the dispersion band in Fig. 2.11(b) in Chapter 2. Once again, we are using an initial multiplying parameter $B = 3.0 \times 10^{-8}$m. And the result is so much different from the previous cases, see Fig. A.4.

In Fig. A.4, although the simulation time is short because of an early overlapping takes place, it is not like the case of equipartition (1^{st} and 2^{nd}

eigenmode as initial condition), the super-recurrence relation (3^{rd} eigenmode as initial condition) or the case of linear-dominated nonlinear oscillation (128^{th} and 384^{th} eigenmode as initial condition). Indeed, the energy distribution among different eigenmode is very hard to predict as the degree of dispersion is so random. What conclusion we can draw from Fig. A.4 is that it looks like only even modes are being excited. From Fig. A.4, energy is fading in eigenmode 256 and is redistributed to eigenmode 254, 258, 260 and 262. Although the plotting itself does not include all eigenmode, it is a reasonable guess for the even mode around eigenmode 256 to be excited first. The energy is assumed to be distributed to both upper even mode and lower even mode in the dispersion band.

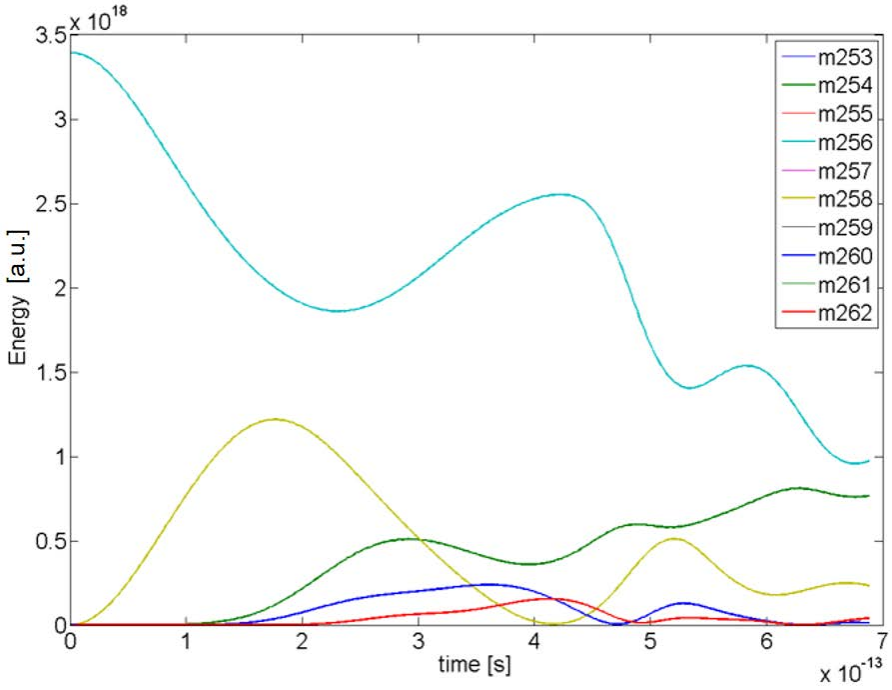

Figure A.4: (Color online) Energy indicator-time graph of several modes using the 256^{th} eigenmode as the initial configuration, with y-axis being the energy-level indicator and the x-axis being the time, the plot stops at 594 oscillations.

A.5 512^{th} eigenfrequency

We will end this section by last looking into the energy indicator-time graph using eigenmode 512 as an initial condition. For the fact that putting energy into a high-frequency mode with large amplitude will lead to a quick equipartition conducted by Zabusky and Deem [25], we perform the numerical calculations in a different way by using a lower initial multiplying parameter $B = 2.5 \times 10^{-8}\text{m}$ instead. The truth is, no matter how we adjust the value of B, equipartition still takes place quickly, see Fig. A.5, this is quite contradicting with the conclusion of Zabusky and Deem [25].

For an initial multiplying parameter $B = 2.5 \times 10^{-8}\text{m}$, this time the overlapping occurs when there are only 547 oscillations, which is the shortest lasting time among different initial configuration. Within the simulation time, one can see from Fig. A.5 that the energy stored in eigenmode 512 initially is quickly redistributed to eigenmode 510, then 508, 506…etc. This set of data tells us that the equipartition or the energy distribution is not a 'one way trip', normally the energy tends to redistribute from one mode to modes with higher frequency, but when there is no such higher mode exists, the energy will transfer backward, that is, to redistribute themselves to lower mode by symmetry. It is like when one climbs up a ladder from the bottom and eventually reaches the top, instead of staying there, he or she climbs down the ladder with the same step of climbing up.

Unluckily, we cannot further study this case by not changing the

system as the overlapping happens too early. If there is a way to prevent the overlapping happens in this Section, we can draw conclusion in a more general way. With the existence of such issue, we can only guess the behaviour beyond overlapping.

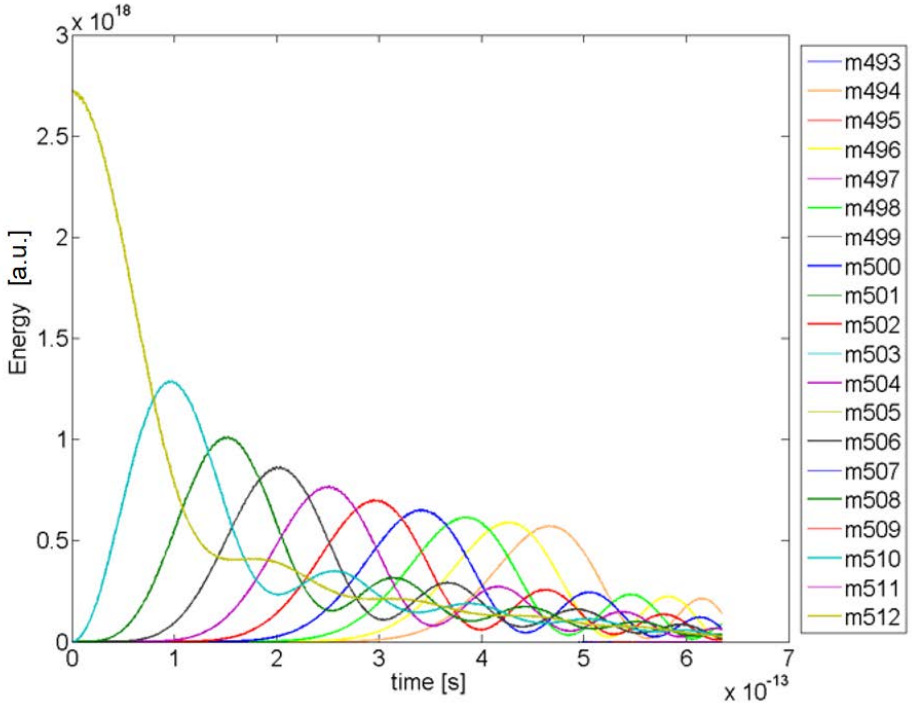

Figure A.5: (Color online) Energy indicator-time graph of several modes using the 512^{th} eigenmode as the initial configuration, with y-axis being the energy-level indicator and the x-axis being the time, the plot stops at 547 oscillations.

References

1. William Crookes, *On Radiant Matter, Lecture delivered before the British Association for the Advancement of Science, at Sheffield, Friday, 22 August 1879* (The Popular Science Monthly, 1880).
2. R. D. Hazeltine, and F. L. Waelbroeck, *The Framework of Plasma Physics: Frontier in Physics*, (Westview Press, 2004).
3. P. A. Sturrock, *Plasma Physics: An Introduction to the Theory of Astrophysical, Geophysical & Laboratory Plasmas*, (Cambridge University Press, 1994).
4. N. Engheta and R. W. Ziolkowski, *Metamaterials: Physics and Engineering Explorations*, (Wiley & Sons, 2006).
5. S. Zouhdi, A. Sihvola, and A. P. Vinogradov, *Metamaterials and Plasmonics: Fundamentals, Modeling, Applications*, (Springer, 2008).
6. D. R. Smith, *What are Electromagnetic Metamaterials?* , (Novel Electromagnetic Materials, The research group of D.R. Smith, 2009).
7. K. H. Fung and C. T. Chan, "Plasmonic modes in periodic metal nanoparticle chains: a direct dynamic eigenmode analysis," Optics Letters **32**, 973 (2007).
8. R. Quidant, C. Girard, J. C. Weeber, and A. Dereux, "Tailoring the transmittance of integrated optical waveguides with short metallic nanoparticle chains," Phys. Rev. B **69**, 085,407 (2004).
9. M. Quinten, A. Leitner, J. R. Krenn, and F. R. Aussenegg, "Electromagnetic energy transport via linear chains of silver nanoparticles," Optics Letters **23**, 1331 (1998).
10. S. A. Tretyakov and A. J. Viitanen, "Line of periodically arranged passive dipole scatters," Electrical Engineering **82**, 353 (2000).
11. A. Alu and N. Engheta, "Theory of linear chains of metamaterial/plasmonic particles as subdiffraction optical nanotransmission lines," Phys. Rev. B **74**, 205,436 (2006).
12. M. Lapine, I. V. Shadrivov, and Y. S. Kivshar, "Colloquium: Nonlinear metamaterials," Rev. Mod. Phys. **86**, 1093 (2014).

13. M. Lapine, M. Gorkunov, and K. H. Ringhofer, “Nonlinearity of a metamaterial arising from diode insertions into resonant conductive elements,” Phys. Rev. E **67**, 065,601 (2003).
14. A. A. Zharov, I. V. Shadrivov, and Y. S. Kivshar, “Nonlinear Properties of Left-Handed Metamaterials,” Phys. Rev. Lett. **91**, 037,401 (2003).
15. V. M. Agranovich, Y. R. Shen, R. H. Baughman, and A. A. Zakhidov, “Linear and nonlinear wave propagation in negative refraction metamaterials,” Phys. Rev. B **69**, 165,112 (2004).
16. Y. Zeng, D. A. R. Dalvit, J. O’Hara, and S. A. Trugman, “Modal analysis method to describe weak nonlinear effects in metamaterials,” Phys. Rev. B **85**, 125,107 (2012).
17. Y. Zeng, W. Hoyer, J. Liu, S. W. Koch, and J. V. Moloney, “Classical theory for second-harmonic generation from metallic nanoparticles,” Phys. Rev. B **79**, 235,109 (2009).
18. J. Shan, J. I. Dadap, I. Stiopkin, G. A. Reider, and T. F. Heinz, “Experimental study of optical second-harmonic scattering from spherical nanoparticles,” Phys. Rev. A **73**, 023,819 (2006).
19. B. K. Canfield, H. Husu, J. Laukkanen, B. Bai, M. Kuittinen, J. Turunen, and M. Kauranen, “Local field asymmetry drives second-harmonic generation in noncentrosymmetric nanodimers,” Nano Letters **7**, 1251 (2007).
20. I. V. Shadrivov, “Nonlinear guided waves and symmetry breaking in left-handed waveguides,” Photonics and Nanostructures: Fundamentals and Applications **2**, 175 (2004).
21. Y. S. Kivshar and G. P. Agrawal, *Optical Solitons: From Fibers to Photonic Crystals*, (Academic Press, San Diego, 2003).
22. E. Fermi, J. Pasta, and S. Ulam, “Studies of the Nonlinear Problems,” Los Alamos Report LA-1940, (1955).
23. J. L. Tuck, Los Alamos Report LA-3990, (1968).
24. N. J. Zabusky and M. D. Kruskal,“Interaction of ‘Solitons’ in a Collisionless Plasma and the Recurrence of Initial States,” Phys. Rev. Lett. **15**, 240 (1965).
25. N.J. Zabusky and G.S. Deem, “Dynamics of Nonlinear Lattices. Localized Optical Excitations, Acoustic Radiations and Strong Nonlinear Behavior,” J. Comp. Phys. **2**, 126 (1967).
26. A. J. Lichtenberg, R. Livi, M. Pettini, and S. Ruffo, “Dynamics of oscillator chains,” Lect. Notes Phys. **728**, 21 (2007).

27. B. Rink, “Proof of Nishida’s conjecture on anharmonic lattices,” Comm. Math. Phys. **261**, 613 (2006).
28. D. Bambusi and A. Ponno, “Resonance, metastability and blow up in FPU,” Lect. Notes Phys. **728**, 191 (2007).
29. G. James and Y. Sire, “Center manifold theory in the context of infinite one-dimensional lattices,” Lect. Notes Phys. **728**, 207 (2007).
30. B. Rink, “An integrable approximation for the Fermi-Pasta-Ulam Lattice,” Lect. Notes Phys. **728**, 283 (2007).
31. N. W. Ashcroft and N. D. Mermin, *Solid State Physics*, edited by F. Seitz and D. Turnbull (Brooks-Cole, Belmont, 1976).
32. M. Stone and P. Goldbart, *Mathematics for Physics: A guided tour for graduated students*, (Cambridge, 2008).
33. C. M. Bender and S. Boettcher, “Real Spectra in Non-Hermitian Hamiltonians Having PT Symmetry,” Phys. Rev. Lett. **80**, 5243 (1998); C. M. Bender, “Making sense of non-Hermitian Hamiltonians,” Rept. Prog. Phys. **70**, 947 (2007).
34. H. Schomerus, “From scattering theory to complex wave dynamics in non-Hermitian PT-symmetric resonators,” Phil. Trans. R. Soc. A **371**, 20120,194 (2013).
35. G. Levai and M. Znojil, “Systematic search for PT-symmetric potentials with real energy spectra,” J. Phys. A **33**, 7165 (2000); A. Mostafazadeh, “Pseudo-Hermiticity versus PT symmetry: The necessary condition for the reality of the spectrum of a non-Hermitian Hamiltonian,” J. Math. Phys. **43**, 205 (2002).
36. A. Lupu, H. Benisty, and A. Degiron, “Switching using PT symmetry in plasmonic systems: positive role of the losses,” Optics Express **21**, 21,651 (2013).
37. R. El-Ganainy, K. G. Makris, D. N. Christodoulides, and Z. H. Musslimani, “Theory of coupled optical PT-symmetric structures,” Optics Letters **32**, 2632 (2007).
38. Z. H. Musslimani, K. G. Makris, R. El-Ganainy, and D. N. Christodoulides, “Optical solitons in PT Periodic Potentials,” Phys. Rev. Lett. **100**, 030,402 (2008).
39. K. G. Makris, R. El-Ganainy, D. N. Christodoulides, and Z. H. Musslimani, “Beam Dynamics in PT Symmetric Optical Lattices,” Phys. Rev. Lett. **100**, 103,904 (2008).

40. A. Regensburger, M. A. Miri, C. Bersch, J. Nager, G. Onishchukov, D. N. Christodoulides, and U. Peschel, “Observation of Defect States in PT-Symmetric Optical Lattices,” Phys. Rev. Lett. **110**, 223,902 (2013).
41. L. Feng, Y. L. Xu, W. S. Fegadolli, M. H. Lu, J. B. E. Oliveira, V. R. Almeida, Y. F. Chen, and A. Scherer, “Experimental demonstration of a unidirectional relectionless parity-time metamaterial at optical frequencies,” Nat. Mater. **12**, 108 (2013).
42. Z. Lin, H. Ramezani, T. Eichelkraut, T. Kottos, H. Cao, and D. N. Christodoulides, “Unidirectional Invisibility Induced by PT-Symmetric Periodic Structures,” Phys. Rev. Lett. **106**, 213,901 (2011).
43. H. Ramezani, T. Kottos, R. El-Ganainy, and D. N. Christodoulides, “Unidirectional nonlinear PT-symmetric optical structures,” Phys. Rev. A **82**, 043,803 (2010).
44. C. W. Ling, M. Xiao, C. T. Chan, S. F. Yu, and K. H. Fung, “Topological edge plasmon modes between diatomic chains of plasmonic nanoparticles,” Optics Express **23**, 2021 (2015).
45. C. W. Ling, J. Wang, and K. H. Fung, “Formation of nonreciprocal bands in magnetized diatomic plasmonic chains,” Phys. Rev. B **92**, 165,430 (2015).
46. C. W. Ling, K. H. Choi, T. C. Mok, Z. Q. Zhang, and K. H. Fung, “Anomalous Light Scattering by Topological PT-Symmetric Particle Arrays.” arXiv:1606.05851 (2016).
47. W. H. Weber and G. W. Ford, “Propagation of optical excitations by dipolar interactions in metal nanoparticle chains,” Phys. Rev. B **70**, 125,429 (2004).
48. J. D. Jackson, *Classical Electrodynamics* (John Wiley and Sons, 1998) Third Edition.
49. C. F. Bohren and D. R. Huffman, *Absorption and Scattering of Light by Small Particles* (John Wiley and Sons, 1998)
50. Filippo Capolino Edited, *Theory and Phenomena of Metamaterials* (Taylor and Francis Group, LLC, 2009)
51. I. Lumerical Solutions, “MS Windows NT Kernel Description,” (1999). from http://www.lumerical.com/tcad-products/fdtd/
52. Y. L. Xu, “Electromagnetic scattering by an aggregate of spheres,” Appl. Opt. **34**, 4573 (1995).

53. N. Stefanou, V. Yannopapas, and A. Modinos, “Heterostructures of photonic crystals: frequency bands and transmission coefficients,” Comput. Phys. Commun. **113**, 49 (1998).
54. J. Ng, Z. F. Lin, C. T. Chan, and P. Sheng, “Photonic Clusters formed by dielectric microspheres: numerical simulations,” Phys. Rev. B **72**, 085,130 (2005).
55. T. C. Mok, Raymond P. H. Wu, C. W. Ling, C. H. Lam, N. Boechler, and K. H. Fung, “Possible Energy Localization by Classical Nonlinear Interaction in Chain of Plasmonic Nanoparticles” Opt. Lett. (manuscript to be submitted).